

University of Windsor

## Scholarship at UWindor

---

Electronic Theses and Dissertations

Theses, Dissertations, and Major Papers

---

2010

# Plug-in Hybrid Electric Vehicle Control Strategies Utilizing Multiple Peaking Power Sources

Kevin Martin  
*University of Windsor*

Follow this and additional works at: <https://scholar.uwindsor.ca/etd>

---

### Recommended Citation

Martin, Kevin, "Plug-in Hybrid Electric Vehicle Control Strategies Utilizing Multiple Peaking Power Sources" (2010). *Electronic Theses and Dissertations*. 198.  
<https://scholar.uwindsor.ca/etd/198>

This online database contains the full-text of PhD dissertations and Masters' theses of University of Windsor students from 1954 forward. These documents are made available for personal study and research purposes only, in accordance with the Canadian Copyright Act and the Creative Commons license—CC BY-NC-ND (Attribution, Non-Commercial, No Derivative Works). Under this license, works must always be attributed to the copyright holder (original author), cannot be used for any commercial purposes, and may not be altered. Any other use would require the permission of the copyright holder. Students may inquire about withdrawing their dissertation and/or thesis from this database. For additional inquiries, please contact the repository administrator via email ([scholarship@uwindsor.ca](mailto:scholarship@uwindsor.ca)) or by telephone at 519-253-3000ext. 3208.

**PLUG-IN HYBRID ELECTRIC VEHICLE CONTROL STRATEGIES  
UTILIZING MULTIPLE PEAKING POWER SOURCES**

By

**KEVIN J. MARTIN**

A Thesis

Submitted to the Faculty of Graduate Studies  
through Mechanical, Automotive and Materials Engineering  
in Partial Fulfillment of the Requirements for  
the Degree of Master of Applied Science at the  
University of Windsor

Windsor, Ontario, Canada

2010

© Copyright 2010 by Kevin J. Martin

**PLUG-IN HYBRID ELECTRIC VEHICLE CONTROL STRATEGIES  
UTILIZING MULTIPLE PEAKING POWER SOURCES**

By

**KEVIN J. MARTIN**

APPROVED BY:

---

N. Kar

Department of Electrical and Computer Engineering

---

J. Johrendt

Department of Mechanical, Automotive and Materials Engineering

---

B. Minaker, Advisor

Department of Mechanical, Automotive and Materials Engineering

---

A. Fartaj, Chair of Defense

Department of Mechanical, Automotive and Materials Engineering

September 16<sup>th</sup>, 2010

## **Author's Declaration of Originality**

I hereby certify that I am the sole author of this thesis and that no part of this thesis has been published or submitted for publication.

I certify that, to the best of my knowledge, my thesis does not infringe upon anyone's copyright nor violate any proprietary rights and that any ideas, techniques, quotations, or any other material from the work of other people included in my thesis, published or otherwise, are fully acknowledged in accordance with the standard referencing practices. Furthermore, to the extent that I have included copyrighted material that surpasses the bounds of fair dealing within the meaning of the Canada Copyright Act, I certify that I have obtained a written permission from the copyright owner(s) to include such material(s) in my thesis and have included copies of such copyright clearances to my appendix.

I declare that this is a true copy of my thesis, including any final revisions, as approved by my thesis committee and the Graduate Studies office, and that this thesis has not been submitted for a higher degree to any other University or Institution.

# Abstract

Conventional automobiles operate with the use of internal combustion engines (ICEs) which run on fossil fuels as a source of energy. However, the conventional ICE provides poor fuel economy, as well as producing air pollutants. A Plug-in Hybrid Electric Vehicle (PHEV) has the potential to run solely on free energy with zero emissions as long as it operates within its all electric range. Active control techniques must be used in order to ensure optimum efficiency of the PHEV once the ICE is operated.

The objective of the proposed research is to create a control strategy utilizing batteries as well as ultracapacitors suitable for a PHEV configuration. The control strategy will be evaluated through numerical models under several driving cycles as well as emergency maneuvers in order to ensure its effectiveness at reducing fuel consumption and improving engine efficiency.

To my parents, Gerald and Diane.

# Acknowledgements

I would like to first of all thank Dr. Bruce Minaker for the post Iron Ring ceremony conversation that would eventually lead to my decision to begin my Masters under his supervision. He permitted my ideas to wander freely and allowed me to discover a path for myself, deepening my independence as a researcher and as an engineer.

It was a pleasure to work in the Vehicle Dynamics and Control Research group, where creative thoughts and inspiration could be found everywhere. Specifically, I would like to thank Dr. Rob Rieveley for all of his assistance, guidance and patience with me. I would also like to thank my colleagues, Hart Honickman and Mike Johnston, for their knowledge and easygoing personalities, which made the last two years very enjoyable in 110C.

I was also very fortunate to receive support from the AUTO21 Network of Centres of Excellence and would like to extend my thanks to my fellow researchers at the University of Ontario Institute of Technology, Memorial University and University of Waterloo.

# Table of Contents

<b>Author’s Declaration of Originality .....</b>	<b>iii</b>
<b>Abstract.....</b>	<b>iv</b>
<b>Acknowledgements .....</b>	<b>vi</b>
<b>List of Tables .....</b>	<b>xii</b>
<b>List of Figures.....</b>	<b>xiii</b>
<b>List of Notation.....</b>	<b>xvii</b>
<b>1 Introduction.....</b>	<b>1</b>
1.1 Electrification of Vehicles .....	1
1.2 Research Outline .....	2
1.3 Thesis Structure .....	3
<b>2 Literature Review .....</b>	<b>4</b>
2.1 Vehicle Dynamics and Simulation.....	4
2.1.1 Longitudinal Vehicle Dynamics .....	5
2.1.2 Driveline Dynamics .....	6
2.1.3 Pneumatic Tire Modeling .....	7



2.2 Hybrid Electric Drivelines .....	9
2.2.1 Batteries .....	9
2.2.2 Ultracapacitors .....	12
2.2.3 Electric Motors.....	13
2.3 Plug-in Hybrid Electric Vehicle Control .....	16
2.3.1 Integrated Hybrid Control Strategies .....	16
2.3.1.1 All Electric Range Control.....	17
2.3.1.2 Blend Mode Control .....	17
2.3.2 Regenerative Braking Systems .....	19
2.3.3 Multiple Peaking Power Sources .....	19
2.4 Drive Cycles.....	21
<b>3 Vehicle Dynamics and Simulation.....</b>	<b>23</b>
3.1 Longitudinal Vehicle Dynamics .....	23
3.2 Tire Forces .....	25
3.2.1 Wheel Speed Stability.....	25
3.2.2 The Magic Formula Tire Model .....	26
3.3 Equivalent Roll Stiffness Model.....	28
3.3.1 Driver Behaviour .....	30
3.3.2 Powertrain and Driveline .....	30
3.3.3 Hydraulic Braking.....	31
3.4 Simulation.....	31
3.5 Validation Results.....	32

3.5.1 Acceleration .....	33
3.5.2 Braking.....	34
3.5.3 Highway Fuel Consumption .....	35
3.5.4 City Fuel Consumption .....	36
<b>4 Drive Cycle Analysis .....</b>	<b>38</b>
4.1 Drive Cycles.....	38
4.1.1 UDDS.....	39
4.1.2 HWFET .....	42
4.1.3 US06 .....	44
4.1.4 SC03.....	47
4.1.5 NYCC .....	50
4.2 ERS Drive Cycle Sensitivity.....	54
<b>5 Hybrid Electric Drivetrain.....</b>	<b>55</b>
5.1 Hybrid Configuration.....	55
5.2 Energy Source.....	56
5.2.1 Battery Capacity.....	57
5.2.2 Battery Model .....	58
5.3 Power Source .....	60
5.3.1 Ultracapacitor Model .....	60
5.4 Traction Motor-Generator.....	61
5.4.1 Motor Generator Model .....	61
5.5 Pacifica EV Performance .....	62

5.5.1 EV Pacifica Acceleration.....	63
<b>6 Hybrid Electric Vehicle Control.....</b>	<b>65</b>
6.1 Integrated Hybrid Control Development .....	66
6.1.1 ON-OFF Control.....	67
6.1.2 Hybrid Control Evaluation.....	68
6.2 Regenerative Braking Optimization .....	71
6.2.1 Brake Performance.....	71
6.2.2 Controllable Hybrid Brake System .....	76
6.2.3 Regenerative Braking Evaluation .....	78
6.3 Multiple Peaking Power Source Control .....	81
6.3.1 Vehicle Velocity .....	82
6.3.2 Ultracapacitor State of Charge.....	82
6.3.3 Peaking Power Source Control Evaluation.....	84
<b>7 Results.....</b>	<b>89</b>
7.1 All Electric Range.....	89
7.1.1 All Electric UDDS .....	90
7.1.2 All Electric HWFET .....	92
7.1.3 All Electric US06.....	93
7.1.4 All Electric SC03 .....	95
7.1.5 All Electric NYCC.....	97
7.2 Blend Mode.....	98
7.2.1 Blend Mode UDDS.....	99

7.2.2 Blend Mode HWFET.....	99
7.2.3 Blend Mode US06.....	102
7.2.4 Blend Mode SC03.....	105
7.2.5 Blend Mode NYCC.....	107
<b>8 Conclusions and Recommendations.....</b>	<b>108</b>
8.1 Thesis Summary.....	108
8.2 Recommendations.....	112
<b>References.....</b>	<b>113</b>
<b>Appendix A: Vehicle Specifications.....</b>	<b>120</b>
<b>Appendix B: Drive Cycles.....</b>	<b>123</b>
<b>Vita Auctoris.....</b>	<b>132</b>

# List of Tables

Table 3.1: Pure Slip Magic Formula.....	27
Table 3.2: Stock Chrysler Pacifica Parameters.....	32
Table 3.3: ERS Acceleration.....	34
Table 3.4: ERS Braking .....	35
Table 3.5: ERS Highway Fuel Consumption.....	36
Table 3.6: ERS City Fuel Consumption .....	37
Table 4.1: UDDS Drive Cycle Characteristics .....	40
Table 4.2: ERS-UDDS Performance .....	41
Table 4.3: HWFET Drive Cycle Characteristics .....	42
Table 4.4: ERS-HWFET Performance .....	44
Table 4.5: US06 Drive Cycle Characteristics .....	45
Table 4.6: ERS-US06 Performance .....	47
Table 4.7: SC03 Drive Cycle Characteristics .....	48
Table 4.8: ERS-SC03 Performance .....	50
Table 4.9: NYCC Drive Cycle Characteristics .....	51
Table 4.10: ERS-NYCC Performance .....	53
Table 5.1: ERS EV Acceleration .....	64
Table 6.1: PPS Control Logic .....	83
Table 7.1: ERS-EV Velocity Variations.....	90

# List of Figures

Figure 2.1: Longitudinal Vehicle Force Depiction .....	5
Figure 2.2: Driveline Components.....	6
Figure 2.3: Longitudinal Tire Behaviour .....	8
Figure 2.4: Steady-State Equivalent Battery Circuit.....	10
Figure 2.5: Randles Equivalent Battery Circuit .....	11
Figure 2.6: Ultracapacitor Equivalent Circuit.....	12
Figure 2.7: Motor Type Comparison Chart .....	14
Figure 2.8: All Electric Range vs. Blend Mode.....	18
Figure 2.9: Hybrid Energy Storage Operation .....	20
Figure 2.10: Urban Dynamometer Driving Schedule .....	22
Figure 3.1: Longitudinal Vehicle Dynamics Model .....	24
Figure 3.2: Behaviour of Magic Formula Tire Model .....	28
Figure 3.3: Equivalent Role Stiffness Model.....	29
Figure 3.4: ERS Acceleration .....	33
Figure 3.5: ERS Braking.....	34
Figure 3.6: ERS Highway Fuel Consumption .....	36
Figure 3.7: ERS City Fuel Consumption .....	37
Figure 4.1: ERS-UDDS Velocity Profile.....	40
Figure 4.2: ERS-UDDS Engine Trace and Fuel Consumption.....	41
Figure 4.3: ERS-HWFET Velocity Profile .....	43

Figure 4.4: ERS-HWFET Engine Trace and Fuel Consumption.....	43
Figure 4.5: ERS-US06 Velocity Profile.....	46
Figure 4.6: ERS-US06 Engine Trace and Fuel Consumption .....	46
Figure 4.7: ERS-SC03 Velocity Profile.....	49
Figure 4.8: ERS-SC03 Engine Trace and Fuel Consumption.....	49
Figure 4.9: ERS-NYCC Velocity Profile.....	52
Figure 4.10: ERS-NYCC Engine Trace and Fuel Consumption .....	52
Figure 5.1: Hybrid Electric Vehicle Configuration .....	56
Figure 5.2: Quasi-static Energy Flow Simulator .....	57
Figure 5.3: 35Ah All Electric Range Simulation.....	58
Figure 5.4: Charge Resistance .....	59
Figure 5.5: Discharge Resistance.....	59
Figure 5.6: Open Circuit Voltage.....	59
Figure 5.7: Motor-Generator Efficiency Contour.....	62
Figure 5.8: ERS EV Acceleration.....	63
Figure 6.1: Vehicle Control Systems .....	65
Figure 6.2: Varying Speed Constant Throttle.....	67
Figure 6.3: Constant Speed Varying Throttle.....	68
Figure 6.4: Integrated Hybrid Control Engine Trace.....	69
Figure 6.5: Integrated Hybrid Control Electric Motor Torque .....	69
Figure 6.6: Engine On-Off Control.....	70
Figure 6.7: Free Body Diagram of a Vehicle under Braking.....	71
Figure 6.8: Ideal Braking Force Distribution.....	73
Figure 6.9: Directional Instability due to Rear Wheel Lockup.....	74
Figure 6.10: Braking Process Analysis.....	76
Figure 6.11: Regenerative Braking Optimization Process.....	78
Figure 6.12: Regenerative Braking On-Off 0.3g .....	79

Figure 6.13: Regenerative Braking On-Off 0.5g .....	79
Figure 6.14: Regenerative Braking On-Off 0.7g .....	80
Figure 6.15: Optimal Regenerative Braking .....	81
Figure 6.16: Battery and Ultracapacitor Currents with a Step Current.....	83
Figure 6.17: Regenerative Braking with Battery Energy Source .....	84
Figure 6.18: Regenerative Braking with Hybrid Power Source .....	85
Figure 6.19: Hybrid Power Source Power Split.....	85
Figure 6.20: Low Speed Ultracapacitor Recharge .....	86
Figure 6.21: Optimal PPS Control Low Power Demand.....	87
Figure 6.22: Optimal PPS Control High Power Demand .....	87
Figure 7.1: ERS-UDDS EV State of Charge .....	90
Figure 7.2: ERS-UDDS EV Currents .....	91
Figure 7.3: ERS-HWFET EV State of Charge .....	92
Figure 7.4: ERS-HWFET EV Currents .....	93
Figure 7.5: ERS-US06 EV Velocity Profile .....	94
Figure 7.6: ERS-US06 EV State of Charge .....	94
Figure 7.7: ERS-US06 EV Currents .....	95
Figure 7.8: ERS-SC03 EV State of Charge .....	96
Figure 7.9: ERS-SC03 EV Currents .....	96
Figure 7.10: ERS-NYCC EV State of Charge .....	97
Figure 7.11: ERS-NYCC EV Currents .....	98
Figure 7.12: ERS-UDDS Blend Mode State of Charge.....	99
Figure 7.13: ERS-HWFET Blend Mode State of Charge.....	100
Figure 7.14: ERS-HWFET Blend Mode EM Torque .....	101
Figure 7.15: ERS-HWFET Blend Mode ICE Torque.....	101
Figure 7.16: ERS-US06 Blend Mode State of Charge .....	102
Figure 7.17: ERS-US06 Blend Mode EM Torque.....	103



Figure 7.18: ERS-US06 Blend Mode ICE Torque ..... 104

Figure 7.19: ERS-SC03 Blend Mode State of Charge..... 105

Figure 7.20: ERS-SC03 Blend Mode EM Torque ..... 106

Figure 7.21: ERS-SC03 Blend Mode ICE Torque..... 106

Figure 7.22: ERS-NYCC Blend Mode State of Charge ..... 107

# List of Notation

The notation throughout this work is used to denote mathematical types. The notations for specific entities are listed below

---

<i>Label</i>	Description
<i>AER</i>	All electric range
<i>BLDC</i>	Brushless direct current
<i>C</i>	Capacitance
<i>C<sub>dl</sub></i>	Double-layer capacitance
<i>C<sub>uc</sub></i>	Ultracapacitor capacitance
<i>CD</i>	Charge depleting
<i>CS</i>	Charge sustaining
<i>DOD</i>	Depth of discharge
<i>ERS</i>	Equivalent roll stiffness
<i>F<sub>x,ij</sub></i>	Longitudinal tire force
<i>HEV</i>	Hybrid electric vehicle
<i>HWFET</i>	Highway Fuel Economy Test
<i>i<sub>L</sub></i>	Leakage current
<i>I<sub>2</sub></i>	Battery current
<i>I<sub>d</sub></i>	Direct stator current

---

---

$I_q$	Quadrature stator current
$I_{uc}$	Ultracapacitor current
<b>ICE</b>	Internal combustion engine
$L_m$	Magnetizing inductance
$L_r$	Rotor inductance
$L_s$	Stator inductance
<b>NYCC</b>	New York City Cycle
$p$	Poles
$p_b$	Brake pressure
<b>PHEV</b>	Plug-in hybrid electric vehicle
<b>PPS</b>	Peaking power source
$Q_0$	Nominal battery capacity
$Q_{uc}$	Ultracapacitor charge
$r$	Wheel radius
$r_e$	Effective wheel radius
$R_{ct}$	Charge-transfer resistance
$R_d$	Diffusion resistance
$R_{in}$	Internal resistance
$R_o$	Ohmic resistance
$R_{uc}$	Ultracapacitor internal resistance
<b>SC03</b>	Speed Correction 03
<b>SOC</b>	State of charge
<b>SR</b>	Slip ratio
$U_d$	Direct voltage component
$U_{load}$	Load voltage

---

---

$U_o$	Non-ohmic overpotential
$U_{oc}$	Open-circuit voltage
$U_q$	Quadrature voltage component
<b>UDDS</b>	Urban Dynamometer Driving Schedule
<b>US06</b>	Supplemental Federal Test Procedure
$V_c$	Ultracapacitor terminal voltage
$x$	Longitudinal displacement
$\dot{x}$	Longitudinal velocity
$\ddot{x}$	Longitudinal acceleration
$y$	Lateral displacement
$\dot{y}$	Lateral velocity
$\ddot{y}$	Lateral acceleration
$\eta_c$	Charge efficiency
$\eta_d$	Discharge efficiency
$\dot{\phi}$	Roll rate
$\ddot{\phi}$	Roll acceleration
$\dot{\psi}$	Yaw rate
$\ddot{\psi}$	Yaw acceleration
$\varphi_d$	Direct stator resolved rotor flux
$\varphi_q$	Quadrature stator resolved rotor flux
$\omega_r$	Rotor frequency
$\omega_v$	Stator voltage frequency
$\omega_w$	Rotational wheel velocity
$\dot{\omega}_w$	Angular wheel acceleration

---

# Chapter 1

## 1 Introduction

The internal combustion engine has been the most prominent propulsion system used for transportation purposes throughout the last century. The depletion of fossil fuel resources and the rise in emissions has resulted in a need for more sustainable transportation methods. As modern society continues to grow, so does the need for an increasing number of vehicles for transportation. Trends predict that the fossil fuels located under the earth's surface are at risk of being entirely consumed in the near future. Hybrid electric vehicles (HEVs) offer superior fuel economy and are a logical step in the direction towards zero emissions vehicles. This chapter offers a brief history of hybrid electric vehicles and the motivation behind such research.

### 1.1 Electrification of Vehicles

All current production vehicles rely on the combustion of fossil fuels as a means of transforming chemical energy to mechanical energy through the use of an internal combustion engine. The combustion of fossil fuels results in the production of nitrogen oxides, carbon monoxides and unburned hydrocarbons, all considered toxins when found in air. The production of gases such as carbon dioxide and methane also contribute to global warming. If the use of fossil fuels continues on its current trend, the world's fossil fuel resources will be completely depleted by approximately 2038 [12].

The concept of HEVs was established in the late 1800s, although the use of the electric motor was to provide additional power when the internal combustion engine could not

provide sufficient amounts. Regenerative braking was also invented around this time, providing a means for recuperating the vehicle's kinetic energy in order to recharge the peaking power source. The complexity of the advancements in the powertrain systems were seen as troublesome and not worth the effort, considering the proven reliability of the IC engine.

The need for reduced emissions and fuel consumption prompted the return of the HEV. Improvements in battery technology and computation power allowed for complex hybrid vehicle drivetrain control. Of utmost importance is the integrated hybrid control, which modulates the internal combustion engine and electric motor. The desired goal of such a control is to achieve minimal fuel consumption while maximizing regenerative capabilities of the braking system.

Implementation and testing of integrated hybrid control can become very costly. The advancements in computation power have allowed for vehicle simulation techniques to be developed in order to safely and accurately model vehicle systems for fractions of the costs of real world tests [7].

## **1.2 Research Outline**

The goals of this research are to develop a plug-in hybrid electric vehicle model, simulate real world drive cycles, and analyze the effect of the integrated hybrid control algorithms when multiple peaking power sources are incorporated in the vehicle model.

The first objective of the research is to develop and validate a highly flexible hybrid vehicle dynamics model. The flexibility is determined through the number of hybrid vehicle configurations which can be achieved in the model and the validation is established through comparison to specifications given by the manufacturer.

The second objective of the research is to implement hybrid controls to optimize the drivetrain capabilities of the given vehicle configuration. The hybrid controls of

significance are the integrated hybrid drivetrain control, regenerative braking control, and the peaking power source control.

Finally, the effect of the developed hybrid controls during real world drive cycles will be evaluated.

### **1.3 Thesis Structure**

This thesis consists of eight chapters and two appendices. In Chapter 1, the social and environmental effects are introduced, providing the motivation for the research. In Chapter 2, the relevant literature regarding existing technology and innovation are discussed. In Chapter 3, vehicle dynamics modeling is established. This chapter mainly includes the applicable equations of motion and longitudinal vehicle dynamics behaviour. In Chapter 4, the drive cycles of interest are evaluated in terms of distance, velocity, acceleration, energy and power. In Chapter 5, plug-in hybrid electric vehicle control strategies are developed. The differences between all electric, charge sustaining and blend modes are described. In Chapter 6, hybrid electric drivetrain components are introduced. The discussion includes modeling of the electric components and their selection for such an application. In Chapter 7, the results of the numerical simulations are provided. Validations of the hybrid vehicle dynamics model and drive cycle implementation are established. Finally, in Chapter 8, implications of the results in Chapter 7 and potential for future work are discussed.

## **Chapter 2**

# **2 Literature Review**

The addition of electrical propulsion components to a conventional vehicle structure allows the vehicle to run potentially with zero emissions and higher efficiency. The complexity of the hybrid electric vehicle drivetrain requires extensive design and development that can be extremely costly at the empirical level. Existing vehicle dynamics models, drivetrain models, and non-linear tire models can be used in conjunction with battery, ultracapacitor and electric motor models in order to develop simulation software for hybrid electric vehicles suitable for evaluating multiple hybrid configurations and control. Each subsystem may contain their own control, while the interaction of the subsystems may also be controlled through some hierarchy of control schemes. This chapter will focus on the state of the art for the development of such a hybrid electric vehicle simulation model.

### **2.1 Vehicle Dynamics and Simulation**

When modeling a vehicle, a fixed axis system with its origin at the centre of mass of the vehicle body is used in order to ensure constant inertial properties. The forward or longitudinal direction of the vehicle is labeled the x-axis, the right or lateral direction of the vehicle is labeled the y-axis, and the downward or vertical direction is labeled the z-axis. Rotation of the vehicle body about the longitudinal axis is known as roll, about the lateral axis is known as pitch, and about the vertical axis is known as yaw. The rotation of each individual wheel will provide four additional degrees of freedom for the system.



Therefore, most vehicle models contain ten degrees of freedom for the vehicle body and wheels. The solution of ten second order differential equations could prove to be challenging; however, with the use of modern numerical mathematics software, this can be done quite easily. Most commercially available vehicle simulation software contains many more degrees of freedom within their models. In order to evaluate preliminary design ideas, the vehicle systems may be simplified and analyzed in particular directions separately with sufficient accuracy.

### 2.1.1 Longitudinal Vehicle Dynamics

Modeling a vehicle in the longitudinal direction is typically done for acceleration and braking purposes. The vehicle is modeled as a single rigid body, and all lateral effects are ignored. Vertical loads at both the front and rear tires represent both the left and right sides of the vehicle lumped as single loads. Figure 2.1 below displays all of the forces acting on the simplified longitudinal vehicle dynamics model.



Figure 2.1: Longitudinal Vehicle Force Depiction

Rolling resistance and aerodynamic drag act against the vehicle body and are modeled as functions of vehicle velocity. The application of Newton's second law on the centre of mass results in:

$$\sum F_x = m_{effective}\ddot{x} = F_{traction} - F_{aerodynamics} - F_{rolling\ resistance} - F_{grade} \quad (2.1)$$

The traction force provided by the propulsion unit is labeled  $F_{\text{traction}}$  and the force required to overcome hill climbing is labeled  $F_{\text{grade}}$ . The grade force is a result of the vehicle weight acting in the longitudinal direction during inclination. This vehicle model is useful for gear optimization, engine selection, fuel consumption and some basic performance estimations [24] [12] [17] [21] [16]. The user must understand the limitations of such a model due to the large number of simplifications and assumptions made. In terms of numerical computation, the model can be simulated easily once it has been arranged into a first order form.

### 2.1.2 Driveline Dynamics

To develop the traction force in the longitudinal model, an analysis of the driveline must be completed. The driveline consists of a propulsion unit, clutch, gearbox, differential, driveshaft, and wheels as illustrated in Figure 2.2.



*Figure 2.2: Driveline Components*

The propulsion unit is typically an internal combustion engine with varying degrees of model complexity. The most common ICE model is completed empirically using dynamometer testing results for varying throttle positions where spark advance, exhaust gas recirculation, air to fuel ratio, and emissions are considered pre-calibrated control variables [24] [21] [9]. Alternatively, the throttle can be modeled as a variable nozzle and the engine modeled as a pump with particular cylinder volume, rotational speed and volumetric efficiency [39] [4]. Propulsion unit power will be the limiting factor in vehicle top speed.

The clutch is used in order to allow the vehicle to come to rest without stalling the engine and is typically modeled as a power loss of the transmission [24] [21]. The second fraction of the transmission model is the gear box, which selects the appropriate gear for a given vehicle speed. The gear box is typically designed to either have a geometric or progressive gear ratio [17] [24].

The differential and driveshafts are characteristically modeled as lumped masses with constant rotational inertia properties classically added to the effective mass of the vehicle. Losses in either the differential or driveshafts may be included in the losses of the transmission. The vehicle wheel is a much more complex component in the driveline and will be discussed in the subsequent section.

### **2.1.3 Pneumatic Tire Modeling**

The forces created to accelerate, brake, and corner a vehicle occur at the road-wheel interface. The vehicle's motion depends completely on these forces and therefore creates a major importance on the accuracy of the tire model. The major difficulty in modeling tires is their non-linear behaviour in both longitudinal and lateral directions. Once the throttle is pressed, the wheel starts to slip slightly, which results in a differential speed between the wheel's spin speed and the ground speed, resulting in the generation of a longitudinal force. The longitudinal force generated is a function of slip ratio and vertical load as seen in Figure 2.3 [16] [24] [35] [33].

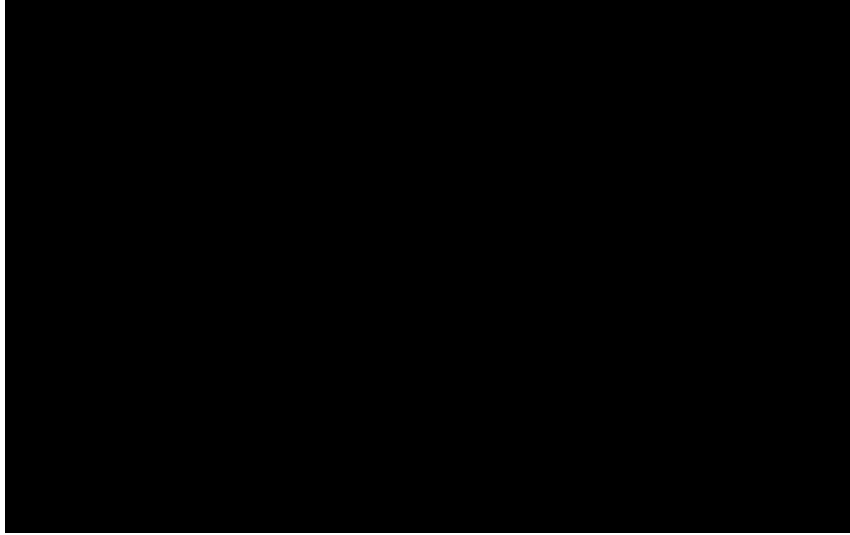


*Figure 2.3: Longitudinal Tire Behaviour*

In order to calculate wheel slip, the tire contact velocity is approximated by the rotational speed of the wheel and the effective tire radius. The relationship for longitudinal slip ratio is defined as:

$$SR = \frac{\omega \cdot r_e}{\dot{x}} - 1 \quad (2.2)$$

As the tire accelerates, in either direction, it deforms at the road-wheel interface, creating a compressed zone and a stretched zone. The unloading of the tire does not occur in the same manner as the loading of the tire, resulting in a hysteresis effect. This hysteresis effect results in what is known as rolling resistance, which opposes the motion of the wheel [16].

To accurately simulate vehicle motion, the tire model must encompass longitudinal slip, lateral slip and the aligning moment. Many empirical tire models exist, though the preferred tire model is the Pacejka Magic Formula. It is a notable improvement from the Calspan model, though the major drawbacks of the formula remain the lack of tire data and the lack of physical interpretation for the various coefficients [47].

## 2.2 Hybrid Electric Drivelines

The electric propulsion system of a hybrid vehicle introduces several new components to the vehicle structure. Traction is generated through the use of one or more electric motors powered by batteries, ultracapacitors or a generator unit coupled to the IC engine. Modeling of such components may be difficult due to their non-linearities and state dependent variables. Each subsystem must be modeled accurately and independently before being integrated.

### 2.2.1 Batteries

Batteries are devices that convert chemical energy into electrical energy. They are typically a reversible energy storage system; therefore, they can be recharged through the reverse chemical process. The requirements for HEV applications include: high specific power, high specific energy, long calendar and cycle life, low initial and replacement costs, high reliability, and high robustness.

Classically, specific energy is the first parameter of concern, as this will affect the range of the vehicle. Power density is ranked next in terms of importance, as it will affect the vehicle's performance under acceleration and braking. Achieving both high energy density and power density is possible, although it comes at increased costs. Battery manufacturers typically specify the coulometric capacity of their batteries. The coulometric capacity is defined as the number of ampere-hours (Ah) gained while discharging the battery at a fixed current rate until a cut-off voltage is achieved. The cut-off voltage is the minimum allowable voltage, which is achieved at zero state of charge. The state of charge, SOC, of the battery is the ratio of the remaining capacity to the fully charged capacity of the battery. A fully charged battery has a SOC of 1, and a fully discharged battery has a SOC of 0. The SOC can be monitored accurately through a combination of voltage correction and current integration [21] [29] [13]. Equation 2.3

shows the relationship between current, nominal battery capacity ( $Q_0$ ) and state of charge. To improve the accuracy of the model, the coulombic efficiency ' $\eta_c$ ' may also be included.

$$SOC = SOC_0 - \int \frac{-\eta_c I_b(t)}{Q_0} dt \quad (2.3)$$

Battery models vary in complexity; the more accuracy required the more complex the model. The most basic of battery models consists of an open-circuit voltage source in series with an internal resistance [21] [29].

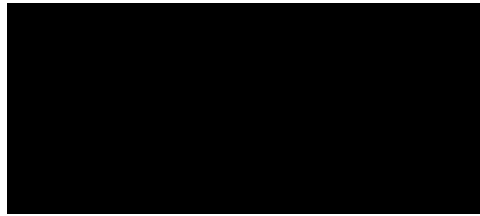


Figure 2.4: Steady-State Equivalent Battery Circuit

The application of Kirchhoff's voltage law for the equivalent circuit yields:

$$U_{oc}(t) - R_{in}(t) \cdot I_2(t) = U_2(t) \quad (2.4)$$

In this model, the open circuit voltage varies with the SOC. The internal resistance is a combination of three different effects. The first is the ohmic resistance ( $R_o$ ), the second is the charge-transfer resistance ( $R_{ct}$ ), and the third is the diffusion resistance ( $R_d$ ). The major drawback of this model is that the resistances do not depend on current. The processes involved are highly non-linear; therefore, models have been developed where fitting techniques are used to interpret results from constant-current tests. Modifications to the original model can be made to include effects of SOC and discharge current.

$$U_{load}(t) = (\kappa_1 - \kappa_3 \cdot I_b(t)) + (\kappa_2 - \kappa_4 \cdot I_b(t)) \cdot q(t) \quad (2.5)$$

The constants  $\kappa_1$  and  $\kappa_2$  create a linear relationship between battery state of charge and open circuit voltage, while the constants  $\kappa_3$  and  $\kappa_4$  vary the battery model for charging and discharging events.

Modeling dynamic effects of a battery requires a more sophisticated model. There are several different models that may be used; of these, the most common is the Randles model [21] [8].



Figure 2.5: Randles Equivalent Battery Circuit

The Randles model includes a double-layer capacitor to reproduce capacitive effects of the charge accumulation/separation that occur at the interface of the electrodes and the electrolyte. Applying Kirchhoff's voltage law once again for the new battery model results in:

$$U_{load}(t) = U_{oc} - R_o \cdot I_2(t) - U_o(t) \quad (2.6)$$

$$R_o \cdot C_{dl} \cdot \frac{d}{dt} U_o(t) = U_{oc} - U_{load}(t) - U_o(t) \cdot \left(1 + \frac{R_o}{R_d + R_{ct}}\right) \quad (2.7)$$

Often this model is altered to include several different effects, such as self-discharge, occurring within the battery. The resistances may be written as functions of discharge current to include more of the nonlinear effects. The most precise battery models include effects of non-linear equilibrium potential, rate dependency, capacity and temperature

effects [8] [15] [4] [39]. Batteries can also be modeled through fitting methods and tabular data from experimental discharge and charging events.

### 2.2.2 Ultracapacitors

Ultracapacitors are devices which store energy in the electric field of an electrochemical double layer. They typically have a substantially higher specific power than batteries but the tradeoff is that their specific energy is substantially lower. Ultracapacitors are useful for applications such as acceleration and hill climbing [12].

Ultracapacitors differ from regular capacitors in material as well as physical process. The energy is stored by the charge separation taking place in the layers that separate the electrolyte and the electrodes. A separator is used to insulate the electrodes as well as to store and immobilize the liquid electrolyte.

An equivalent circuit of an ultracapacitor can be derived for physical modeling. The simplest model consists of a capacitor in series with a resistor.

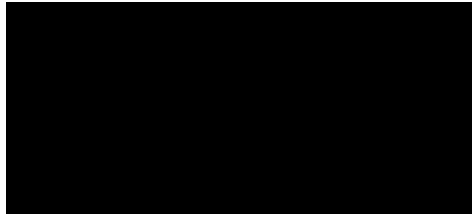


Figure 2.6: Ultracapacitor Equivalent Circuit

The application of Kirchhoff's voltage law results in:

$$R_{uc} \cdot I_{uc}(t) - \frac{Q_{uc}(t)}{C_{uc}} + U_{load}(t) = 0 \quad (2.8)$$

$$I_{uc}(t) = -\frac{d}{dt} Q_{uc}(t) = 0 \quad (2.9)$$



Dynamic modeling of ultracapacitors also contains modifications similar to those from the battery models, though the basic equivalent circuit is seen as more accurate in ultracapacitors [21].

### **2.2.3 Electric Motors**

In electric and hybrid electric vehicles the electric motor provides a traction force through a transmission and the driven wheels. The motor is usually reversible, allowing it to convert electrical power from the batteries into mechanical power to drive the vehicle, but also to convert mechanical power back into electrical power to recharge the batteries. The latter of the two modes is known as generator mode, which occurs during the process of regenerative braking. Desired characteristics of a traction motor are high efficiency, low cost, high specific power, good controllability, fault tolerance, low noise, and uniformity of operation.

Several different types of electric motors exist, and they can be organized into two main categories: commutator motors and commutatorless motors. Direct current (DC) motors are categorized as commutator motors as they contain commutators and brushes. Alternating current (AC) motors such as induction and switched reluctance motors are categorized as commutatorless. Commutatorless motors provide higher efficiency, higher power density and lower operating cost, which are all important aspects to the design of a HEV. This work will focus on the use of induction motors. Figure 2.4 shows the specific power of different types of electric motors suitable for traction motors in EVs and HEVs.

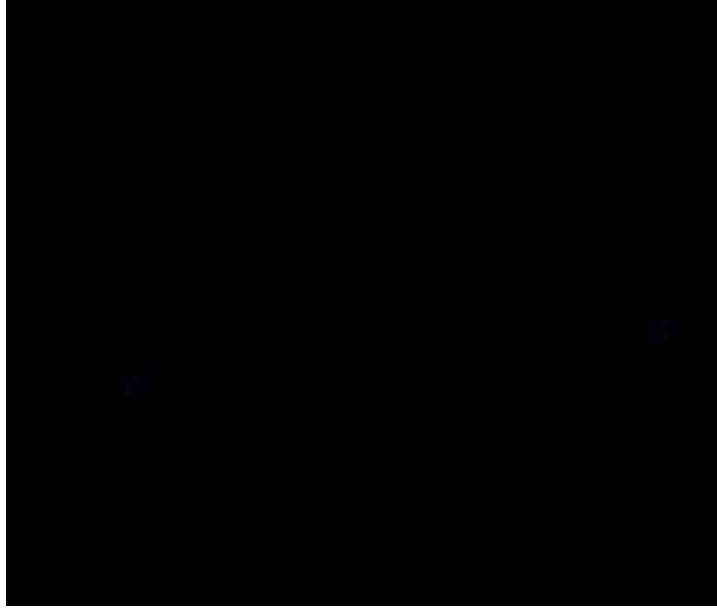


Figure 2.7: Motor Type Comparison Chart

Induction motors require an AC power source, usually supplied by an inverter with a DC source. Induction motors are modeled using a two-phase reference frame. The reference frame consists of a direct axis labeled 'd', and a quadrature axis labeled 'q'. The most convenient reference frame is the synchronous reference frame which rotates at the frequency of the magnetic field developed in the stator. Electrical circuit analysis of the stator can be calculated using Kirchhoff's voltage law.

$$\begin{aligned}
 U_q(t) = \sigma \cdot L_s \cdot \frac{d}{dt} I_q(t) + \left( R_s + \frac{L_m^2 \cdot R_r}{L_r^2} \right) \cdot I_q(t) + \omega_v(t) \cdot \sigma \cdot L_s \cdot I_d(t) \\
 - \frac{L_m \cdot R_r}{L_r^2} \cdot \varphi_q(t) + \frac{L_m}{L_r} \cdot p \cdot \omega_r(t) \cdot \varphi_d(t)
 \end{aligned} \tag{2.10}$$

$$\begin{aligned}
 U_d(t) = \sigma \cdot L_s \cdot \frac{d}{dt} I_d(t) + \left( R_s + \frac{L_m^2 \cdot R_r}{L_r^2} \right) \cdot I_d(t) - \omega_v(t) \cdot \sigma \cdot L_s \cdot I_q(t) \\
 - \frac{L_m \cdot R_r}{L_r^2} \cdot \varphi_d(t) + \frac{L_m}{L_r} \cdot p \cdot \omega_r(t) \cdot \varphi_q(t)
 \end{aligned} \tag{2.11}$$

The equations describing the state of the rotor are:

$$0 = \frac{d}{dt} \varphi_q(t) - \frac{L_m \cdot R_r}{L_r} \cdot I_q(t) + \frac{R_r}{L_r} \cdot \varphi_q(t) + (\omega_v(t) - p \cdot \omega_r(t)) \cdot \varphi_d(t) \quad (2.12)$$

$$0 = \frac{d}{dt} \varphi_d(t) - \frac{L_m \cdot R_r}{L_r} \cdot I_d(t) + \frac{R_r}{L_r} \cdot \varphi_d(t) - (\omega_v(t) - p \cdot \omega_r(t)) \cdot \varphi_q(t) \quad (2.13)$$

$$\sigma = 1 - \frac{L_m^2}{(L_s \cdot L_r)} \quad (2.14)$$

The d-q axis stator currents are  $I_d(t)$  and  $I_q(t)$ , the d-q axis stator voltages are  $U_d(t)$  and  $U_q(t)$ , and the d-q axis stator resolved rotor fluxes are  $\varphi_d(t)$  and  $\varphi_q(t)$ . The stator resolved rotor and stator inductances are  $L_r$  and  $L_s$ , the stator resolved rotor and stator resistances are  $R_r$  and  $R_s$ , and the magnetizing inductance is  $L_m$ . The frequency of the stator voltage is represented by  $\omega_v(t)$ , and the frequency of the magnetic field induced in the rotor is given by the number of poles,  $p$ , multiplied by the rotor speed,  $\omega_r(t)$  [21] [20] [12] [13].

The magnetic field induces a torque on the rotor which can be found through an energy balance. Stator voltage components and the AC frequency are set by the electronic frequency converter. The main power electronics of the motor system is the inverter, which converts the DC supply voltage to a variable frequency three phase AC source.

The losses of the system come from ohmic resistance, slip and controller efficiency. In order to solve the equations of the system, the stator voltages and frequency must be known from the control strategy. Equations 2.10-2.13 can then be integrated to solve for the currents and fluxes of the d-q reference frame. A common control strategy is to impose zero d-axis voltage and to modulate the q-axis voltage as a function of supply voltage [21]. Alternatively, empirical modeling of the motor may be conducted to develop an efficiency contour for a given motor once the motor controller has been implemented [1].

## **2.3 Plug-in Hybrid Electric Vehicle Control**

The integration of conventional vehicle components with electric propulsion components results in a vast number of potential hybrid electric configurations. A series hybrid is characterized by a configuration in which the electric motor alone provides the traction force for the vehicle. The power can be provided by either the battery or by a generator driven by an ICE. Alternatively, a parallel hybrid vehicle is characterized by a configuration in which either the electric motor or the internal combustion engine can provide the traction force for the vehicle. Several other configurations exist, though they are typically a combination of the series and parallel types [19] [7] [14] [25].

As the complexity of the vehicle configuration is increased, so are the demands for control. Each vehicle component must have its own control, though the interaction of the various subsystems must also be controlled. In order to achieve the optimal result, three main types of subsystem interaction control are required: integrated hybrid control, regenerative braking control, and multiple power source control.

### **2.3.1 Integrated Hybrid Control Strategies**

The goal of integrated HEV control is to determine the optimal power split at each instant of time that minimizes the total fuel consumption of the vehicle [38] [19]. Classical hybrid electric vehicles charged their batteries solely from fuel transformed through the internal combustion engine and generator; therefore, they typically hold the SOC at some constant value where the battery efficiency is greatest. In contrast, plug-in hybrid electric vehicles recharge their batteries at the end of a driving event, allowing the battery to run through a range of depletion levels. The energy gained during plug-in charging can be taken from natural or free resources, where zero emissions are produced. As a result, it is desired that the initial battery state be fully charged and that the final state be completely discharged. This ensures that the vehicle has used the total amount of energy available

from the battery during the driving event [26]. In order for the battery to achieve zero SOC at the end of the driving event, two strategies are available; all electric control and blend mode control.

### **2.3.1.1 All Electric Range Control**

The purpose of the All Electric Range Control (AER) is to allow the vehicle to utilize its entire battery range before switching to fuel for energy [26] [45]. If the vehicle has an all electric range of 40 miles and travels 20 miles daily, the vehicle can be recharged at the end of each day and never consume any fuel, acting as an electric vehicle. Once the SOC reaches the minimum threshold, charge sustaining mode (CS) is automatically initiated. Charge sustaining mode holds the battery state of charge near constant to ensure the battery does not reach dangerously low levels, which will affect battery life. For plug-in hybrid electric vehicles with large AERs, this control strategy is the most fuel efficient. For PHEVs with small AERs, a charge depleting mode such as blend mode control is most fuel efficient [26]. The battery state of charge for all electric control can be seen in Figure 2.8 where B represents EV mode operation and A represents CS mode operation.

### **2.3.1.2 Blend Mode Control**

Blend mode control uses both the IC engine and the electric motor until the SOC of the battery reaches the minimum threshold. Given that fuel and battery split the energy demand, the blend mode reaches the CS mode much later than AER control. The engine is only operated when it can perform within its optimal efficiency range, but is also dependent on the battery SOC, throttle position and prior knowledge of trip distance [26] [45] [25]. The battery state of charge throughout blend mode operation is seen in Figure 2.8.

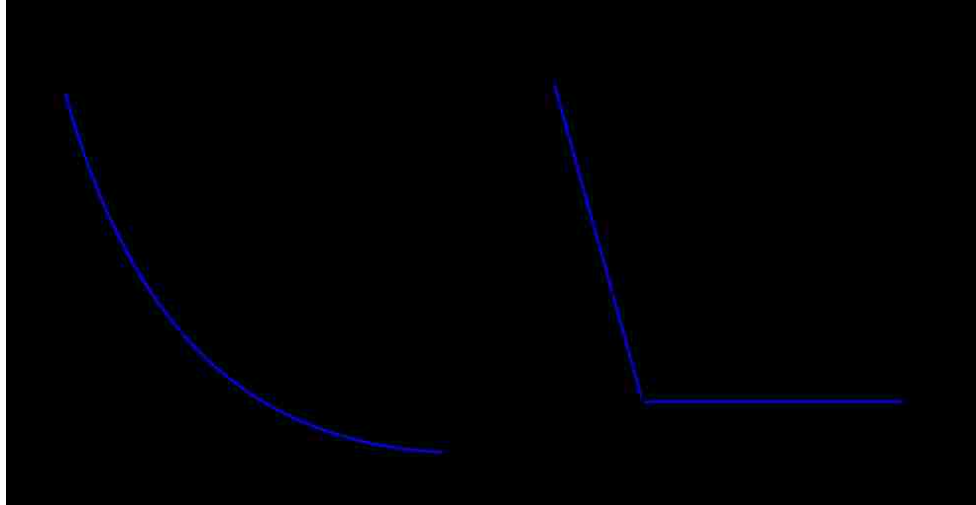


*Figure 2.8: All Electric Range vs. Blend Mode*

As the engine operates in a high efficiency range, the electric motor is used as a power modulator [7]. The engine and motor can also be used for power assist purposes, increasing acceleration performance or downscaling to save mass [41]. The integration of the two subsystems results in a complex situation of control. Three types of blend mode control exist: dynamic programming, intelligent control techniques such as fuzzy logic, and optimal control [38] [19] [18]. All of these have been successfully implemented, although optimal control tends to require information that is unknown for a given driving event, such as SOC and total distance; therefore, optimal control may prove too complex for practical use [19] [26] [10].

The selection of the control strategy and control type will be based strongly on the topology of the vehicle as well as the performance index. The input variables must be easily measurable and the control scheme must be robust and reliable [25] [19]. System efficiencies of plug-in hybrid electric vehicles have been nearly doubled in test configurations when compared to conventional vehicles [31].

### **2.3.2 Regenerative Braking Systems**

One of the most important features of a hybrid electric vehicle is the ability to recapture significant amounts of energy during braking. Conventional braking systems dissipate kinetic energy as heat through friction. Conversely, HEVs run the motor as a generator, recharging the batteries and improving fuel efficiency and range [1] [12] [37] [44].

Regeneration is limited by the available capabilities of the traction motor and the battery system. Due to the limitations of the batteries and motor, a friction braking system must be used for emergency braking and bringing the vehicle to rest [48]. Hybrid control must also be developed for the hybrid braking system. The purpose of the hybrid braking control is to ensure maximum regenerative torque upon a braking request. As the maximum regenerative torque is being provided, the controller must also modulate the friction brakes to meet driver demand. Previous active safety systems such as anti-lock braking (ABS), electronic braking force distribution (EBD), traction control (TC) and electronic stability program (ESP) can all be incorporated into the hybrid braking scheme. The control strategy must monitor the battery SOC, battery temperature, and available motor torque in order to guarantee optimal braking [1] [37] [48].

### **2.3.3 Multiple Peaking Power Sources**

The use of traction batteries provides many advantages such as recuperation of energy when braking, idling on electric power to avoid emissions, driving on electrical power in specific cases where the IC engine has poor emissions, and decreased fuel consumption [2] [42]. However, the battery is very rate sensitive and has limited power capabilities. The introduction of a secondary power source to a hybrid vehicle can allow the system to overcome some of the downfalls of lone energy storage. Limitations on drive range are a result of poor energy density and limitations on acceleration and regenerative braking are

a result of poor power density. The hybridization of ultracapacitors and batteries allows compensation for the lower specific energy of the ultracapacitors and the lower specific power of the batteries [12] [6] [49].

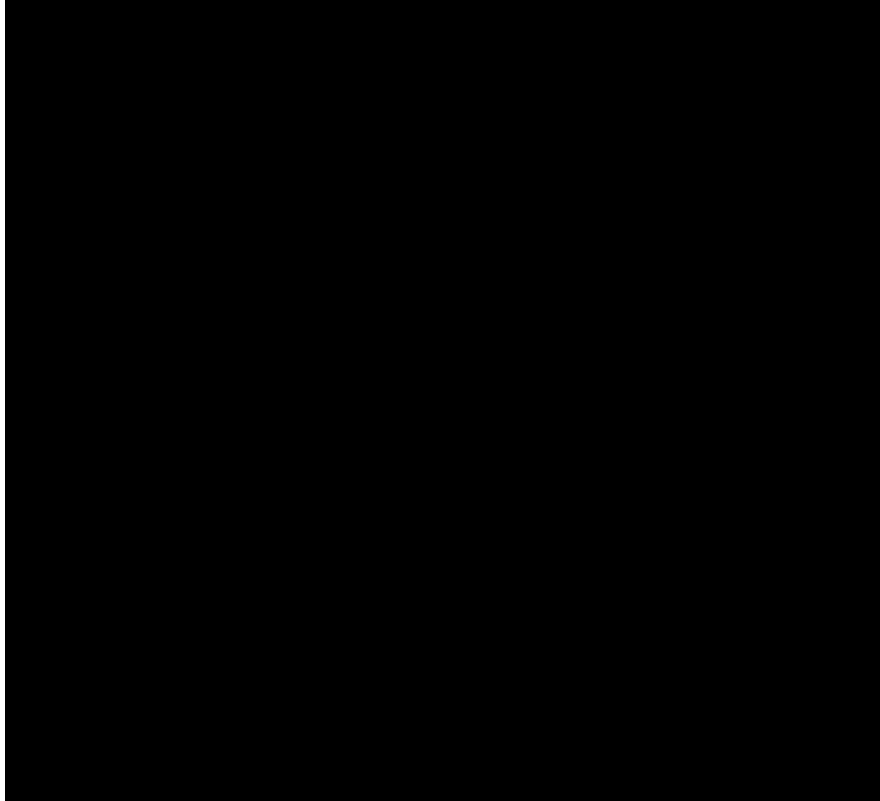


*Figure 2.9: Hybrid Energy Storage Operation*

Ultracapacitors have the ability to absorb high currents with high frequencies over nearly endless cycles without performance deterioration, making them an ideal counterpart for batteries, which can be extremely sensitive to large discharge and charge rates [6] [11] [36]. Acceleration and regenerative braking tend to cause large currents which exceed battery limitations.

The integration of ultracapacitors and batteries results in the need for a control strategy to regulate their current demands. The ultracapacitor SOC is controlled based on vehicle speed, high SOC at low speed and low SOC at high speed. The low SOC at high speed is



to ensure that maximum regenerative braking can be achieved even with high battery SOC [36] [11]. The ideal case will allow the ultracapacitors to take full loads for short pulses and not cause any sudden spikes in battery current. In other words, the ultracapacitor handles the transients of the system, while the battery handles the majority of the steady-state demand [3]. The addition of ultracapacitors to a battery energy storage system can significantly improve power and vehicle range without any increase on cost or vehicle mass [36].

## 2.4 Drive Cycles

To model the range and efficiency of a proposed HEV, it is important to have relevant drive data for simulation purposes. Before driving data was available, constant velocity tests were customary [12]. It is obvious that constant velocity tests would produce only moderately accurate results as real driving scenarios would be ignored. Many corporations have gone through the task of instrumenting fleets of vehicles in order to develop real world driving data, also known as drive cycles. They are a useful tool for comparative studies between HEVs, although their accuracy could be questioned. Drive cycles allow for simulation in which the vehicle undergoes realistic driving patterns of everyday use. The development of real world drive cycles has created a push towards standardized hybrid electric vehicle fuel consumption calculations. The Society of Automotive Engineers Journal J1711 sets forth a standard for evaluating HEV fuel consumption under testing of four primary drive cycles: UDDS, HWFET, US06, and SC03 [31] [41]. The velocity profile of the UDDS drive cycle can be seen in Figure 2.10.

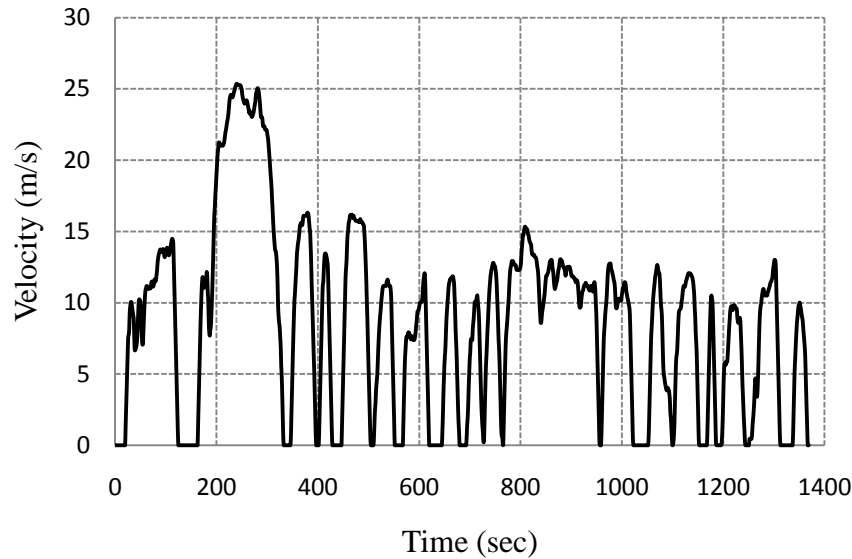


Figure 2.10: Urban Dynamometer Driving Schedule

According to current federal test procedure standards, the vehicle must not miss the speed trace by more than 2 mph (0.89 m/s) at any point in time [31]. Fuel displacement benefits of PHEVs will also be influenced by the frequency of recharging events [30].

The availability of drive cycle data has created a large market of HEV simulations for hybrid electric vehicle control optimization. Some preliminary results show a lack in correlation between simulation and empirical testing. Suggestions have been made that errors may be a result of unexpected engine on/off behaviour as a result of throttle uncertainty [43] [28]. Driver aggressiveness, range and the exclusion of effects such as thermal behaviour, component wear and weather conditions have also been linked to the inaccuracies of the simulation results [34] [43]. Despite some early discrepancies, drive cycles remain the main estimator of fuel economy and all electric range for plug-in hybrid electric vehicles [46].

## **Chapter 3**

# **3 Vehicle Dynamics and Simulation**

Vehicle dynamics may be analyzed in several different ways. Typically models are developed for isolated analysis of a particular case. Vehicle models range in complexity from a simple one degree of freedom model to extremely complicated multibody systems. Although modeling of an entire vehicle and all of its subsystems would prove to be the most accurate, the time consumption of such models is undesirable. The development of a vehicle dynamics model must reduce the model complexity of the entire system, be implemented in a common PC programming language, include interactions of the subsystems of interest, and be only as accurate as necessary, saving valuable computation time.

In order to model the full vehicle system, subsystems for the suspension, engine, driveline, and chassis should also be incorporated. The inputs of the engine and driveline subsystems will originate from driver demand as throttle and brake. The inputs of the chassis and body subsystems will originate from the driver steer angle and road geometry. The following sections will focus on the development of a vehicle dynamics model for hybrid electric vehicle simulation purposes.

### **3.1 Longitudinal Vehicle Dynamics**

The primary direction of interest when developing a vehicle dynamics model for HEV applications is the forward or longitudinal direction. Classically, HEVs are modeled using some form of drive cycle in order to optimize their integrated control. Lateral

effects are ignored due to low cornering speeds and vertical effects are ignored due to assumed flat road geometry.

The vehicle is modeled as five masses; one lumped mass and four wheel masses. The single lumped mass includes the mass of the body, engine, driveline, fuel, passengers, and any other payload. It has a sole degree of freedom, translation in the longitudinal direction. The four wheel masses are each assigned a degree of freedom, rotation about the wheel center. A schematic of the longitudinal vehicle dynamics model can be seen in Figure 3.1.



Figure 3.1: Longitudinal Vehicle Dynamics Model

The equations of motion of the system can be derived from Newton's second law as:

$$\sum F_x = m\ddot{x} = F_{x,fl} + F_{x,fr} + F_{x,rl} + F_{x,rr} + F_{x,wind} + F_{x,g} + F_r \quad (3.1)$$

$$\sum M_w = I_w \dot{\omega}_w = T_{engine} - M_{rolling\ resistance} - M_{Fx} - T_{brake} \quad (3.2)$$

The torque output from the engine through the drivetrain is labeled  $T_{engine}$ , the moment created about the wheel centre due to rolling resistance is labeled  $M_{rolling\ resistance}$ , the longitudinal contact patch friction force is labeled  $M_{Fx}$ , and the torque developed by the braking system based on brake pedal position is labeled  $T_{brake}$ . The wheel moment equation is applied separately for each wheel in the model. The driveline is modeled using classical modeling techniques discussed in Section 2.1.2 and the tire forces are generated from the tire model introduced in the following section.

## 3.2 Tire Forces

The tire model is the single most important part in a vehicle dynamics model. It is responsible for transferring forces from the vehicle to the road and vice versa. In order to model a tire, first the tire characteristics must be estimated or obtained from experimental tests. All tire compounds are different and therefore no model will be able to model all tire behaviour.

Friction in the tire is generated through two main effects; adhesion and hysteresis. Adhesion is a result of the molecular bonds generated between the exposed surface of atoms of rubber and road material in the contact area, where as hysteresis is a result of a difference in loading and unloading forces.

Tractive and lateral forces are a function of normal force, slip angle and slip ratio. Slip is always present in the tire even with no tractive driving or braking forces. All forces acting at the road tire interaction surface are assumed to occur at the centre of the contact patch.

### 3.2.1 Wheel Speed Stability

The slip ratio has alternate definitions under driving and braking conditions. Under driving a slip ratio of one is defined as wheel spin and under braking a slip ratio of one is defined as fully locked. Peak longitudinal forces occur at slip ratios of 0.15 to 0.3, slip ratios smaller than those at peak values tend to converge, though larger values of slip tend to diverge rapidly until torque is reduced [27].

The definition of slip ratio works well for forward velocities but has inherent problems when low speeds and negative velocities are considered. It is desired to modify the definition of slip ratio to contain all cases of acceleration and braking in all directions, forward and reverse. The corrected calculation of slip ratio is shown in Equation 3.3.

$$SR = -\frac{\dot{x} - \omega \cdot r_e}{|\dot{x}|} \quad (3.3)$$

This correction has addressed the issue of negative velocities, though does not address the singularity in wheel slip as the wheel speed approaches zero. The solution is to derive a first order differential equation for longitudinal slip.

$$\dot{SR} = -\frac{1}{B}(\dot{x} - \omega \cdot r_e - SR \cdot |\dot{x}|) \quad (3.4)$$

The solution found from Equation 3.4 results in oscillations at low vehicle speeds. To eliminate these oscillations, a damping term which is only active at low speeds is introduced.

$$F_{x,damping} = 2\zeta\dot{x}\sqrt{\frac{F_z C_s}{gB}} \quad (3.5)$$

The damping term is activated in the wheel speed equation at speeds lower than 0.15 m/s where  $\zeta$  is the damping coefficient,  $C_s$  is the longitudinal stiffness, and  $B$  is equivalent to that found in Equation 3.4 and is experimentally determined ( $0 < B < 1$ ). The sign of the damping term must switch at each time step to ensure sufficient oscillation reduction in the wheel speeds [32].

### 3.2.2 The Magic Formula Tire Model

The function of the tire model is to establish the forces and moments occurring at the tire road contact patch and resolve these to the wheel centers and hence into the vehicle chassis. The forces needed for vehicle handling are: longitudinal tractive or braking force, lateral cornering force, vertical normal force, and the aligning moment.

The tire model must continually receive information about the position, orientation, and velocity at each wheel center and also the topography of the road surface [5].

The Magic Formula Tire model was introduced by Bakker in 1986 and has seen widespread acceptance in vehicle dynamics literature [5]. The Magic Formula relates lateral force to slip angle, aligning moment to slip angle and longitudinal force to slip ratio. Previously completed experiments show a high correlation between the Magic Formula and actual data. The equations of the Magic Formula are summarized in Table 3.1.

General Formula	Longitudinal Force
$y(x) = D \sin[C \tan^{-1}\{Bx - E(Bx - \tan^{-1}(Bx))\}]$	$X_x = \kappa$
$Y(X) = y(x) + S_v$	$Y_x = F_x$
$x = X + S_h$	$D_x = \mu_x F_z$
$B = \text{stiffness factor}$	$\mu_x = b_1 F_z + b_2$
$C = \text{shape factor}$	$BCD_x = (b_3 F_z^2 + b_8) e^{-b_5 F_z}$
$D = \text{peak factor}$	$C_x = b_0$
$S_h = \text{horizontal shift}$	$E_x = (b_6 F_z^2 + b_7 F_z + b_8)(1 - b_{13} \text{sgn}(\kappa + S_{hx}))$
$S_v = \text{vertical shift}$	$B_x = BCD_x / C_x D_x$
$B = (dy/dx_{(x=0)}) / CD$	$S_{hx} = b_9 F_z + b_{10}$
$C = (2/\pi) \sin^{-1}(y_s/D)$	$S_{vy} = b_{11} F_z + b_{12}$
$D = y_{max}$	$\text{Brake force only } (b_{11} = b_{12} = b_{13} = 0)$
$E = (Bx_m - \tan(\pi/2C)) / (Bx_m - \tan^{-1}(Bx_m))$	

Table 3.1: Pure Slip Magic Formula

The value of Y(X) is either the lateral force, aligning moment, or longitudinal force. The value of x is the corresponding input to the model, either slip angle or slip ratio. The horizontal and vertical shifts are associated with the addition of camber effects and

physical features such as conicity and ply steer and are related to the lateral and aligning moment formulae. The peak factor,  $D$ , determines the upper limit of the transmissible force. The shape factor,  $C$ , controls the stretching of the curve in the  $x$  direction and has typical values of 1.3, 1.65 and 2.4 for lateral, longitudinal and aligning moment respectively. The stiffness factor,  $B$ , is multiplied by  $C$  and  $D$  to create the slope at the origin. The curve factor,  $E$ , effects the transition in the curve and the position of the peak value. The coefficients  $b_0$  through  $b_{13}$  are listed in Appendix A. The resulting longitudinal force versus slip ratio and normal load can be seen in Figure 3.2.

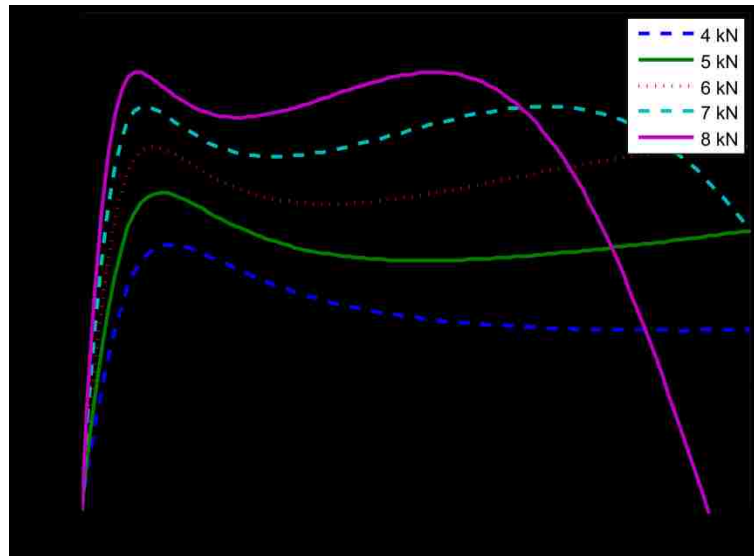


Figure 3.2: Behaviour of Magic Formula Tire Model

### 3.3 Equivalent Roll Stiffness Model

The Equivalent Roll Stiffness (ERS) model is developed from the lumped mass model by treating the front and rear suspensions as rigid axles connected to the body by revolute joints [5]. The model also includes yaw effects as a result of steer inputs from the driver. The ERS model has been proven successful in implementation for variable torque distribution control in [22] [40]. The inclusion of lateral effects in the vehicle dynamics



model results in eight degrees of freedom: longitudinal translation, lateral translation, yaw rotation, roll rotation, and the four rotations of the wheels.



Figure 3.3: Equivalent Role Stiffness Model

Despite the minimum requirements of longitudinal vehicle dynamics isolation for HEV applications, the Equivalent Roll Stiffness model allows for some expansion of the desired simulations. The developed controls may now be tested for sensitivity in cornering as well as emergency maneuvers through the ERS model. The resulting equations of motion can be written according to Newton's second law as [40] [27] [22]:

$$\sum F_x = m(\ddot{x} - \dot{y}\dot{\psi}) + (m_r l_r - m_f l_f)\dot{\psi}^2 - 2m_s h\dot{\psi}\dot{\phi} \quad (3.6)$$

$$\sum F_y = m(\ddot{y} - \dot{x}\dot{\psi}) + (m_f l_f - m_r l_r)\ddot{\psi} - m_s h\ddot{\phi} \quad (3.7)$$

$$\sum M_z = I_{zz}\ddot{\psi} + (m_f l_f - m_r l_r)\dot{x}\dot{\psi} + (m_f l_f - m_r l_r)\dot{y} - I_{xz}\ddot{\phi} \quad (3.8)$$

$$\sum M_x = I_{xx}\ddot{\phi} - I_{xz}\ddot{\psi} \quad (3.9)$$

$$\sum F_x = m\ddot{x} = F_{x,fl} + F_{x,fr} + F_{x,rl} + F_{x,rr} + F_{x,wind} + F_{x,g} + F_r \quad (3.10)$$

$$\sum F_y = m\ddot{y} = F_{y,fl} + F_{y,fr} + F_{y,rl} + F_{y,rr} + F_{y,wind} + F_{y,g} \quad (3.11)$$

$$\sum M_z = l_f(F_{y,fl} + F_{y,fr}) - l_r(F_{y,rl} + F_{y,rr}) - \frac{t}{2}(F_{x,rr} + F_{x,fr} - F_{x,rl} - F_{x,fl}) \quad (3.12)$$

$$\sum M_x = (m_s g h - K_s)\varphi - C_s \dot{\varphi} - m_s h(\ddot{y} + \dot{x}\dot{\psi}) \quad (3.13)$$

The estimation of the roll stiffness for the ERS model is done by separately analyzing the roll stiffness,  $K_s$ , and roll damping,  $C_s$ , of the front and rear axle. The estimation of roll damping is obtained by assuming equivalent linear damping and using the positions of the dampers relative to the roll centers to calculate the required coefficients. The estimation of the roll stiffness is done in a similar manner, although contributions of the anti-roll bars must also be included. To further understand the developed ERS model, examination of its subsystems will be conducted in the following sections.

### 3.3.1 Driver Behaviour

The ERS driver model contains three control variables: throttle, brake and steer angle. The throttle is a closed loop PID controller set for vehicle speed correction. A control gain for driver aggressiveness may also be selected.

The steer angle can be calculated from a set of five different functions: no steer, steady steer, double lane change, sinusoid, increasing sinusoid, or ramp. All steer functions contain an initializing time delay and a final time delay [40].

### 3.3.2 Powertrain and Driveline

The ERS powertrain is modeled as a quasi-static engine efficiency map with idle and redline limitation parameters. The engine is coupled to a non-linear torque converter, modeled by a fourth order polynomial, and an automatic transmission. The model allows for flexible powertrain configurations including: front wheel drive, rear wheel drive, and all wheel drive. The differential and gear efficiencies are also built-in to the powertrain

and driveline subsystem. Operating efficiency is calculated as a ratio of power out to fuel power utilized. All engine thermal effects are neglected in the ERS model [40].

### 3.3.3 Hydraulic Braking

The ERS model employs a classical hydraulic braking system to decelerate the vehicle. The braking torque is generated through friction between the pads and rotors and is modeled as [5]:

$$B_T = n\mu_b p_b A_b R_d \quad (3.14)$$

Where  $n$  is the number of friction surfaces,  $\mu_b$  is the coefficient of friction between the pads and the rotor,  $p_b$  is the brake pressure,  $A_b$  is the brake piston area, and  $R_d$  is the radius to the center of the pad. The brake pressure is modulated through a close looped feedback controller set for speed correction. Thermal effects of the braking system are neglected.

## 3.4 Simulation

Once the set of ordinary differential equations that represent the system have been developed, the ODEs must then be rewritten into first order form for numerical integration. The program chosen for the numerical integration of the vehicle model is MATLAB®. MATLAB contains several ODE solvers suitable for systems of differential equations. The ODE45 routine is an explicit Runge-Kutta (4,5) formula with moderate accuracy requiring only the solution at the preceding time step, making it suitable for the given vehicle model. Numerical stiffness may hinder simulation time of this solver if not considered; however, this is not expected to occur in the present study.

### 3.5 Validation Results

Preceding the hybridization of the ERS model, validity of the model must be established. Due to the longitudinal nature of the simulations, the ERS model will be validated using four primary tests: longitudinal acceleration, longitudinal braking, highway fuel consumption, and city fuel consumption. The tests will be conducted using a model of a stock Chrysler Pacifica. The parameters of the Pacifica can be seen in Table 3.2.

<b>Item</b>	<b>Value</b>
Vehicle mass	2299 kg
Aerodynamic drag coefficient	0.355
Frontal Area	2.84 m <sup>2</sup>
Effective rolling radius	0.432 m
Distance from center of gravity to front axle	1.3293 m
Distance from center of gravity to rear axle	1.6247 m
Height of center of gravity	0.644 m
Automatic transmission ratios	2.84, 1.57, 1, 0.69

*Table 3.2: Stock Chrysler Pacifica Parameters*

### 3.5.1 Acceleration

To evaluate the accuracy of the ERS model, the stock Pacifica configuration will be modeled and tested in a drag strip acceleration simulation. The results of the ERS acceleration test are seen in Figure 3.4.

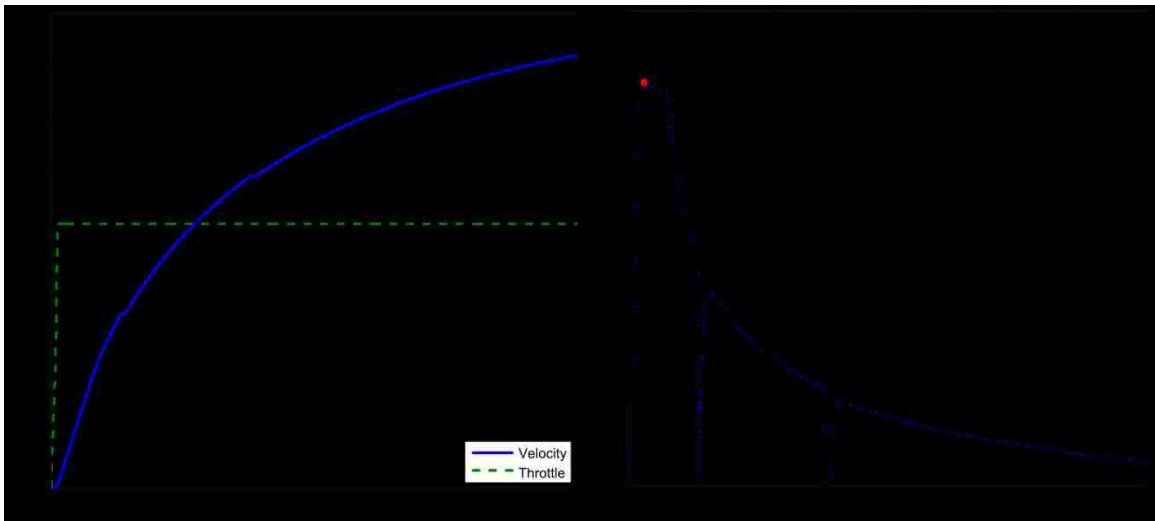


Figure 3.4: ERS Acceleration

Figure 3.4 shows the velocity and acceleration time history of the ERS drag strip acceleration simulation. Close examination of the results shows transmission gear shifts at 5 and 13.5 seconds. Table 3.3 lists the corresponding acceleration times for the Pacifica from an empirical test. Correlation of the times from Table 3.3 to the times found by the ERS model will prove validity in acceleration.

Acceleration	Time (seconds)	ERS Time (seconds)	Relative Error (%)
0-30 mph	3.1	3.18	2.54
0-40 mph	4.7	4.51	4.12
0-50 mph	6.8	6.59	3.13
0-60 mph	9.3	8.94	3.94

0-70 mph	12.6	11.94	5.37
0-80 mph	16.4	16.47	0.42
0-90 mph	22.0	22.37	1.66
0-100 mph	29.6	31.68	6.78

Table 3.3: ERS Acceleration

The results from the ERS model show a correlation coefficient of 0.998. Relative errors are calculated and found to be less than 10% during all operational speeds. The relative errors are a result of many factors including: model inaccuracies, parameter estimations, and lack of experimental data (i.e. temperature, wind conditions, road surface, etc.). The correlation of the results with empirical test data has proven the ERS model valid in acceleration.

### 3.5.2 Braking

To evaluate the accuracy of the ERS model, the stock Pacifica configuration will be modeled and tested in a braking simulation. The results of the ERS braking test are seen in Figure 3.5.

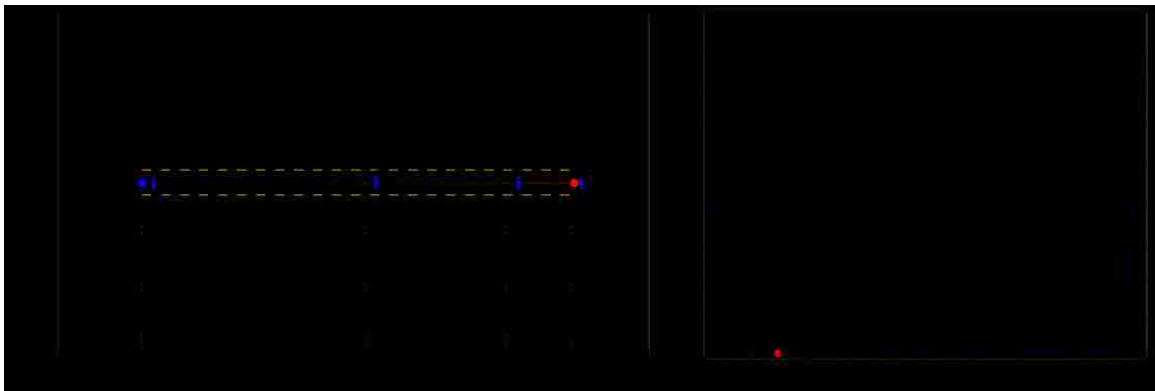


Figure 3.5: ERS Braking

Figure 3.5 shows the vehicle position and acceleration time history for the braking event. Table 3.4 lists the corresponding braking distance for the Pacifica from an empirical test. Correlation of the distance from Table 3.4 to the distance found by the ERS model will prove validity in braking.

<b>Braking</b>	<b>Distance</b>	<b>ERS Distance</b>
70-0 mph (112.6 kph)	182ft (55.4 m)	171ft (52.1 m)

*Table 3.4: ERS Braking*

The results from the ERS model show a stopping distance of 52.1 m in 3.38s. Therefore, the ERS model out performs the empirical test in braking. The main factors resulting in the improved braking performance are: the virtual ABS, lack of engine torque, and model inaccuracies. The relative error is found to be 6%, which is within the expectable range; therefore, the ERS model has proven valid under braking.

### **3.5.3 Highway Fuel Consumption**

To evaluate the accuracy of the ERS powertrain model, the stock Pacifica configuration will be modeled and tested for highway fuel consumption. A varying throttle with average speed equivalent to the EPA highway test of 21.55 m/s will be used. The results of the ERS highway fuel consumption simulation are seen in Figure 3.6.

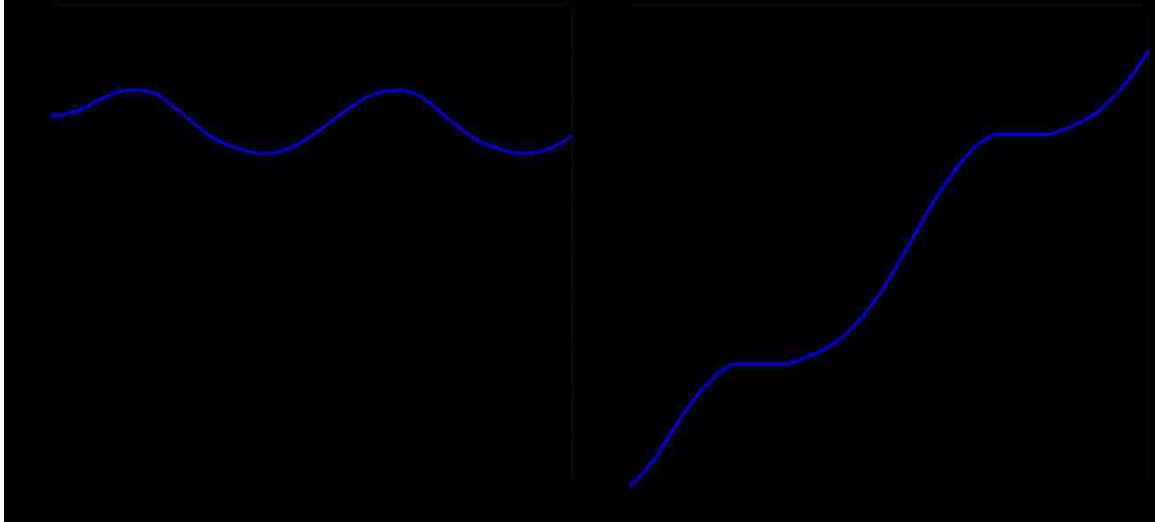


Figure 3.6: ERS Highway Fuel Consumption

Table 3.5 lists the corresponding advertised highway driving fuel consumption for the Pacifica. Correlation of the fuel consumption listed in Table 3.5 to the fuel consumption found by the ERS model will prove validity in highway fuel consumption.

Driving Condition	Fuel Consumption	ERS Fuel Consumption
Highway Driving	22 mpg (10.7 L/100km)	20.6 mpg (11.4 L/100km)

Table 3.5: ERS Highway Fuel Consumption

The ERS model displaced significantly more fuel than the listed highway fuel consumption. This is a result of inaccuracies in the engine fuel map as well as an over estimation in the advertised fuel consumption. Although the difference is significant, the ERS highway fuel consumption numbers will be taken as the benchmark for highway fuel consumption and improvement through hybridization.

### 3.5.4 City Fuel Consumption

To evaluate the accuracy of the ERS powertrain model, the stock Pacifica configuration will be modeled and tested for city fuel consumption. A varying throttle with an average



speed equivalent to the EPA city driving test of 8.75 m/s will be used. The results of the ERS city fuel consumption simulation are seen in Figure 3.6.

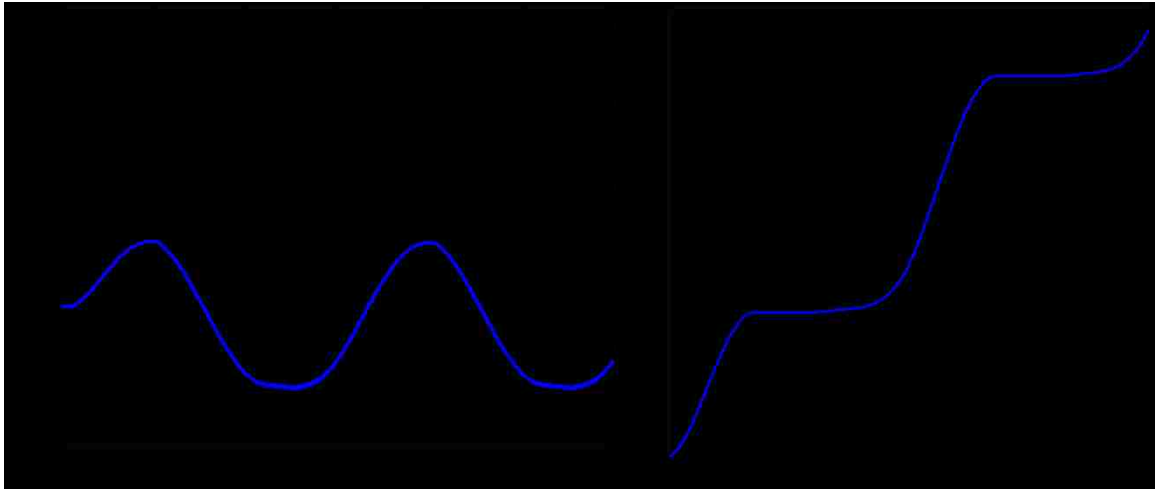


Figure 3.7: ERS City Fuel Consumption

Table 3.6 lists the corresponding advertised city driving fuel consumption for the Pacifica. Correlation of the fuel consumption listed in Table 3.6 to the fuel consumption found by the ERS model will prove validity in city fuel consumption.

Driving Condition	Fuel Consumption	ERS Fuel Consumption
City Driving	17 mpg (13.8 L/100km)	16.5 mpg (14.2 L/100km)

Table 3.6: ERS City Fuel Consumption

The ERS model displaced approximately the equivalent amount of fuel as the listed city fuel consumption. The inaccuracies in the engine fuel map, as well as an over estimation in the advertised city fuel consumption led to the discrepancies in the results of the ERS model. The ERS city fuel consumption numbers will be taken as the benchmark for city fuel consumption and improvement through hybridization.

## **Chapter 4**

# **4 Drive Cycle Analysis**

The accuracy of fuel economy predictions by manufacturers has been questioned for many years. The development of the Environmental Protection Agency's driving cycles has allowed for more valid testing procedures as a means of estimating fuel economy. The EPA city fuel consumption and highway fuel consumption are calculated from the Urban Dynamometer Driving Schedule and the Highway Fuel Economy Test Driving Schedule respectively.

Fuel economy is just one of the many uses of drive cycle simulation. Drive cycles can also be used for driveline design, driveline optimization and design of driveline control. They allow the designer to minimize fuel consumption, component costs and diagnose potential problems before a concept vehicle is developed. Other drive cycles from various countries around the world are also available and provide useful data for vehicle assessment. The following sections will demonstrate the value of drive cycle simulation and evaluate the stock Pacifica's performance using the ERS model under various drive cycles.

### **4.1 Drive Cycles**

A drive cycle is an array of velocity data with a corresponding time frequency. Typically the time frequency is 1Hz and the total time ranges from 500 seconds to 1500 seconds. The most common drive cycles used for evaluation in North America are the Urban Dynamometer Driving Schedule (UDDS) and the EPA Highway Fuel Economy Test

Driving Schedule (HWFET). These particular drive cycles are the EPA standards for city and highway fuel consumption and emissions testing. Other common drive cycles used for performance and emissions evaluation are the US06 or Supplemental FTP Driving Schedule, the Speed Correction 03 Driving Schedule and the New York City Cycle.

Tracking of a drive cycle is a complex task for a dynamic driver model. The driver model acts as a controller to track the reference vehicle velocity. The driver model can either be predictive, looking forward in time, or reactive, looking at the current desired state. The predictive model follows the drive cycle more closely, though the reactive model tends to contain a time lag. All of the simulations in the following sections will use a reactive driver model. The accuracy of the driver model may also be evaluated by the accuracy of the drive cycle trace found within the results.

#### 4.1.1 UDDS

The Urban Dynamometer Driving Schedule, UDDS, was developed to represent city driving conditions. It is currently used for light duty vehicle testing and EPA city fuel consumption. The characteristics of the drive cycle are summarized in Table 4.1.

Drive Cycle	UDDS
Total Time (min)	22.81
Max. Speed (km/h)	91.24
Average Speed (km/h)	31.50
Distance Travelled (km)	11.99
Propulsion Energy (kWh)	
Per cycle	2.9323
Per km	0.2445

---

Braking Energy (kWh)	
Per cycle	1.2946
Per km	0.1079
Ratio of Braking Energy to Propulsion Energy	0.4414

---

*Table 4.1: UDDS Drive Cycle Characteristics*

Table 4.1 shows that the UDDS cycle has a low average speed and a high braking ratio which would suggest high fuel consumption and low engine efficiency. Also notable is the low propulsion energy per km. Low propulsion energy is typical of less aggressive driver behaviour. In order to develop ERS-UDDS benchmarks, the ERS model will attempt to trace the drive cycle in simulation. The results of the ERS-UDDS simulation are seen in Figure 4.1 and Figure 4.2.

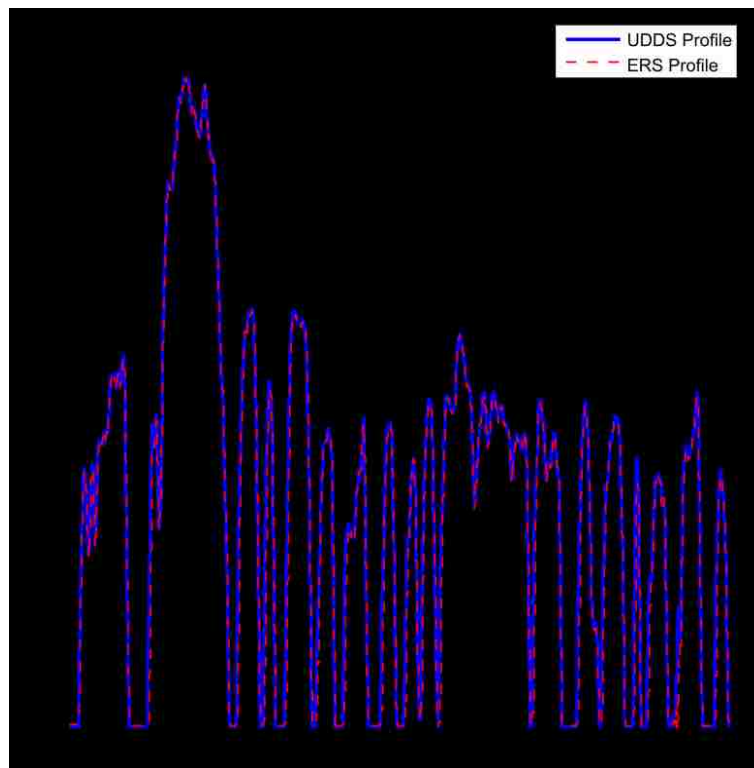


*Figure 4.1: ERS-UDDS Velocity Profile*

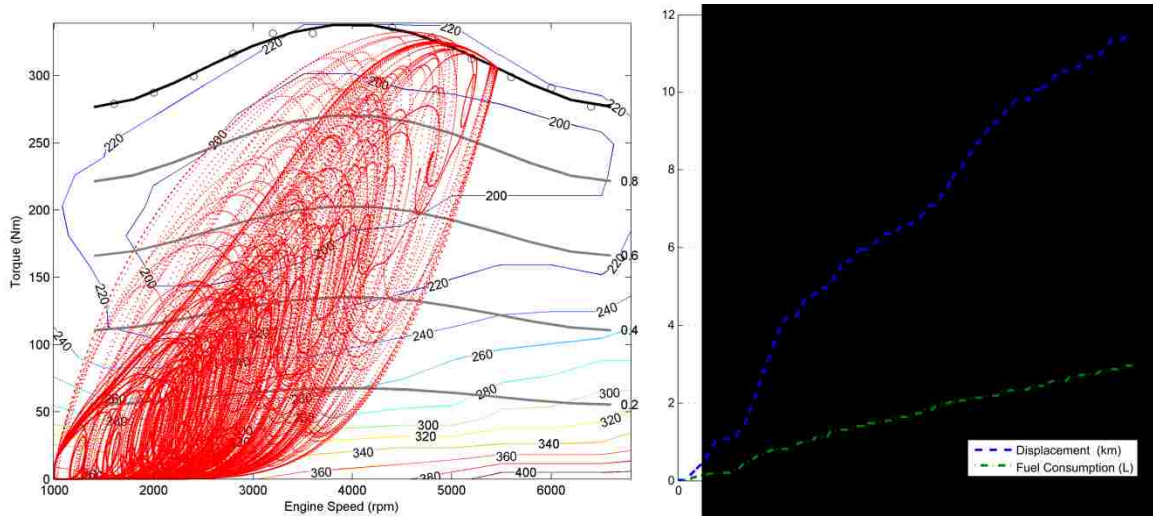


Figure 4.2: ERS-UDDS Engine Trace and Fuel Consumption

Figure 4.2 shows the ERS engine model spends a large portion of time operating at low throttle; therefore, with poor engine efficiency. The maximum velocity variation, average velocity variation, and ERS fuel consumption are summarized in Table 4.2.

Maximum Velocity Variation	Average Velocity Variation	ERS Fuel Consumption
3.48 m/s	0.31 m/s	23.6 L/100km

Table 4.2: ERS-UDDS Performance

The maximum velocity variation is rather large due the reactive driver model, though the average velocity variation shows the ERS model is able to trace the UDDS cycle accurately.

The fuel consumption is calculated to be significantly higher than the estimated value in Section 3.5.4. This is a result of vehicle idling and low speed operation not present in the prior simulation. The results found in this section will now be the benchmark for the ERS-UDDS cycle.

### 4.1.2 HWFET

The EPA Highway Fuel Economy Test Driving Schedule, HWFET, was developed to represent highway driving conditions. It is currently used for light duty vehicle testing and EPA highway fuel consumption. The characteristics of the drive cycle are summarized in Table 4.3.

Drive Cycle	HWFET
Total Time (min)	12.75
Max. Speed (km/h)	96.44
Average Speed (km/h)	77.60
Distance Travelled (km)	16.51
Propulsion Energy (kWh)	
Per cycle	3.5927
Per km	0.2175
Braking Energy (kWh)	
Per cycle	0.3953
Per km	0.0239
Ratio of Braking Energy to Propulsion Energy	0.1100

*Table 4.3: HWFET Drive Cycle Characteristics*

Table 4.3 shows that the HWFET cycle has a high average speed and a low braking ratio which would suggest minimum fuel consumption and high engine efficiency. The low propulsion energy per km is also a characteristic of less aggressive driving. In order to develop ERS-HWFET benchmarks, the ERS model will attempt to trace the drive cycle

in simulation. The results of the ERS-HWFET simulation are seen in Figure 4.3 and Figure 4.4.

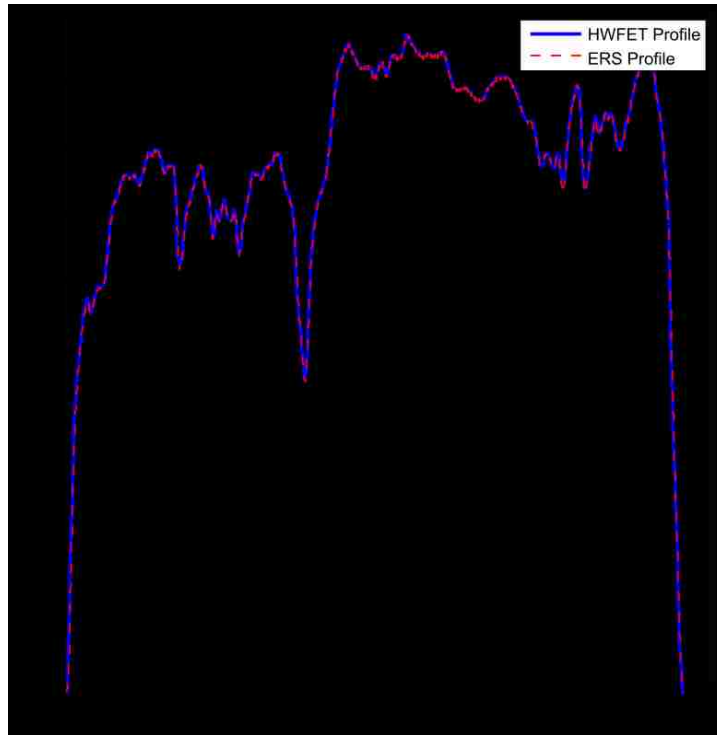


Figure 4.3: ERS-HWFET Velocity Profile

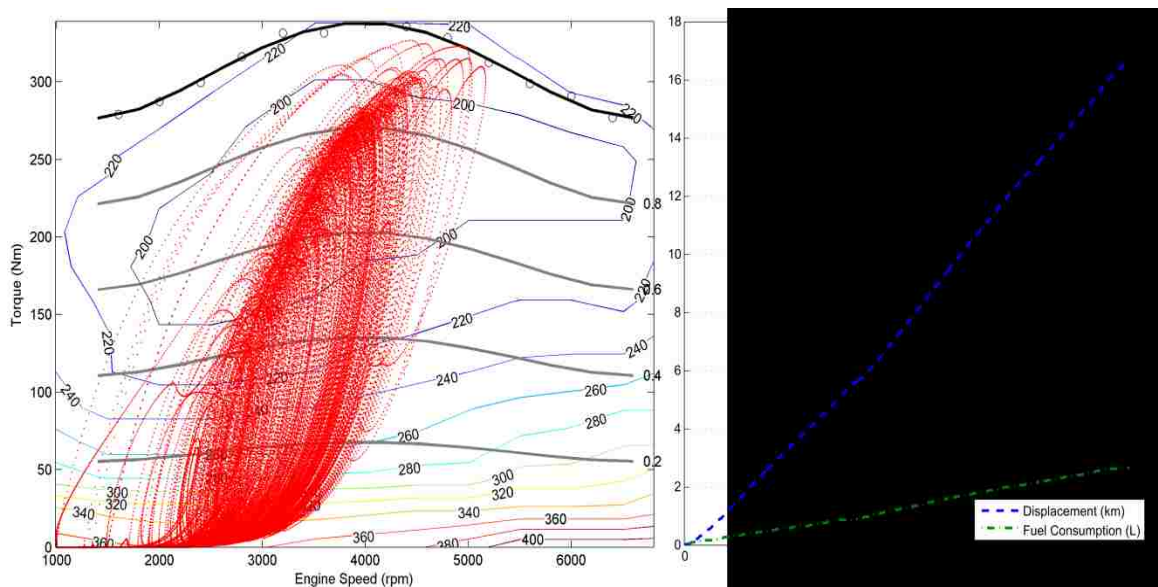


Figure 4.4: ERS-HWFET Engine Trace and Fuel Consumption

Figure 4.4 shows the ERS engine model spends a large portion of time operating in high efficiency regions of the engine map. The maximum velocity variation, average velocity variation, and ERS fuel consumption are summarized in Table 4.4.

<b>Maximum Velocity Variation</b>	<b>Average Velocity Variation</b>	<b>ERS Fuel Consumption</b>
0.81 m/s	0.03 m/s	13.0 L/100km

*Table 4.4: ERS-HWFET Performance*

The maximum velocity variation and the average velocity variation show the ERS model is able to trace the HWFET cycle accurately. The fuel consumption is calculated to be approximately equal to the estimated value in Section 3.5.3. The slight variation is due to more aggressive driver behaviour and an increase in vehicle braking not present in the prior simulation. The results found in this section will now be the benchmark for the ERS-HWFET cycle.

### **4.1.3 US06**

The US06 or Supplemental FTP Driving Schedule was developed to test the exhaust emissions of light duty vehicles at high speeds under aggressive driving conditions. It also attempts to address the shortcomings of the UDDS cycle with rapid speed fluctuations. The characteristics of the US06 drive cycle are summarized in Table 4.5.



<b>Drive Cycle</b>	<b>US06</b>
Total Time (min)	10.00
Max. Speed (km/h)	129.28
Average Speed (km/h)	77.22
Distance Travelled (km)	12.89
Propulsion Energy (kWh)	
Per cycle	4.4994
Per km	0.3489
Braking Energy (kWh)	
Per cycle	1.3797
Per km	0.1070
Ratio of Braking Energy to Propulsion Energy	0.3066

*Table 4.5: US06 Drive Cycle Characteristics*

Table 4.5 shows that the US06 cycle has a high average speed and a moderate braking ratio which would suggest moderate fuel consumption and high engine efficiency. The high propulsion energy per km suggests high driver aggression. In order to develop ERS-US06 benchmarks, the ERS model will attempt to trace the drive cycle in simulation. The results of the ERS-US06 simulation are seen in Figure 4.5 and Figure 4.6.

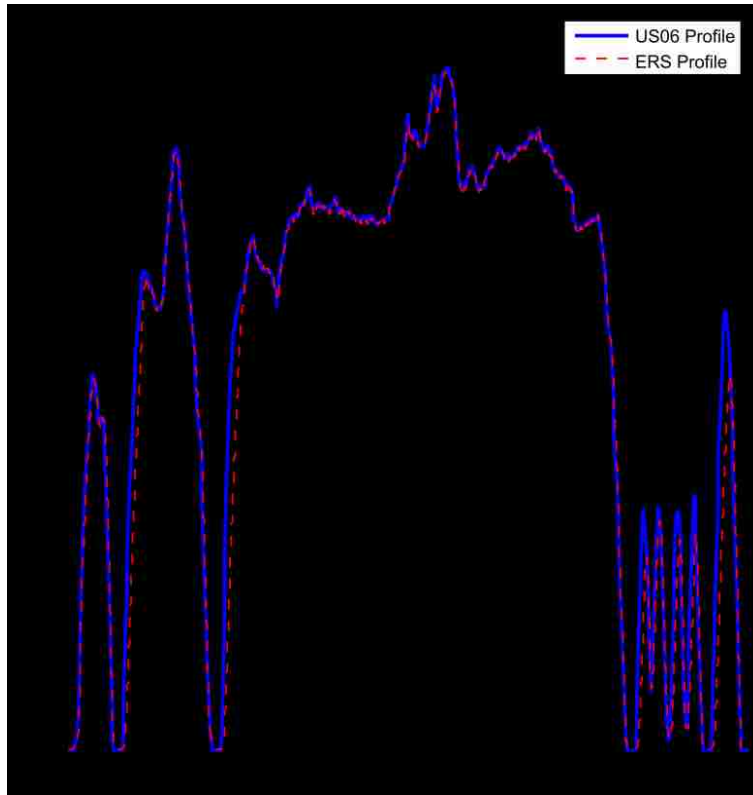


Figure 4.5: ERS-US06 Velocity Profile

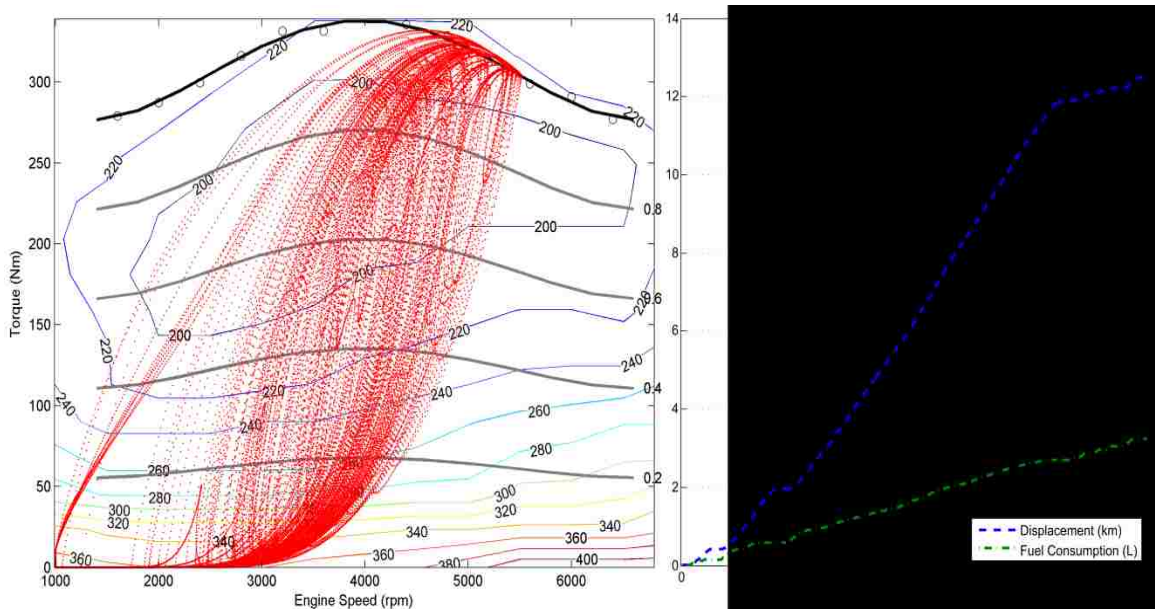


Figure 4.6: ERS-US06 Engine Trace and Fuel Consumption

Figure 4.6 shows the ERS engine model spends a large portion of time at low throttle; therefore, operating with poor engine efficiency. The maximum velocity variation, average velocity variation, and ERS fuel consumption are summarized in Table 4.6.

<b>Maximum Velocity Variation</b>	<b>Average Velocity Variation</b>	<b>ERS Fuel Consumption</b>
10.39 m/s	0.66 m/s	22.8 L/100km

*Table 4.6: ERS-US06 Performance*

The maximum velocity variation is large due to the high driver aggression associated with the US06 drive cycle in conjunction with the reactive driver model. However, the average velocity variation shows the ERS model is able to trace the US06 cycle accurately.

The fuel consumption found is comparable to that found from the ERS-UDDS simulation in Section 4.1.1. This result indicates that the fuel consumption is more sensitive to velocity than driver aggression. Reduced aggression during braking events would have seen the fuel consumption decrease to values nearing the ERS-HWFET benchmark. The results found in this section will now be the benchmark for the ERS-US06 cycle.

#### **4.1.4 SC03**

The Speed Correction 03 Driving Schedule was developed in order to show the engine load and emissions associated with the use of air conditioning units in vehicles. It is currently used for light duty vehicle testing and emissions calculations. The characteristics of the drive cycle are summarized in Table 4.7.

<b>Drive Cycle</b>	<b>SC03</b>
Total Time (min)	10.00
Max. Speed (km/h)	88.22
Average Speed (km/h)	34.52
Distance Travelled (km)	5.76
Propulsion Energy (kWh)	
Per cycle	1.543
Per km	0.2677
Braking Energy (kWh)	
Per cycle	0.7406
Per km	0.1285
Ratio of Braking Energy to Propulsion Energy	0.4799

*Table 4.7: SC03 Drive Cycle Characteristics*

Table 4.7 shows that the SC03 cycle has a low average speed and a high braking ratio which would suggest high fuel consumption and low engine efficiency. In order to develop ERS-SC03 benchmarks, the ERS model will attempt to trace the drive cycle in simulation. The results of the ERS-SC03 simulation are seen in Figure 4.7 and Figure 4.8.

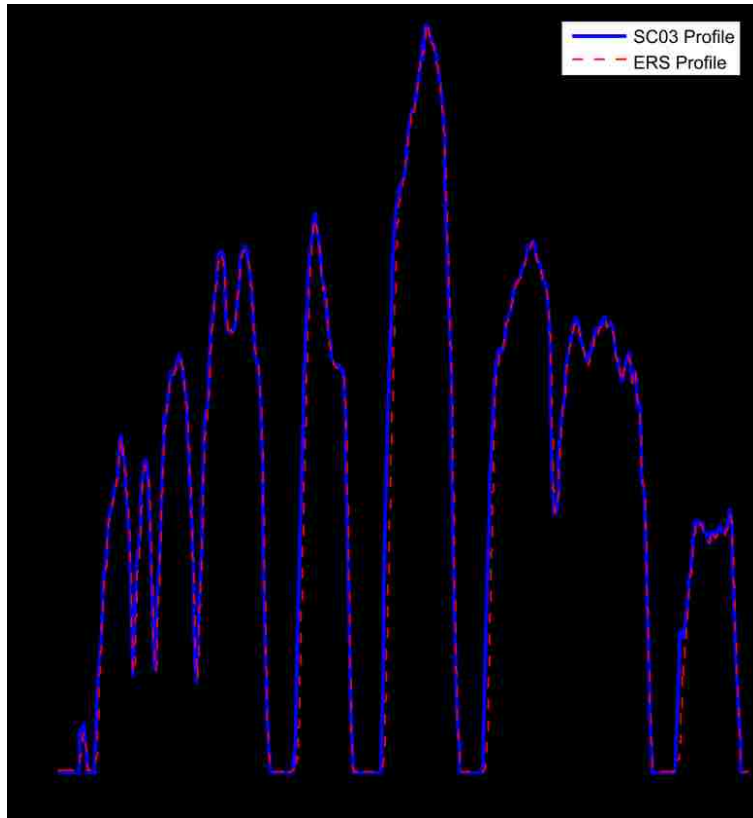


Figure 4.7: ERS-SC03 Velocity Profile

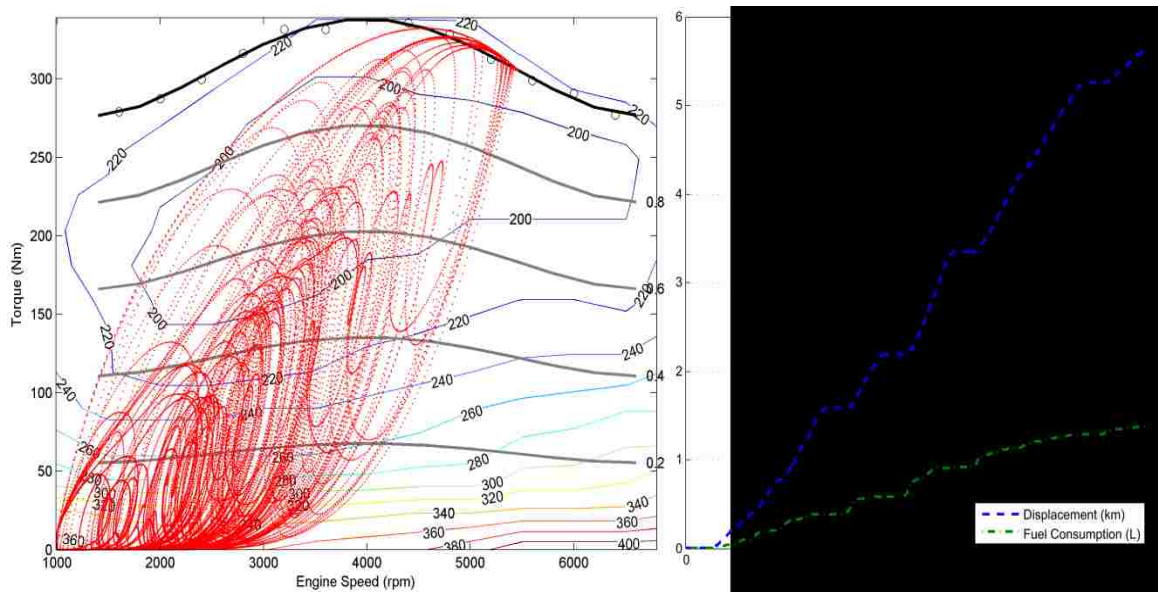


Figure 4.8: ERS-SC03 Engine Trace and Fuel Consumption

Figure 4.8 shows the ERS engine model spends a large portion of time at low throttle; therefore, operating with poor engine efficiency. The maximum velocity variation, average velocity variation and ERS fuel consumption are summarized in Table 4.8.

<b>Maximum Velocity Variation</b>	<b>Average Velocity Variation</b>	<b>ERS Fuel Consumption</b>
6.47 m/s	0.26 m/s	22.2 L/100km

*Table 4.8: ERS-SC03 Performance*

The maximum velocity variation is large due to the high driver aggression associated with the SC03 drive cycle in conjunction with the reactive ERS driver model. However, the average velocity variation shows the ERS model is able to trace the SC03 cycle accurately.

The fuel consumption found is comparable to that found from the ERS-UDDS and ERS-US06 simulations suggesting city driving with moderate to high driver aggression. The results found in this section will now be the benchmark for the ERS-SC03 cycle.

#### **4.1.5 NYCC**

The New York City Cycle, NYCC, was developed for light duty vehicles to simulate low speed urban driving with frequent stops. It is currently used for vehicle testing and emissions regulations. The characteristics of the drive cycle are summarized in Table 4.9.

<b>Drive Cycle</b>	<b>NYCC</b>
Total Time (min)	9.96
Max. Speed (km/h)	44.59
Average Speed (km/h)	11.41

---

Distance Travelled (km)	1.89
Propulsion Energy (kWh)	
Per cycle	0.6098
Per km	0.3210
Braking Energy (kWh)	
Per cycle	0.4081
Per km	0.2148
Ratio of Braking Energy to Propulsion Energy	0.6692

---

*Table 4.9: NYCC Drive Cycle Characteristics*

Table 4.9 shows that the NYCC cycle has a low average speed and a high braking ratio which would suggest high fuel consumption and low engine efficiency. The high propulsion energy per km also suggests aggressive driving. In order to develop ERS-NYCC benchmarks, the ERS model will attempt to trace the drive cycle in simulation. The results of the ERS-NYCC simulation are seen in Figure 4.9 and Figure 4.10.

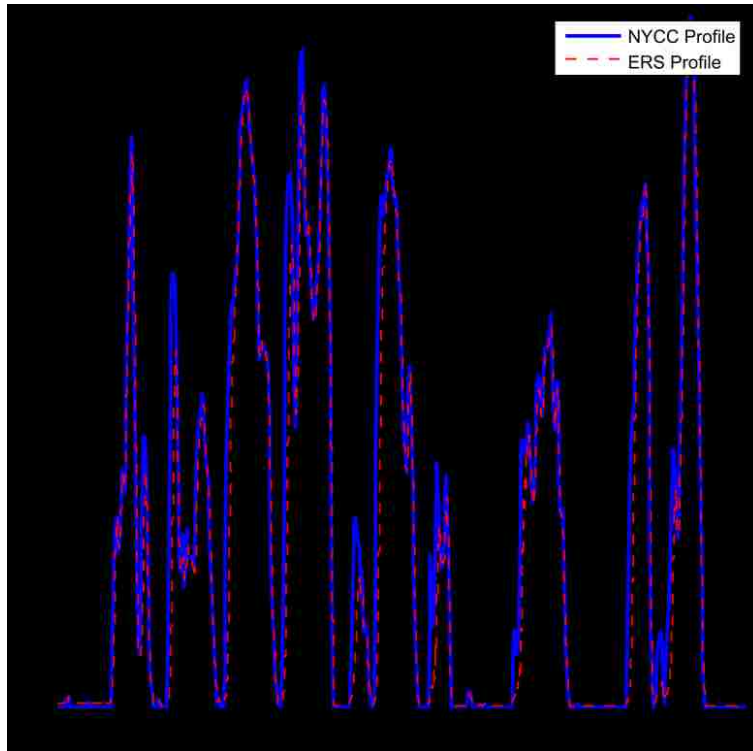


Figure 4.9: ERS-NYCC Velocity Profile

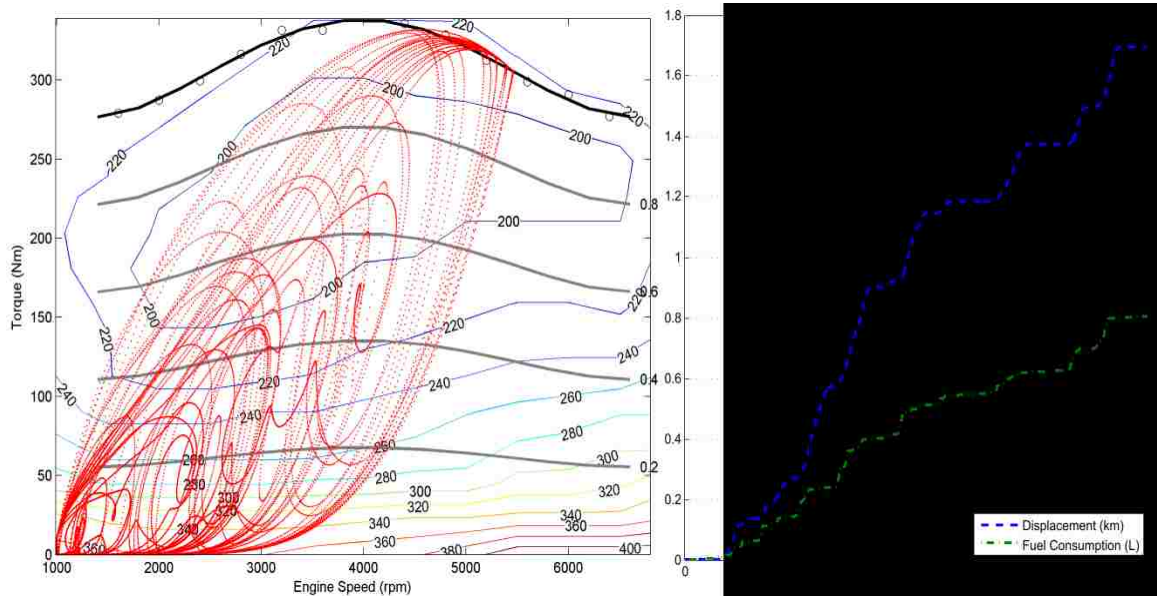


Figure 4.10: ERS-NYCC Engine Trace and Fuel Consumption



Figure 4.10 shows the ERS engine model spends a large portion of time at low throttle; therefore, operating with poor engine efficiency. The maximum velocity variation, average velocity variation, and ERS fuel consumption are summarized in Table 4.10.

<b>Maximum Velocity Variation</b>	<b>Average Velocity Variation</b>	<b>ERS Fuel Consumption</b>
6.32 m/s	0.34 m/s	49.2 L/100km

*Table 4.10: ERS-NYCC Performance*

The maximum velocity variation is large due to the high driver aggression associated with the NYCC in conjunction with the reactive ERS driver model. However, the average velocity variation shows the ERS model is able to trace the NYCC cycle accurately.

The fuel consumption found is drastically larger than the fuel consumption of any other drive cycle. This is a result of the low speed nature of the drive cycle and the frequent vehicle idling. The results found in this section will now be the benchmark for the ERS-NYCC cycle.

## **4.2 ERS Drive Cycle Sensitivity**

The simulation results seen in section 4.1.1 through section 4.1.5 all show some common results characteristic of the ERS model. Of notable importance is the sensitivity of the system to vehicle velocity and driver throttle. The range of vehicle speeds found within a drive cycle will greatly affect the total fuel consumption at the end of the event. If the vehicle velocity is near shift speeds, the fuel consumption will increase due to the decrease in engine rpm during shifting events.

The driver throttle or driver aggressiveness will also play some importance on the total fuel consumption. Due to the nature of the given engine fuel consumption map, increased driver aggression during acceleration events will increase engine efficiency and improve fuel consumption so long as braking aggression is decreased.

The low driver throttle common in all simulations suggests the engine selection is poor if fuel consumption is of importance.

The previous sections have developed ERS benchmarks for various drive cycles. These standards will be used to evaluate the hybrid control schemes in future chapters.

## **Chapter 5**

# **5 Hybrid Electric Drivetrain**

Hybrid electric vehicle architecture results in highly complex designs and configurations. The overall objective of the hybrid electric vehicle will determine which drivetrain configuration is optimal. Once the topology has been chosen, component selection must be made in order to maintain performance and predictability when compared to conventional vehicles. This chapter will focus on the methodology of component selection and evaluate the ERS model operating as an EV.

### **5.1 Hybrid Configuration**

As a result of limitations on the hybrid conversion project, the hybrid configuration was predetermined. The stock Pacifica is a FWD vehicle; therefore, the electric driveline was incorporated onto the rear wheels. To avoid extremely complex configurations, the electric driveline is assumed to act independently on the rear wheels and the mechanical driveline to act independently on the front wheels. This is a parallel configuration in which either driveline can provide propulsion or braking forces. Due to the project requirements of developing a plug-in type hybrid electric vehicle, each independent drivetrain must be able to provide equivalent performance. The resulting configuration can be seen Figure 5.1 below.

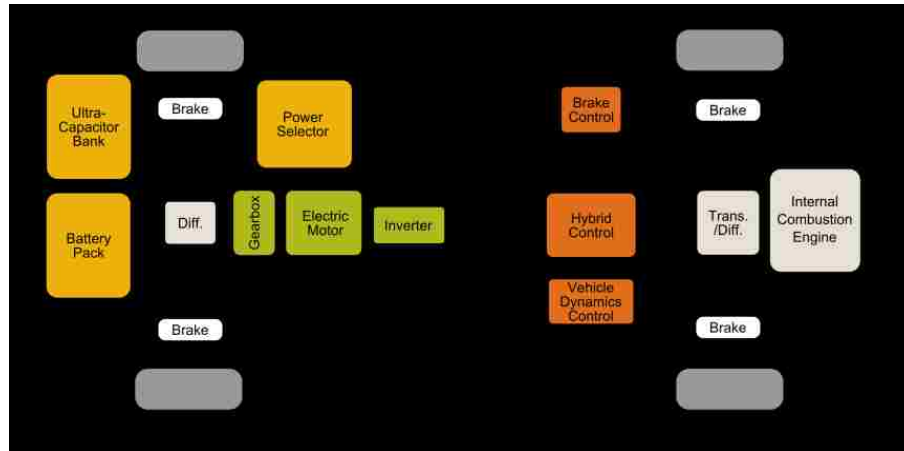


Figure 5.1: Hybrid Electric Vehicle Configuration

The advantages of such a configuration are: simplicity, ability to modulate torque between the front and rear axles, ease of implementation, and complete independence of the driveline. The main disadvantages for this configuration are: the lack of electric motor on the front wheels for maximized torque regeneration, no direct connection between the engine and the generator, and no lateral torque vectoring. The existing ICE drivetrain will be referred to as the mechanical driveline and the integrated electric components will be referred to as the electric driveline. The component selection of the specified electric drivetrain can be made autonomously from the mechanical driveline due to the system independence. The following sections will outline the methodology in component selection.

## 5.2 Energy Source

Advancements in technology have resulted in particularly energy dense batteries appropriate for hybrid electric vehicle applications. Though batteries with very high performance are available, a balance between performance and cost must be met. Of the battery parameters available, two specific design parameters of the battery are of interest: capacity and power. The battery capacity will determine the all electric range of the vehicle, whereas the power will determine the vehicle's maximum speed in EV mode.

The selection of the battery power is dependent on the motor power and will be discussed in the electric motor selection section.

### 5.2.1 Battery Capacity

As set out by the AUTO21 proposal, the PHEV design should result in an all electric range of 40 miles, also known as a PHEV40. Therefore, after the vehicle has travelled 40 miles, the SOC of the batteries should be minimal, at which time the charge sustaining vehicle strategy is implemented. To approximate the battery capacity needed for a PHEV40, a quasi-static backward calculating model is created. The energy flow diagram of the range simulator is seen below.



*Figure 5.2: Quasi-static Energy Flow Simulator*

Efficiencies of the batteries, motor and gear system are approximated through manufacturers' data. The effective mass of the vehicle is calculated based upon the addition of battery and motor mass as well as inertial components of the wheels, engine, and gears. The state of charge for a battery with a capacity of 35Ah is plotted against distance in Figure 5.3.

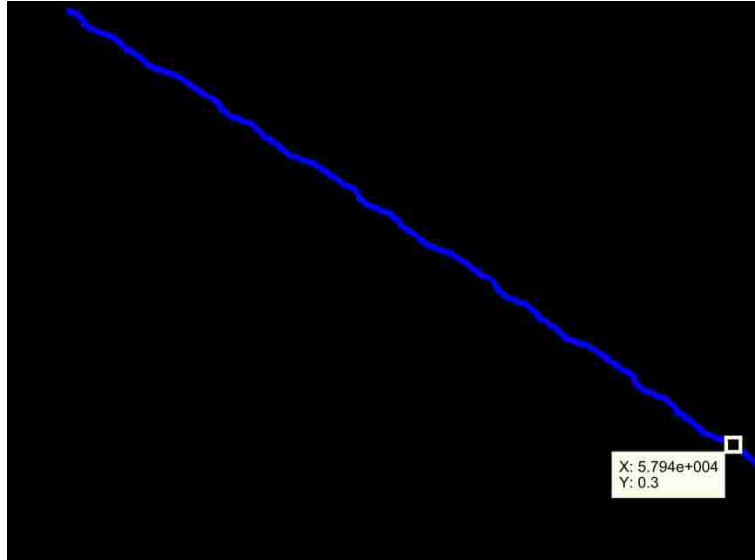


Figure 5.3: 35Ah All Electric Range Simulation

The reduction of weight, addition of a power source and optimization of regenerative braking may increase the AER. A battery with a capacity of 35Ah will be used as the original estimate for the hybridization of the Pacifica. Although the battery capacity is high, it is attainable in the current market.

### 5.2.2 Battery Model

High precision battery models useful for dynamic simulation contain many non-linearities. In order to accurately model the non-linearities of equilibrium potential, rate dependency, capacity and temperature, experimental data and interpolation techniques are used. The internal resistances in charging and discharging as well as the open circuit voltage are seen as functions of state of charge and cell temperature in Figure 5.4, Figure 5.5, and Figure 5.6 respectively.

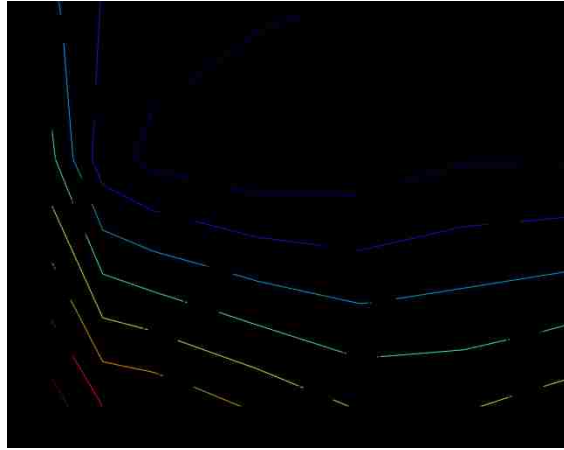


Figure 5.4: Charge Resistance

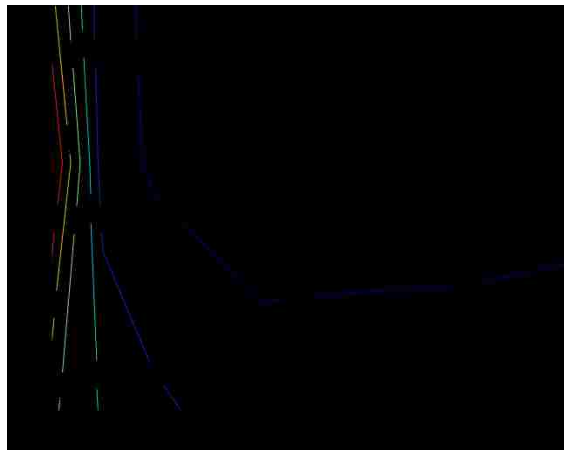


Figure 5.5: Discharge Resistance

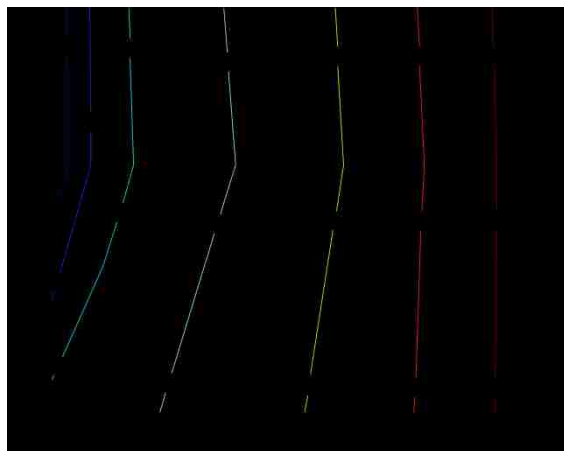


Figure 5.6: Open Circuit Voltage

Although the temperature data may be available, thermal effects of the battery model are assumed negligible due to external cooling. The exclusion of thermal effects helps to simplify the battery model and reduce simulation time when interpolation techniques are used. The simple equivalent circuit will be used to evaluate battery currents. Dynamic effects are ignored due to the incorporation of ultracapacitors in the hybridized power system.

### 5.3 Power Source

Ultracapacitors are highly power dense, making them ideal for regenerative braking and hill climbing of electric vehicles. Modeling of ultracapacitors is done through three parameters: the capacitance, the series resistance, and the dielectric leakage resistance. The following section will expand on these ultracapacitor parameters, as well as define ultracapacitor efficiency.

#### 5.3.1 Ultracapacitor Model

The ultracapacitors are modeled according to the procedure discussed in the literature review, due to its proven accuracy. The electric potential of the ultracapacitor can be obtained as:

$$\frac{dV_C}{dt} = -\left(\frac{i+i_L}{C}\right) \quad (5.1)$$

The integration of the electric potential results in the terminal voltage of the ultracapacitor.

$$V_C = \left[ V_{C0} - \int_0^t \frac{i}{C} e^{t/CR_L} dt \right] e^{-(t/CR_L)} \quad (5.2)$$

Typically the leakage current is very small and can be neglected. The efficiencies of the ultracapacitor in charging and discharging can be calculated from Equation 5.3 and 5.4 respectively.



$$\eta_d = \frac{V_t}{V_c} \quad (5.3)$$

$$\eta_c = \frac{V_c}{V_t} \quad (5.4)$$

Equations 5.3 and 5.4 indicate that the energy loss in the ultracapacitor is due to the presence of an internal resistance. To ensure optimum operating efficiency, the ultracapacitor voltage should be maintained above 60% of its maximum voltage where the relationship remains linear [12].

## 5.4 Traction Motor-Generator

The traction motor must be selected to provide enough power to generate speeds found within the all electric range as well as provide sufficient amounts of regenerative braking. Typically drive cycles may contain velocities of up to 100km/h for extended periods of time; therefore, the motor will be sized according to a continuous speed approximately equal to 100km/h. In order to calculate the necessary motor power, the maximum power criterion under traction condition is evaluated.

$$P(\dot{x} = 100km/h) = (F_{x,wind} + F_r)\dot{x} \quad (5.5)$$

At 100 km/h, approximately 16kW of power is continuously required. To ensure power for adequate regenerative braking and equivalent performance at high and low speeds a motor with 32kW of continuous power is selected. The performance specifications of the traction motor can be seen in Appendix A.

### 5.4.1 Motor Generator Model

Once the motor has been selected, a motor model must be created. Modeling the motor controller and dynamics can be complex and are outside of the spectrum of this study. To model the motor and inverter, a steady state efficiency map is used. The time lag of

the motor is approximated in the dynamic state of motor torque. The efficiency contour of the motor and integrated inverter can be seen in Figure 5.7.

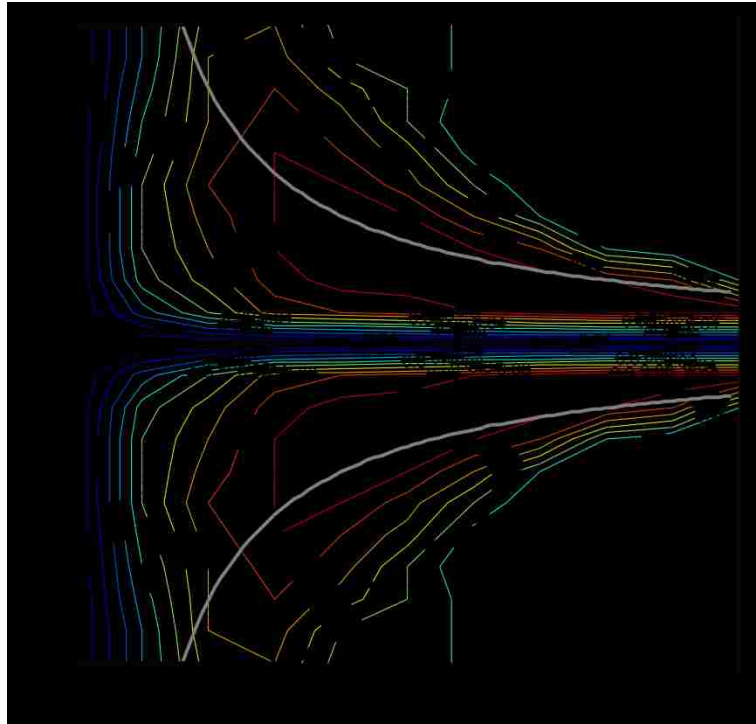


*Figure 5.7: Motor-Generator Efficiency Contour*

The selection of batteries should also allow for 32kW of continuous power to ensure the motor and batteries are compatible. The integration of the electric and mechanical drivelines is the focus of this study and will be developed in the subsequent chapter.

## **5.5 Pacifica EV Performance**

In order to evaluate the electric drivetrain performance, the electric components selected in the previous sections will be integrated into the ERS model. As with the mechanical drivetrain model in ERS, longitudinal simulations of acceleration and braking are of particular interest. Though regenerative braking could be conducted, its optimization will be conducted later in this study. The simulation of highway and city fuel consumption

would prove trivial as the vehicle would be run solely on electric power and would therefore have zero fuel consumption.

### 5.5.1 EV Pacifica Acceleration

To evaluate the Pacifica's acceleration in electric vehicle mode, a drag strip acceleration ERS simulation will be conducted. The proposed electric drivetrain should provide equivalent performance to the acceleration found in section 3.4.1. The results from the acceleration simulation are seen in Figure 5.8.

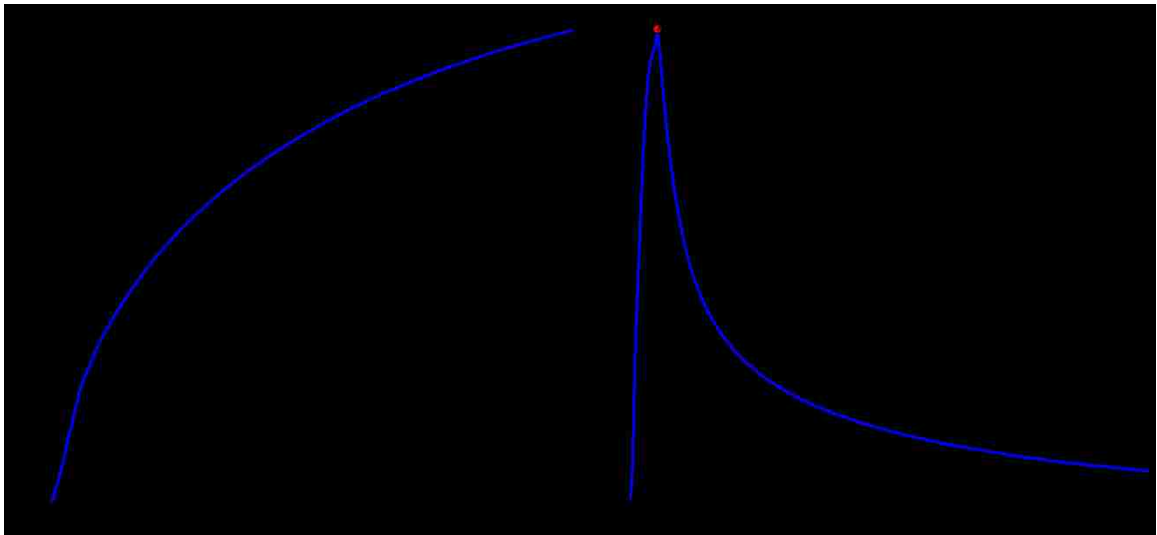


*Figure 5.8: ERS EV Acceleration*

Figure 5.6 shows the velocity and acceleration time history of the ERS model in EV configuration. The characteristics of the electric motor require no gear shifting, increasing driveline efficiency and performance.

The results of the ERS EV acceleration show adequate performance at low speeds and a significant drop off in performance at approximately 70 km/h. Table 5.1 summarizes the differences in acceleration times between the mechanical and electrical drivelines.

<b>Acceleration</b>	<b>Mechanical Driveline</b>	<b>Electric Driveline</b>
0-30 mph (48 km/h)	3.18 seconds	4.42 seconds
0-40 mph (64 km/h)	4.51 seconds	7.35 seconds
0-50 mph (80 km/h)	6.59 seconds	11.57 seconds
0-60 mph (96 km/h)	8.94 seconds	17.78 seconds

*Table 5.1: ERS EV Acceleration*

Due to the low speed nature of drive cycles and the high efficiency of the internal combustion engine at high throttles, the EV acceleration performance is sufficient for the hybrid configuration under consideration.

## Chapter 6

# 6 Hybrid Electric Vehicle Control

The ability of a hybrid electric vehicle to minimize fuel consumption and maximize range is highly dependent upon the energy management control strategy employed. The proposed configuration suggests multiple control strategies to maximize system efficiency. The control systems of interest are the integrated hybrid control, regenerative braking control, and multiple peaking power source control. A schematic of their interaction is seen in Figure 6.1. This chapter focuses on the development of the control systems under investigation.

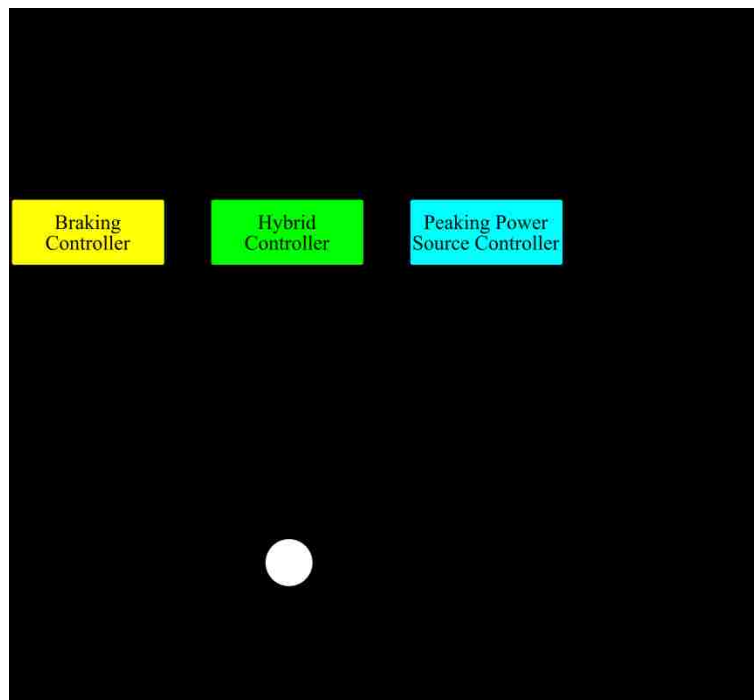


*Figure 6.1: Vehicle Control Systems*

## 6.1 Integrated Hybrid Control Development

The integrated hybrid control modulates the demands on the electric motor and internal combustion engine to ensure optimum efficiency of both systems. The integrated hybrid control is active with positive throttle and passive under braking. The control between mechanical and electrical braking will be discussed in the following section.

As the throttle is pressed a demand for positive torque is requested from the driveline. To ensure predictable vehicle performance, the integrated hybrid controller must match the requested torque with a combination of engine torque and electric motor torque.

$$T_{req} = Throttle \cdot T_{max} = Throttle_{EM} \cdot T_{EM} + Throttle_{ICE} \cdot T_{ICE} \quad (6.1)$$

The objective of the controller is to select the most optimal torque demands from the electric motor and internal combustion engine in order to minimize fuel consumption, providing it satisfies the constraint of Equation 6.1. The trivial solution would suggest that all the requested torque be provided by the electric motor to ensure no fuel consumption. Given prior knowledge of trip distance, this may become the optimal solution. Due to the lack of trip data, maximum brake specific fuel consumption is set as a function of battery state of charge as seen in Equation 6.2.

$$BSFC_{max} = BSFC_{eng,min} (c_1 \cdot SOC_{bat} + c_2 \cdot SOC_{ucap})^{c_3} \quad (6.2)$$

The minimum achievable brake specific fuel consumption of the engine is labeled as  $BSFC_{eng,min}$ , the constants  $c_1$  and  $c_2$  are the respective power ratios of the battery and ultracapacitor, and the constant  $c_3$  is a shape factor which is experimentally determined based upon the desired engine on-off behaviour.

### 6.1.1 ON-OFF Control

The secondary function of the integrated hybrid controller is the on/off switching of the internal combustion engine. Due to the poor fuel efficiency of the ICE at low torque, the ICE is turned off, saving fuel which would be wasted at the idle speed. In order to determine the speed and throttle at which to turn on/off the engine, two preliminary simulations were conducted. The first simulation ran the ERS model at constant throttle with varying velocity as seen in Figure 6.2. The results of the simulation indicate negligible sensitivity of fuel consumption to varying velocity with constant throttle. The second simulation ran the ERS model at constant velocity and varying throttle as seen in Figure 6.3. The results of the simulation show high sensitivity of fuel consumption to driver throttle. The resulting conditions of the on/off control will be evaluated in the following section.

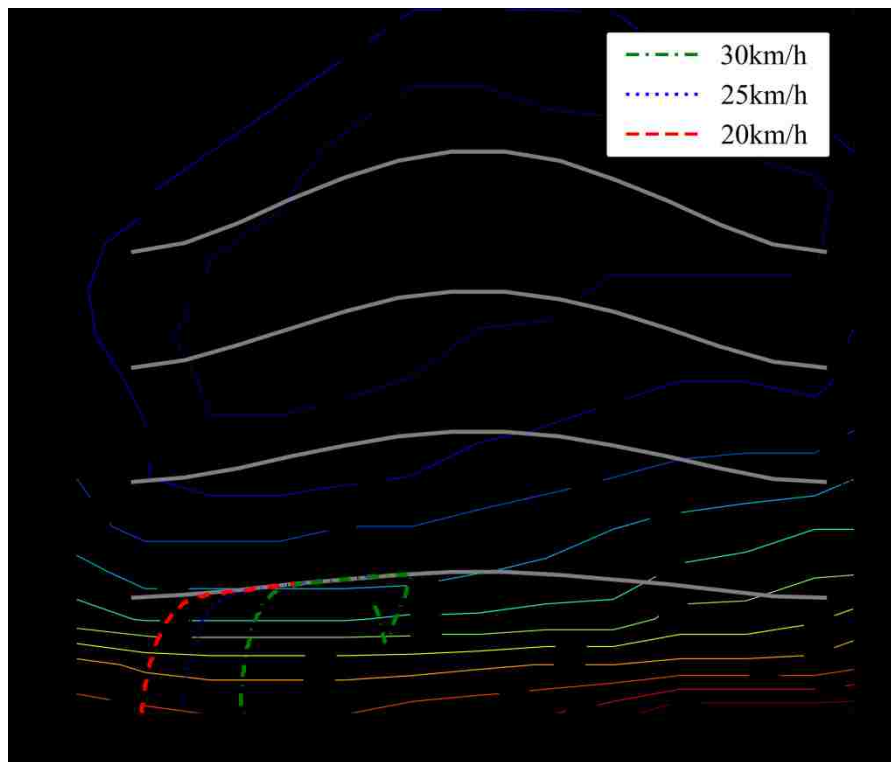


Figure 6.2: Varying Speed Constant Throttle

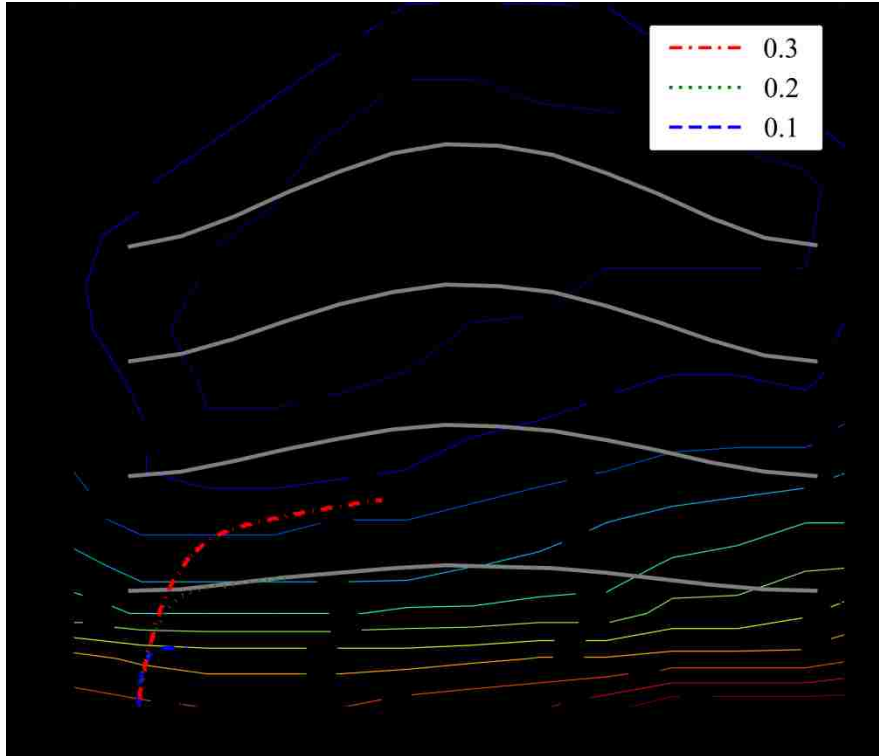


Figure 6.3: Constant Speed Varying Throttle

### 6.1.2 Hybrid Control Evaluation

Prior to hybrid control evaluation, analysis of the driving event in particular must hold some consideration. When analyzing complex systems such as hybrid electric vehicles, the isolation of the control scheme is of utmost priority. The driving events selected for vehicle simulation in the following sections were chosen logically in order to isolate the systems of interest.

The integrated hybrid controller must be developed to contain high sensitivity to battery state of charge. As the state of charge decreases the acceptable internal combustion engine efficiency also decreases. In order to test the integrated hybrid controller, simulations were run with varying SOC as seen in Figure 6.4 and Figure 6.5.



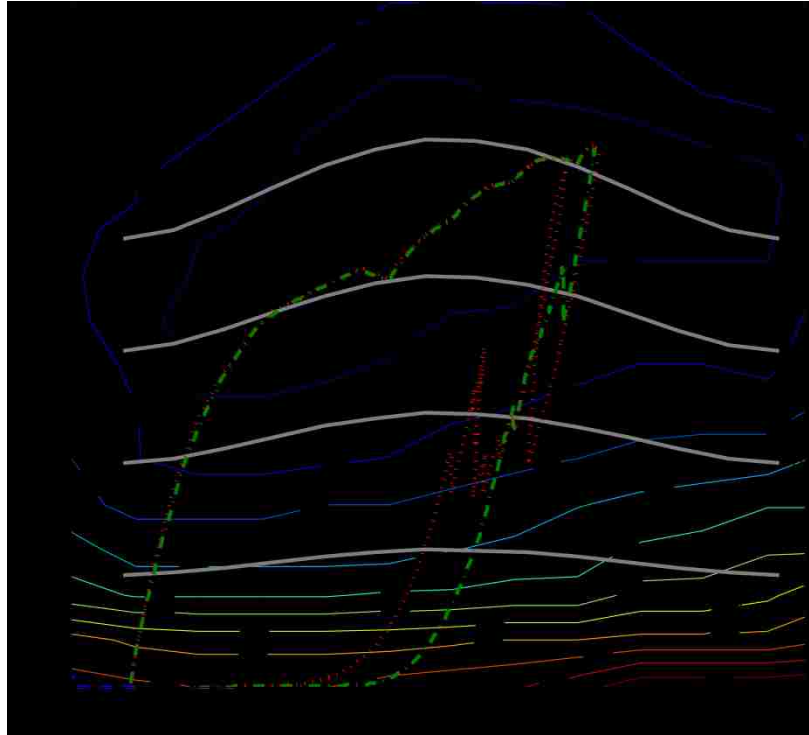


Figure 6.4: Integrated Hybrid Control Engine Trace

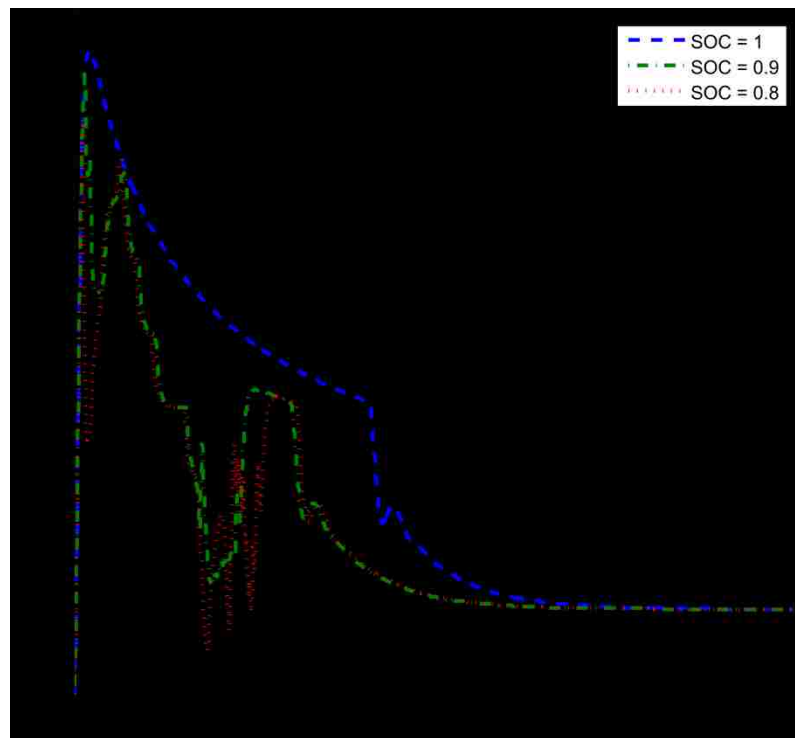


Figure 6.5: Integrated Hybrid Control Electric Motor Torque

The results from Figure 6.4 clearly indicate reduced work from the ICE when the state of charge is high. The torque produced by the electric motor compensates for the remainder of the load requested by the driver that is beyond that acceptable efficiency range of the engine.

As the request for torque and velocity decreases the internal combustion engine efficiency decreases as well. At low speeds and low throttles it is desirable to turn off the engine to save fuel that would be wasted at idle speed. A simulation of constant low vehicle speed is seen in Figure 6.6.

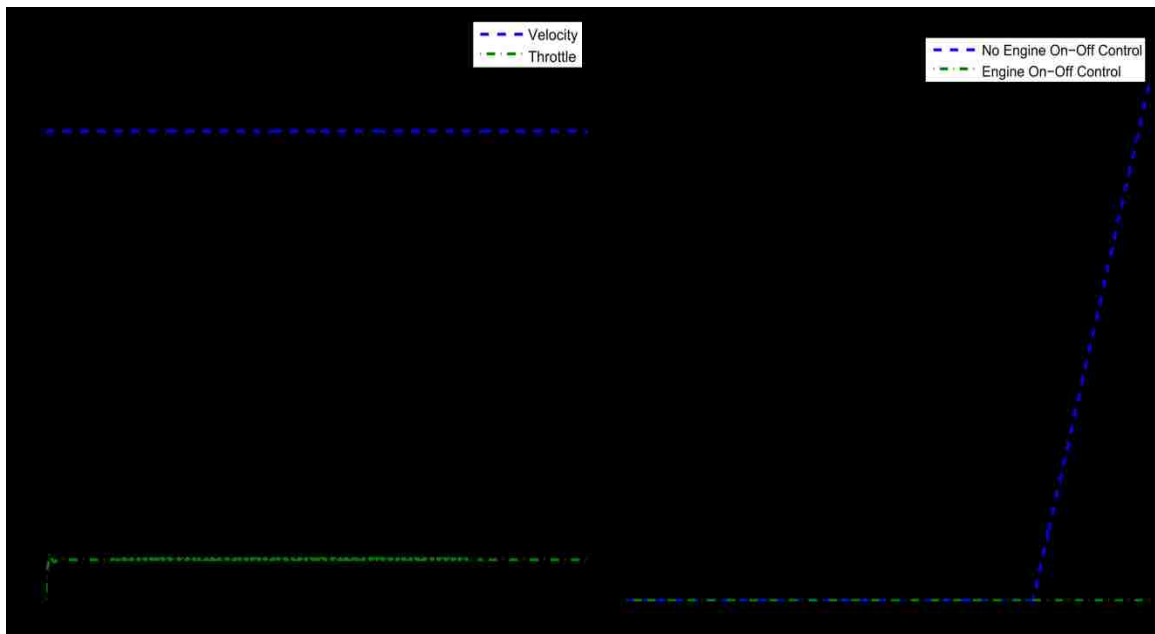


Figure 6.6: Engine On-Off Control

The simulation uses the developed integrated hybrid control to determine the engine on-off strategy. The engine on-off control saves 0.053 L/100km of fuel during the 60 second constant speed event. Due to the low speed nature of drive cycles, the engine on-off control should substantially improve fuel consumption.

## 6.2 Regenerative Braking Optimization

One of the most important reasons for improved efficiency in HEVs is the utilization of regenerative braking. As opposed to the use of hydraulic brakes and dissipating the vehicle's energy through friction as heat, the electric motor is used as a generator converting the vehicle's kinetic energy back into electric energy to recharge the batteries. Braking performance may not be compromised for regenerative purposes; the design must preserve capabilities of quickly reducing vehicle speed and maintaining vehicle stability. In the case of emergency braking or high demand braking, the regenerative braking system typically cannot handle such high torques; therefore, a friction braking system must also be implemented in the design. Analysis of the braking dynamics of a vehicle system will allow for assessment of energy potential.

### 6.2.1 Brake Performance

The objective of the vehicle brake system is to quickly reduce vehicle speed while keeping the vehicle travel directionally stable and controllable under various road conditions. When modeling a vehicle for braking performance, aerodynamic and rolling resistance forces are neglected as they are usually far smaller than the braking forces. Figure 6.7 shows the free body diagram of a vehicle during a braking event.



*Figure 6.7: Free Body Diagram of a Vehicle under Braking*

The application of Newton's second law in the longitudinal directions yields:

$$m\ddot{x} = F_{bf} + F_{br} \quad (6.3)$$

The maximum braking force is limited by the tire-ground adhesion coefficient and is approximately proportional to the normal load on the tire. During braking, the normal load on the tire will vary with deceleration rate; therefore, the braking force should also vary with deceleration. The greater the deceleration demand, the more load is transferred from the rear tires to the front tires. The normal load on the front and rear wheels found from the equilibrium moments about the contacts points can be found from Equations 6.4 and 6.5.

$$W_f = \frac{mg}{L} \left( L_b + h_g \frac{\ddot{x}}{g} \right) \quad (6.4)$$

$$W_r = \frac{mg}{L} \left( L_a - h_g \frac{\ddot{x}}{g} \right) \quad (6.5)$$

To maximize braking, the braking forces must be proportional to their normal loads.

$$\frac{F_{bf}}{F_{br}} = \frac{W_f}{W_r} = \frac{L_b + h_g \cdot \ddot{x}/g}{L_a + h_g \cdot \ddot{x}/g} \quad (6.6)$$

Providing the braking forces are proportional to the load transfer on the tires, the vehicle will achieve its maximum deceleration. The maximum deceleration rate is found from Equation 6.7.

$$|\ddot{x}_{max}|_{\mu} = \frac{F_{bf,max} + F_{br,max}}{m} = \frac{(W_f + W_r)\mu}{m} = g\mu \quad (6.7)$$

Following the ideal braking curve with hydraulic brakes would require a system with complex controls. In traditional braking systems, the braking forces are applied at either a fixed or two fixed proportions to ensure simplicity and vehicle stability. The implication of such a system results in only one particular situation where all tires lock simultaneously. The actual force distribution can be calculated from Equation 6.8.

$$\frac{F_{bf}}{F_{br}} = \frac{\beta}{1-\beta} \quad (6.8)$$

The braking proportion that is distributed to the front wheels is represented by  $\beta$ . The corresponding road adhesive coefficient for the fixed brake proportion is found from Equation 6.9.

$$\mu_0 = \frac{L\beta - L_b}{h_g} \quad (6.9)$$

The normalized ideal braking force distribution curve with fixed brake portioning can be seen in Figure 6.8.

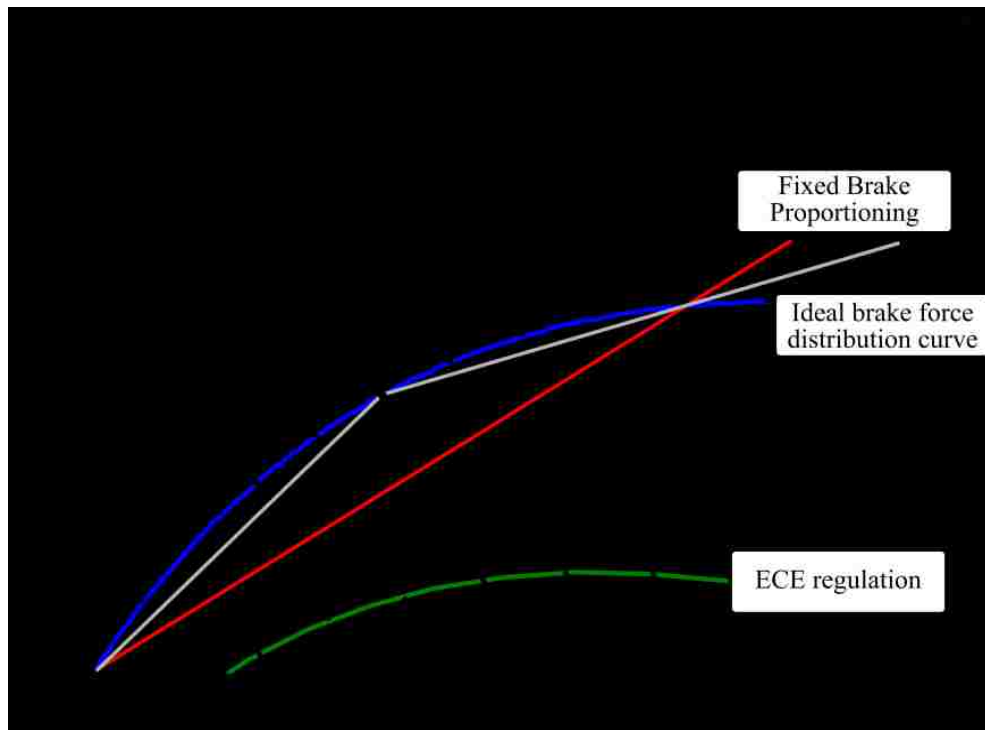


Figure 6.8: Ideal Braking Force Distribution

Therefore, when braking on roads with adhesive coefficient less than  $\mu_0$ , the front wheels will lock first, and when braking on roads with adhesive coefficient more than  $\mu_0$ , the rear wheels will lock first. Locking of the rear wheels first will cause a loss in directional stability. As the wheels are locked, they lose their ability to support lateral forces and as

a result the lateral forces generated at the front tires alone are enough to create a yaw moment. External forces such as side wind, road chamber, or centrifugal force may also contribute to the generated yaw moment. As the motion progresses the moment arm of the vehicle inertia increases until the vehicle reaches  $90^\circ$  and then decreases until the vehicle is completely reversed. An illustration of this type of vehicle behaviour is seen in Figure 6.9.

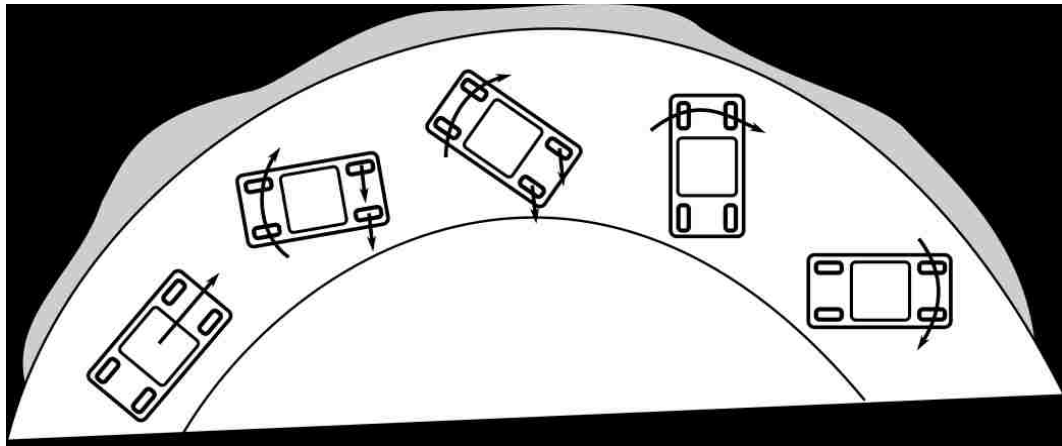


Figure 6.9: Directional Instability due to Rear Wheel Lockup

In the case where the front wheels lock first, the driver loses the ability to steer the vehicle; however, the vehicle remains stable and continues to travel forward until the brake force is released. This is a result of the corrective moment of the vehicle's inertia when lateral movement of the front wheels occurs. It is then evident that the desired case is to have the front wheels lock first if all wheels cannot lock simultaneously. Anti-lock braking system (ABS) attempts to correct this by limiting the braking force to a range of slip which maximizes the braking force while maintaining controllability.

In order to design a braking system, all of the braking events that may occur must be analyzed. The understanding of all the events will not only allow for an increase in braking performance, but also allow for an increase in energy captured during regenerative braking.

When the front wheels are locked first and the rear wheels remain unlocked the forces generated at the wheels are calculated from Equation 6.10 and 6.11.

$$F_{bf} = \frac{mg\mu}{L} \left( L_b + \frac{\ddot{x}}{g} h_g \right) \quad (6.10)$$

$$F_{br} = \frac{L-\mu h_g}{\mu h_g} F_{bf} - \frac{mgL_b}{L} \quad (6.11)$$

Equations 6.10 and 6.11 are used to generate what are known as f-lines. In the reverse case, where the front wheels are unlocked and the rear wheels are locked the equation for the rear braking force becomes:

$$F_{br} = \frac{-\mu h_g}{L+\mu h_g} F_{bf} + \frac{\mu mg L_a}{L+\mu h_g} \quad (6.12)$$

Equation 6.12 is used to generate what are known as r-lines. F-lines and r-lines can be used to analyze any possible braking event with a given fixed brake proportion. As the brakes are applied along the fixed brake proportioning line,  $\beta$ , if the road adhesion coefficient is less than  $\mu_0$ , the front wheels will lock first and the force distribution will move along the f-lines. If the road adhesion coefficient is more than  $\mu_0$ , the rear wheels will lock first and the force distribution will move along the r-lines. The implication is that for a given deceleration, the force distribution can be manipulated as long as it remains along the constant deceleration line [35] [12] [16] [24]. This is the exact effect that may be exploited to increase regenerative braking efficiency.

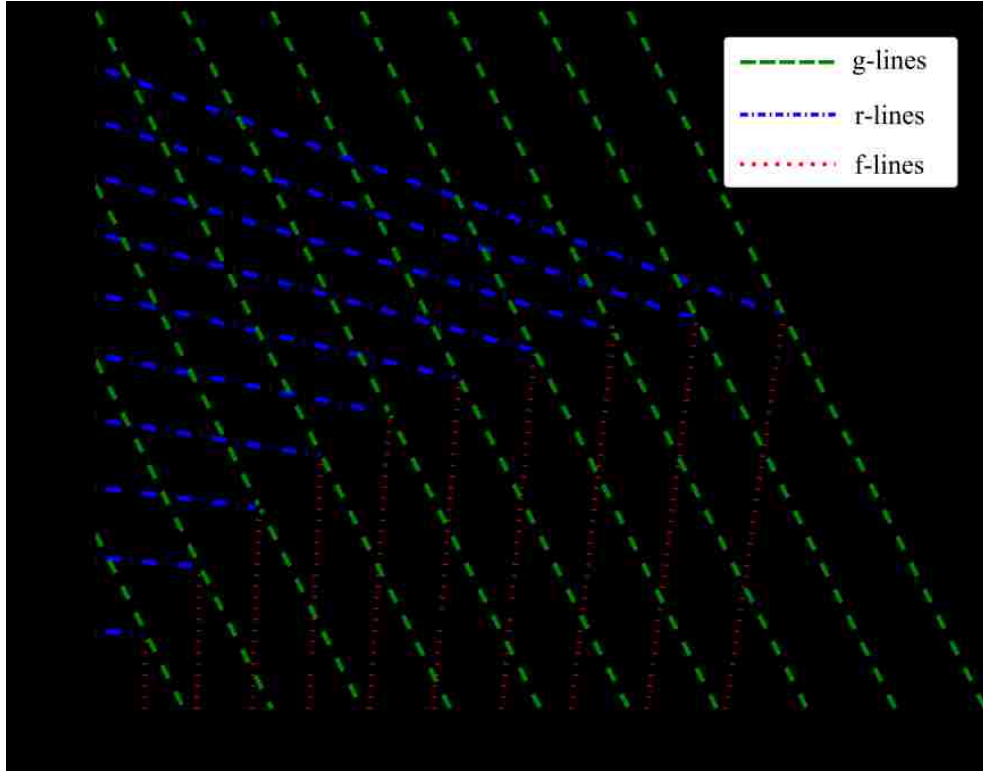


Figure 6.10: Braking Process Analysis

### 6.2.2 Controllable Hybrid Brake System

In the case of HEVs and regenerative braking, individual wheel forces may be controlled in order to achieve maximum energy recuperation. If the electric motor is placed on the front axle, the proportioning should be controlled so that it follows the ECE regulation curve. The ECE regulation curve dictates the minimum braking force on the rear wheels and for passenger cars is calculated from Equation 6.13 [12].

$$\frac{\dot{x}}{g} \geq 0.1 + 0.85(\mu - 0.2) \quad (6.13)$$

If the electric motor is placed on the rear axle, the proportioning needs to maximize the force generated by the rear tires near the onset of rear wheel lockup. In the case where electric motors are placed on both axles the control will maximize regenerative braking based upon motor efficiency. Due to motor placement on the rear axle, the objective of



this particular control strategy aims to distribute more braking force to the rear wheels, under the condition of the rear wheels never locking prior to the front wheels on a road with any adhesive coefficient.

As the vehicle brakes with an acceleration of  $\ddot{x}$  on a road with adhesive coefficient  $\mu$ , and  $\ddot{x}/g < \mu$ , the braking forces on the front and rear wheels can be subjectively applied as long as the total braking forces meets the requirements of Equation 6.3. To maintain braking performance, it is required that no wheel be locked and that the minimum braking force on the rear wheels meet the requirements of the ECE regulation curve. As a result of maximizing rear wheel regenerative force the condition of the ECE regulation curve will always be met.

The deceleration rate is calculated through the driver model as a linear function of vehicle speed and desired speed. The optimized braking process can be seen in Figure 6.11. The maximum braking torque available from the electric motor is determined as a function of vehicle speed and gear ratio. If the electric motor can produce enough braking force to decelerate the vehicle at the desired speed, the electric motor is used alone (a). If the braking force required is larger than the available regenerative force, the maximum regenerative force is produced and the remainder of the braking force is calculated from Equation 6.3 (b). The front braking force can be increased until the onset of rear wheel lockup which can be calculated from Equation 6.12 (c). To further increase deceleration, the regenerative force must be reduced to allow for an increase in front braking force (d).

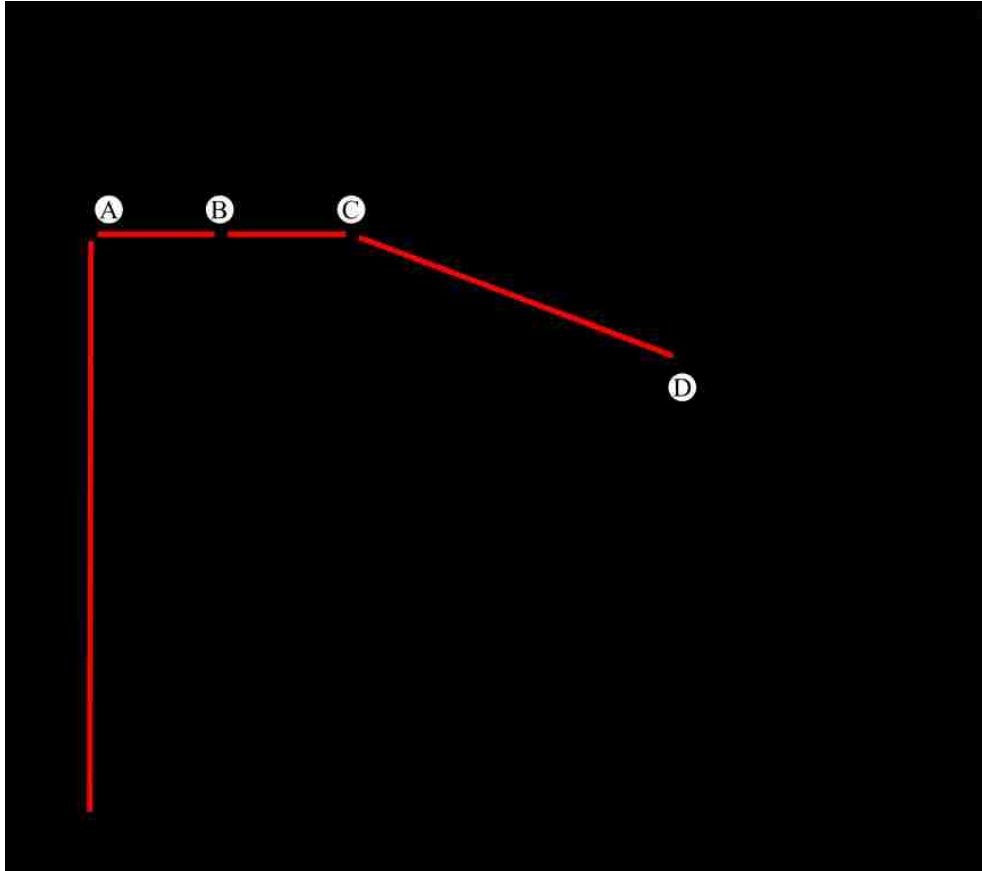


Figure 6.11: Regenerative Braking Optimization Process

### 6.2.3 Regenerative Braking Evaluation

The developed regenerative braking control must maintain braking performance while recovering as much kinetic energy as possible. In order to evaluate the braking performance, the vehicle velocity will be compared between regenerative control on and regenerative control off cases. The recovered energy during the braking event will be compared using the battery state of charge for the on and off cases. The results of the hybrid electric vehicle braking tests at 0.3g, 0.5g and 0.7g can be seen in Figure 6.12, Figure 6.13 and Figure 6.14 respectively.

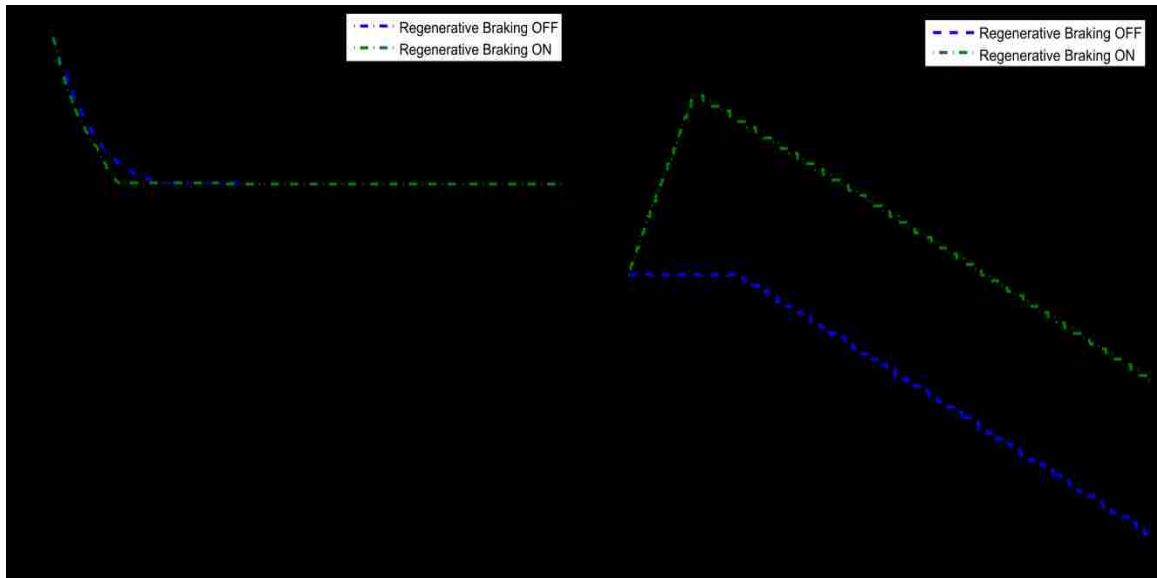


Figure 6.12: Regenerative Braking On-Off 0.3g

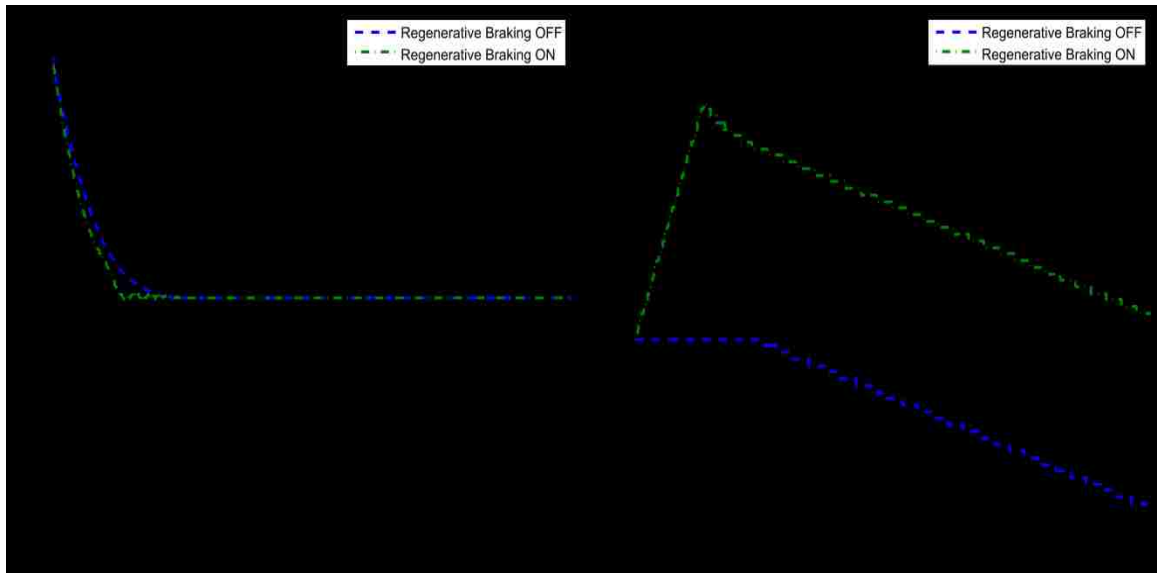


Figure 6.13: Regenerative Braking On-Off 0.5g

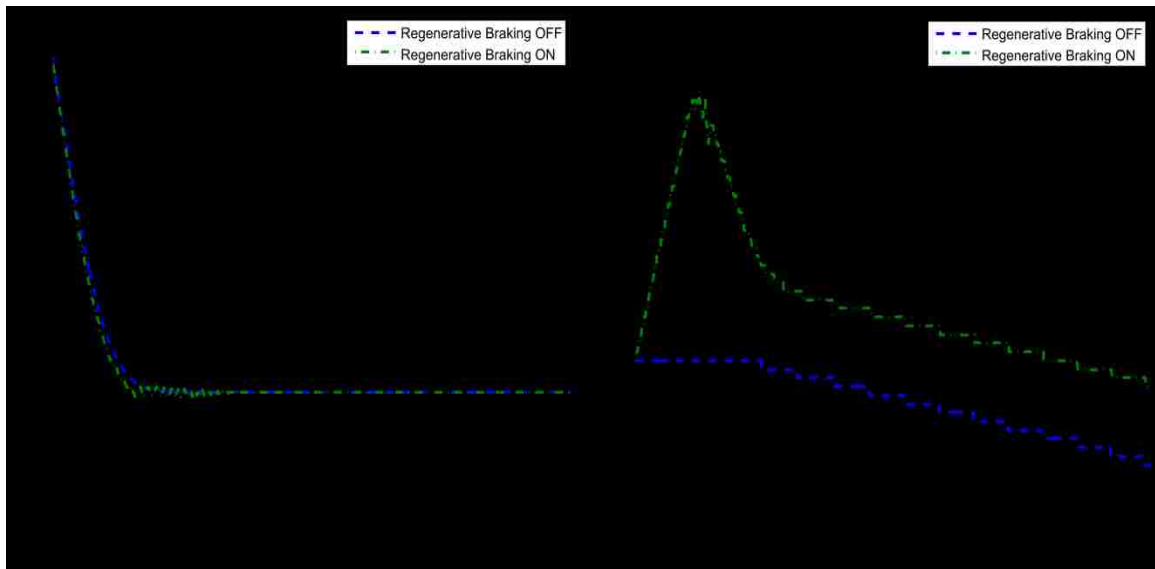


Figure 6.14: Regenerative Braking On-Off 0.7g

As seen in Figures 6.12 through 6.14 the braking performance under regenerative braking mode is improved from the stock braking performance. This is a result of the electric motor increasing the braking torque on the rear wheels during the braking event. The implications of such a result suggest that the mechanical braking system is activated too quickly under braking. Decreasing the threshold of the onset of the mechanical brakes could further optimize the energy recovery of the system.

The state of charge between the separate events appears to differ very slightly. This is ultimately a result of the duration of the braking event being approximately equal for all of the cases analyzed. Decreasing the mechanical braking will result in longer stopping durations and therefore more recovered energy. The improved performance of the hybrid system allows for some decrease in the mechanical braking effort. The results of the optimal regenerative braking system can be seen in Figure 6.15.

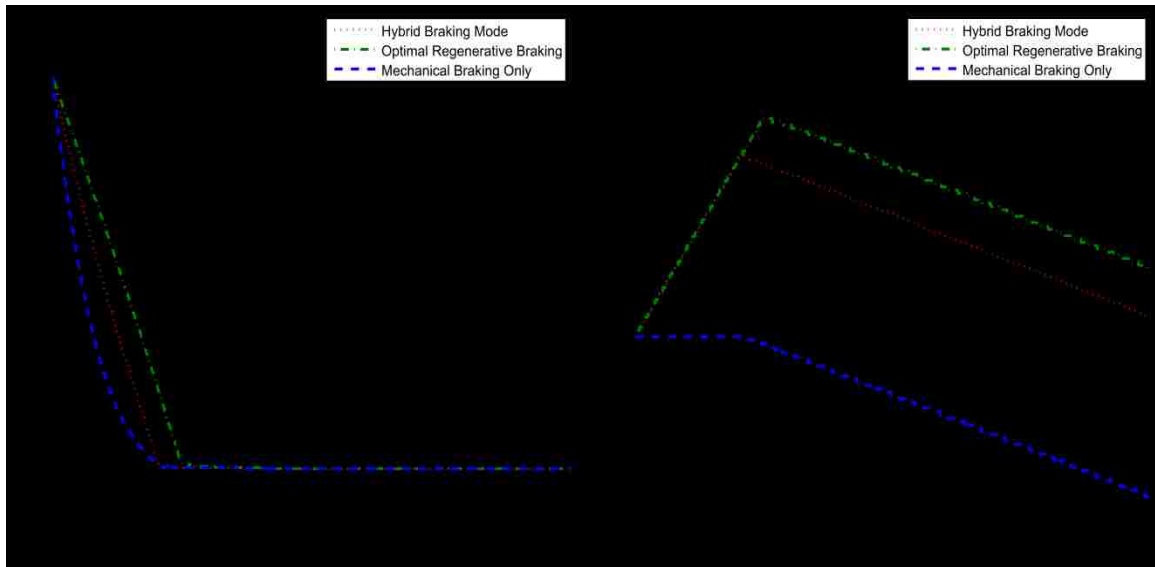


Figure 6.15: Optimal Regenerative Braking

The optimal energy recovery braking system shows the limit of recoverable energy using the electric motor exclusively. The improvement in energy recovered comes at the expense of performance. The hybrid braking mode shows a compromise between the optimal energy recovery and the mechanical braking performance. The hybrid braking mode is capable of recovering approximately 85% of the total available braking energy at the given deceleration rate with equivalent performance to the mechanical braking system. Given electric motor and battery efficiencies, this amount is reduced to 60%-70%. At higher deceleration rates the percentage of recovered energy will decrease, and at lower rates the percentage of recovered energy will increase. This effect will optimize recovered energy during regular braking events and optimize performance during emergency braking events.

### 6.3 Multiple Peaking Power Source Control

The function of the peaking power source (PPS) control is to guarantee high discharge currents and frequencies are delivered through the power source and that steady and low currents are delivered through the energy source. A DC/DC converter is placed

connecting the batteries and the ultracapacitors as a result of varying voltage of the ultracapacitors. The DC/DC converter may have upwards of 98% efficiency during operation. The current fractions from the ultracapacitor and battery will be calculated according to capability of the ultracapacitor given a vehicle state, capacitor state of charge, and driver throttle.

### 6.3.1 Vehicle Velocity

In order to preserve performance of the electric driveline, the ultracapacitor state of charge must contain sensitivity to vehicle velocity. At rest, the ultracapacitors should maintain high state of charge for acceleration and hill climbing events. At high vehicle velocities, the ultracapacitor state of charge should remain low in order to recover energy during braking events. The desired ultracapacitor SOC will determine the interaction between the power source and energy source. The relation between desired ultracapacitor state of charge and vehicle velocity can be seen in Equation 6.14

$$SOC_{ucap,desired} = -\frac{\dot{x}(1-SOC_{min})}{v_{max}} + 1 \quad (6.14)$$

Where  $v_{max}$  is the vehicle speed at which under maximum regenerative braking the ultracapacitor will become completely charged. The optimization of  $v_{max}$  will be conducted in the evaluation of the PPS control.

### 6.3.2 Ultracapacitor State of Charge

As the state of charge of the ultracapacitor decreases, its ability to produce power also decreases. At low ultracapacitor SOC, the battery must provide power to the traction motor as well as to the ultracapacitor to increase ultracapacitor SOC, making this the most undesirable state of the PPS system. At high ultracapacitor SOC, the ultracapacitors and batteries are used simultaneously to provide traction force. A summary of the logic of the control system can be seen in Table 6.1.

Battery SOC	Ultracapacitor SOC	Load Current	Battery Current	Ultracapacitor Current
HIGH	HIGH	Positive	$mI_{load}$	$nI_{load}$
HIGH	HIGH	Negative	0	0
HIGH	LOW	Positive	$I_{load}$	0
HIGH	LOW	Negative	0	$I_{load}$
LOW	HIGH	Positive	0	$I_{load}$
LOW	HIGH	Negative	$I_{load}$	0
LOW	LOW	Positive	$mI_{load}$	$nI_{load}$
LOW	LOW	Negative	0	$I_{load}$

Table 6.1: PPS Control Logic

The parameters ‘m’ and ‘n’ are the respective power ratios of the power source and energy source and can be tuned for optimization. The complexity of the systems grows with the consideration of possible interactions between the batteries and ultracapacitors as a function of vehicle velocity. The desired battery and ultracapacitor response to a step input can be seen in Figure 6.16.

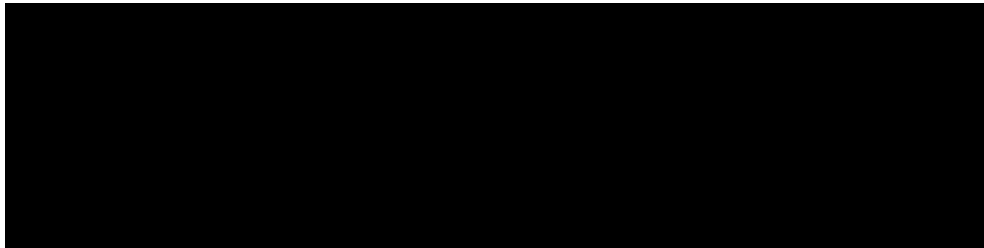


Figure 6.16: Battery and Ultracapacitor Currents with a Step Current

### 6.3.3 Peaking Power Source Control Evaluation

To determine the effectiveness of the peaking power source control, a select number of conditions will be evaluated. Of primary importance is the objective of the hybridization of the power source system. A regenerative braking simulation utilizing solely a battery is compared to the developed hybrid power source system.

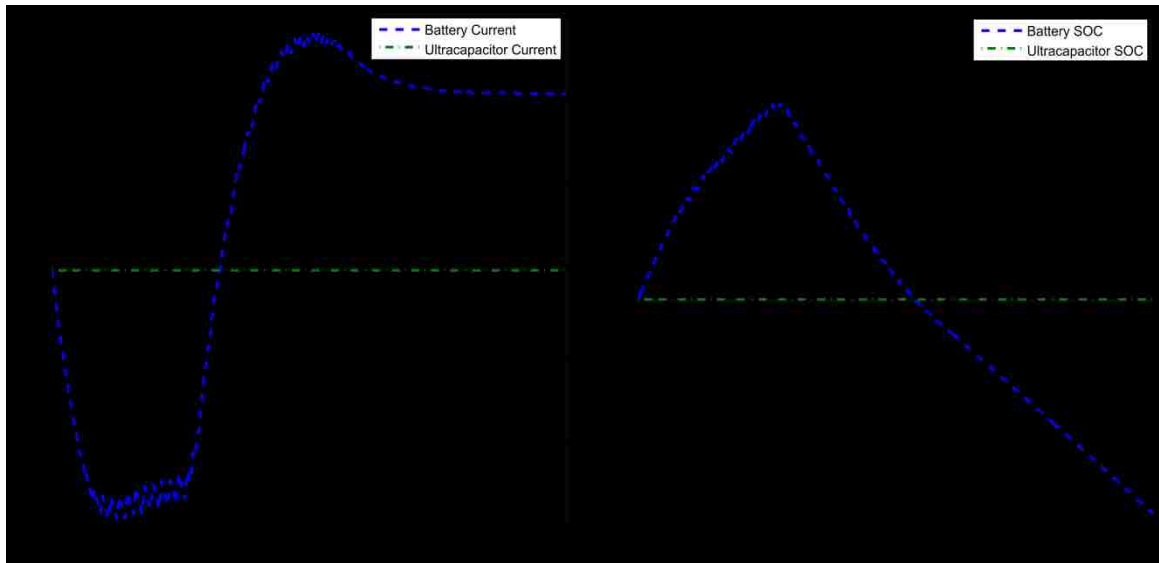


Figure 6.17: Regenerative Braking with Battery Energy Source

Figure 6.17 shows the results for the current and state of charge of the simulation utilizing a battery to recover energy during braking. Due to the limitations of the battery, the majority of the available energy must be wasted as heat in either the mechanical brakes or in a resistor bay.

The simulation was rerun with the proposed hybrid power source as seen in Figure 6.18. Upon comparing Figure 6.17 to Figure 6.18 it is evident that the addition of the ultracapacitor substantially improves energy recovery. Figure 6.17 shows that ultracapacitor's ability to recharge at high currents allows for more energy recovery



throughout the braking event. It is also notable that the battery maintains comparable energy recovery during the two events.

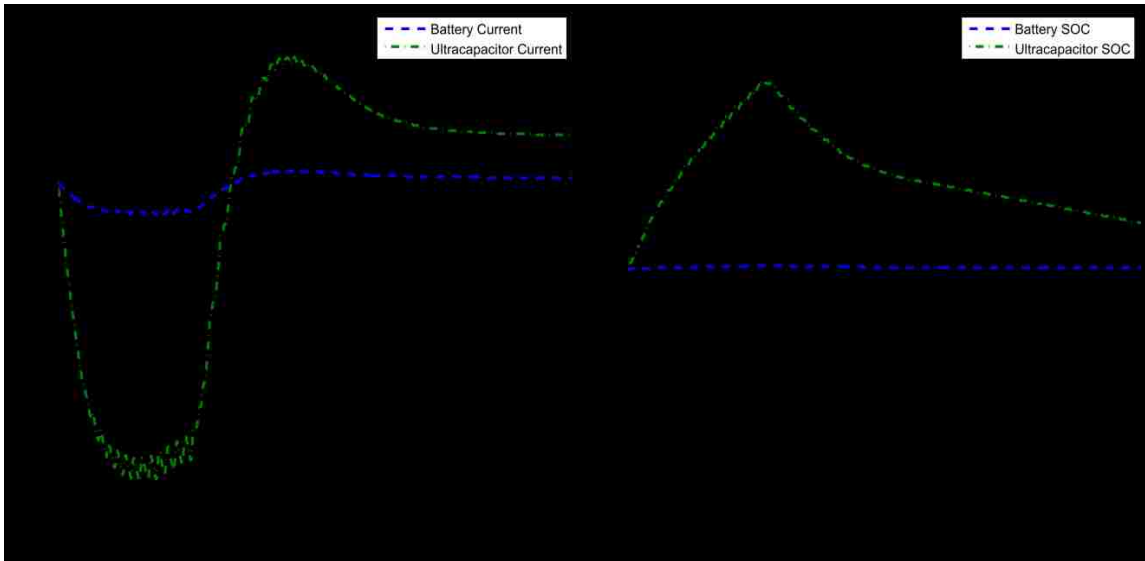


Figure 6.18: Regenerative Braking with Hybrid Power Source

To demonstrate the equivalent effect under propulsion, an acceleration event follows the previous braking event. Figure 6.19 shows the resulting battery and ultracapacitor current and state of charge for the event.

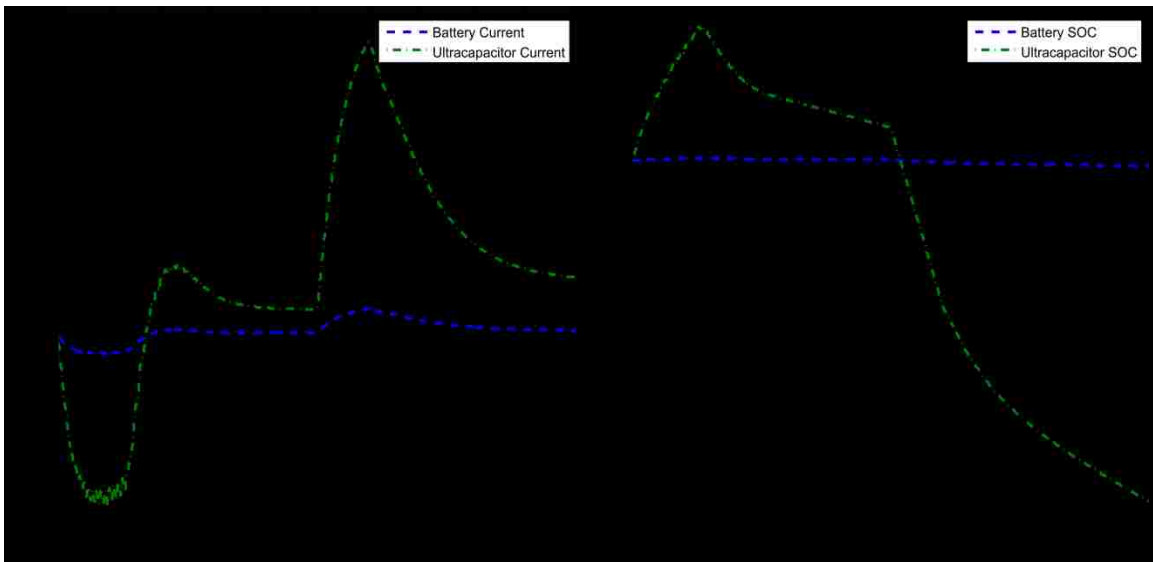


Figure 6.19: Hybrid Power Source Power Split

At low velocity and throttle, the output power of the hybrid power system is also low. If the state of charge of the ultracapacitor is lower than the desired SOC, the battery may have the ability to transfer charge to the ultracapacitor. The developed peak power source control does exactly this as seen in Figure 6.20.

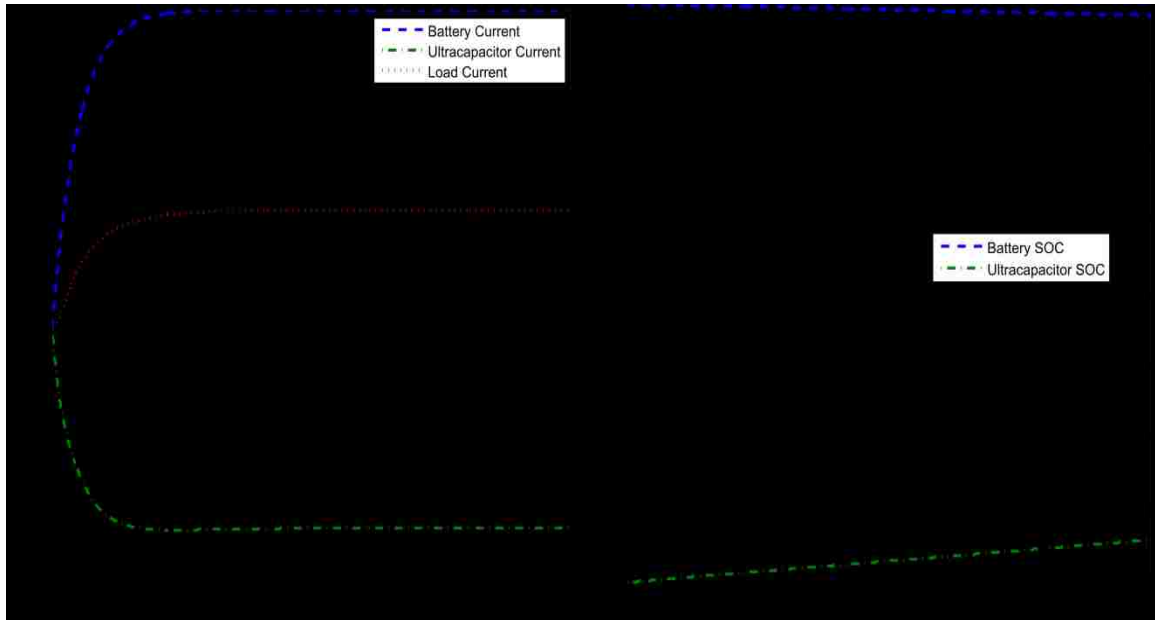


Figure 6.20: Low Speed Ultracapacitor Recharge

Although the load current is low, the battery current remains high, transferring a portion of its current to the load and the remainder to the ultracapacitor for recharge. The state of charge for the ultracapacitor and battery in Figure 6.20 clearly show this.

Upon further analysis of Figures 6.17 through 6.20, it is evident that the ultracapacitor state of charge will vary more frequently than required. In order to ensure the minimum charge transfer between the battery and ultracapacitor, the battery must always deliver current until the current limit is reached. Once the battery current is saturated, the ultracapacitor will then modulate in order to develop the remainder of the load current. This will ensure the minimum use of the DC-DC converter, and therefore improve system efficiency.

The optimal peaking power source control attempts to minimize variations in ultracapacitor state of charge while maintaining vehicle performance. Figure 6.21 and Figure 6.22 show the results of high and lower power demands to the optimal PPS controller.

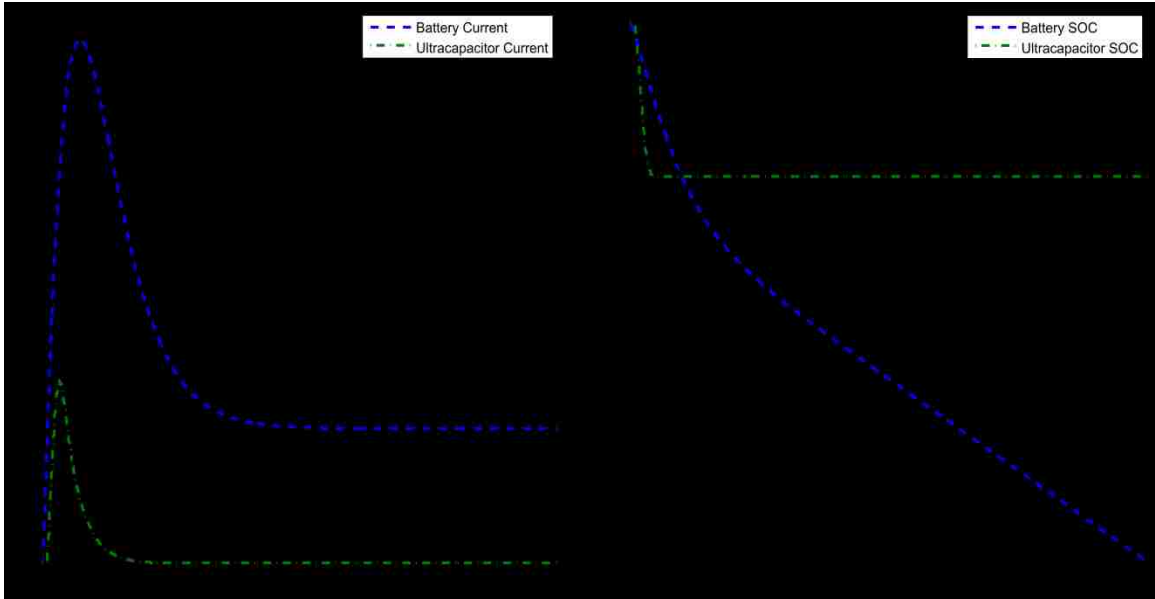


Figure 6.21: Optimal PPS Control Low Power Demand

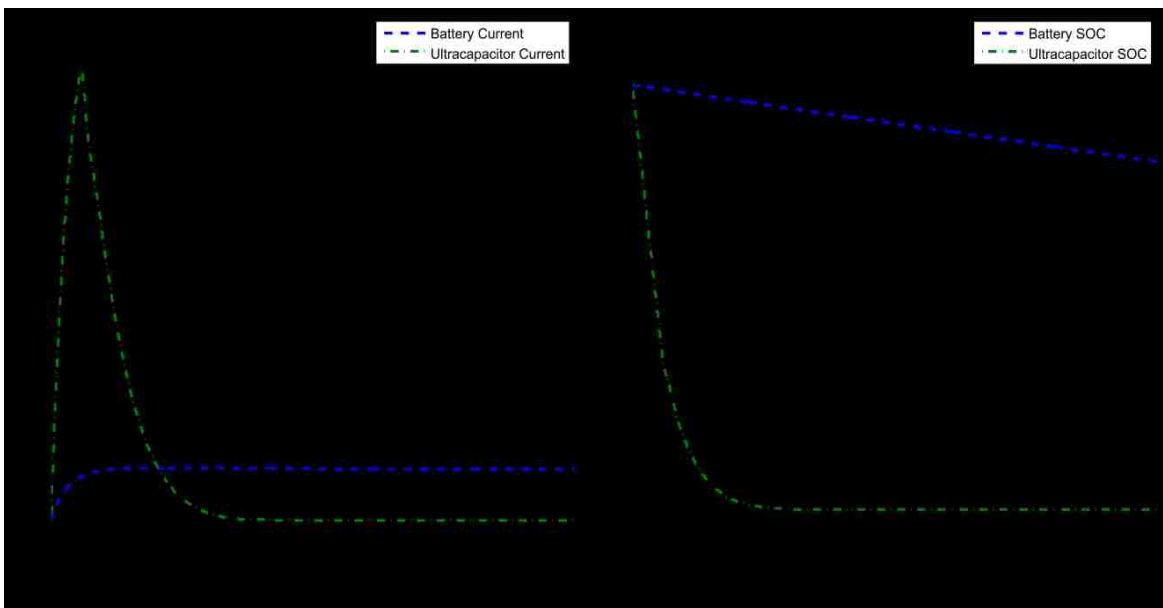


Figure 6.22: Optimal PPS Control High Power Demand

During the low power demand in Figure 6.21, the battery provides the majority of the load current and the ultracapacitor supplements the remainder. Under high power demands the reverse is true, the ultracapacitor provides the majority of the load current and the battery supplements the remainder. In either event, the ultracapacitor current is minimized.

# Chapter 7

## 7 Results

The preceding chapters have developed a flexible hybrid electric vehicle model suitable for numerical simulation. The model has shown reduction in fuel consumption, maximization of regenerative capabilities, and utilization of multiple power sources. In previous chapters, the simulations were designed to show isolation of the given system under consideration. This chapter focuses on the effectiveness of the hybrid model as a whole using drive cycle simulation in order to compare to the stock Pacifica results seen in Chapter 4.

### 7.1 All Electric Range

Although the hybridized Pacifica contains an internal combustion engine, the potential for zero emissions remains through the use of the electric driveline. The ERS model was simulated through the identical drive cycles as outlined in Chapter 4 in electric vehicle mode. The velocity variations outlined in Table 7.1 demonstrate that the electric drivetrain more narrowly follows the desired velocity profile.

Drive Cycle	Maximum Velocity Variation	Average Velocity Variation
UDDS	0.90 m/s	-0.02 m/s
HWFET	0.57 m/s	-0.01 m/s
US06	10.32 m/s	2.30 m/s

SC03	1.05 m/s	-0.04 m/s
NYCC	0.84 m/s	0.00 m/s

*Table 7.1: ERS-EV Velocity Variations*

These results suggest that either the time lag is greater for the mechanical driveline or the electric driveline is more sensitive to throttle input. It should be noted that the US06 drive cycle contains large variations due to the complete state of charge depletion of the ultracapacitor. A means for correcting this will be the focus of the blend mode control in Section 7.2. The following sections will assess the developed electric vehicle configuration for all electric use and range.

### 7.1.1 All Electric UDDS

The all electric ERS model is able to trace the UDDS velocity profile very accurately as outlined in Table 7.1. The state of charge of the ultracapacitor and battery throughout the drive cycle can be seen in Figure 7.1.

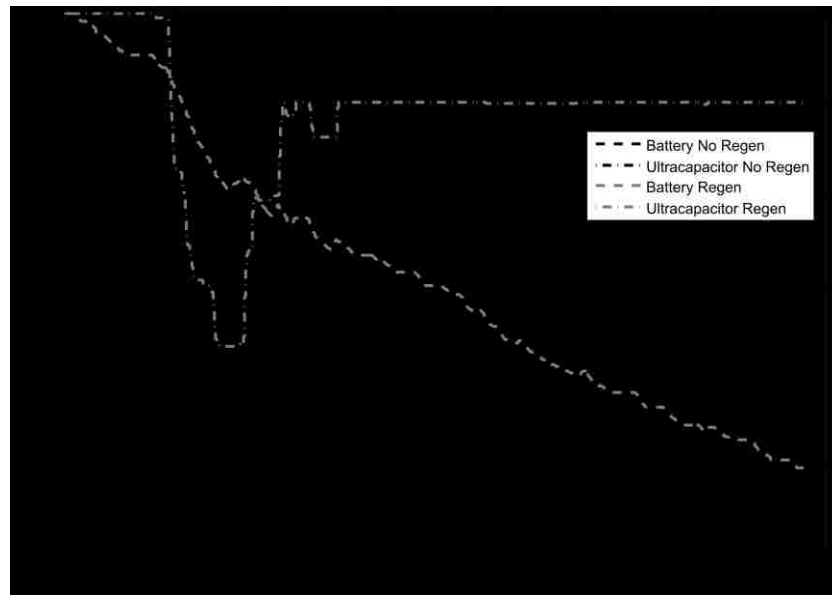


*Figure 7.1: ERS-UDDS EV State of Charge*

The state of charge is also an indication of the power requirements of the cycle. Due to the low usage of the ultracapacitor and high used of the battery it can be stated that the UDDS cycle is a low power high energy cycle.

The simulation was conducted with and without regenerative braking to determine the effectiveness of the braking system at recovering energy. Figure 7.1 shows an increase in battery state of charge of 0.03 and no change in ultracapacitor state of charge over the 1369 second cycle. The final battery state of charge of 0.74 suggests an all electric range of approximately 34.97 km. The significantly lower estimation of all electric range is a result of the increase in system complexity, component models and the addition of the ultracapacitor.

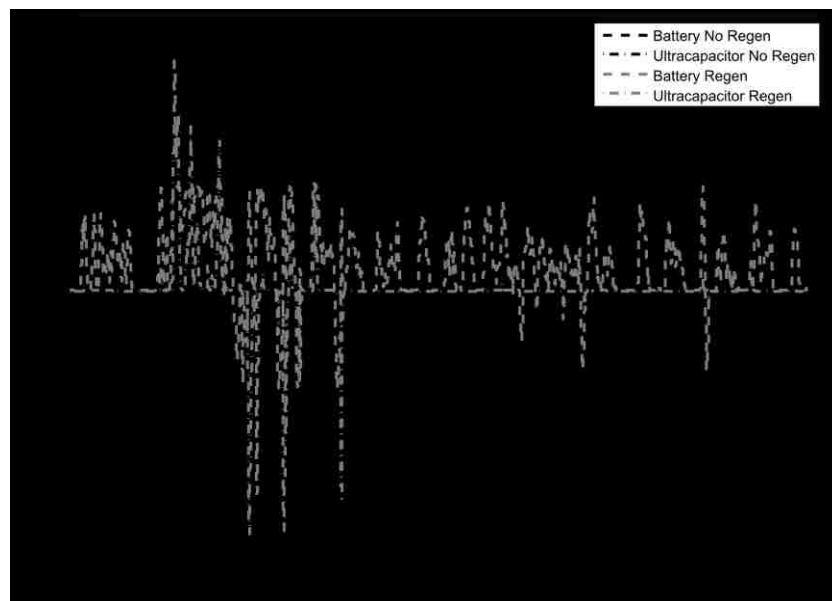


Figure 7.2: ERS-UDDS EV Currents

Figure 7.2 shows the battery and ultracapacitor currents for regenerative and non regenerative braking systems during the UDDS cycle. The increase in battery state of charge is a result of the negative currents from the electric motor. It is also important to note that the power source control does not transfer power from the ultracapacitor to the

battery. Once the ultracapacitor is completely saturated the remaining charge is wasted in a resistor bank. The low speed nature of the UDDS cycle results in large losses in kinetic energy due to the electric motor's inability to regain charge at low vehicle speeds.

### 7.1.2 All Electric HWFET

The all electric ERS model is able to trace the HWFET velocity profile very accurately, despite its high speed nature, as seen in Table 7.1. The state of charge of the ultracapacitor and battery are seen in Figure 7.3.

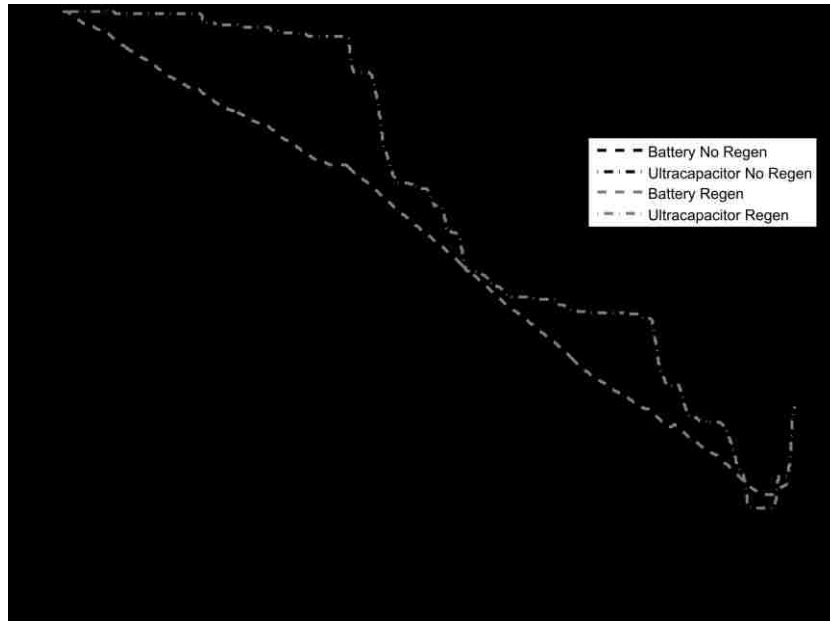


Figure 7.3: ERS-HWFET EV State of Charge

The ultracapacitor and battery state of charge implies the power and energy requirements for the HWFET drive cycle are comparable. The final battery state of charge of 0.58 suggests an all electric range of approximately 27.67 km, significantly less than the estimated value found from the UDDS cycle or the assessment in Chapter 5. The large decrease in estimated all electric range is a result of the increase in driver aggressiveness and vehicle speed in the HWFET drive cycle. The battery and ultracapacitor currents for the HWFET cycle are seen in Figure 7.4.



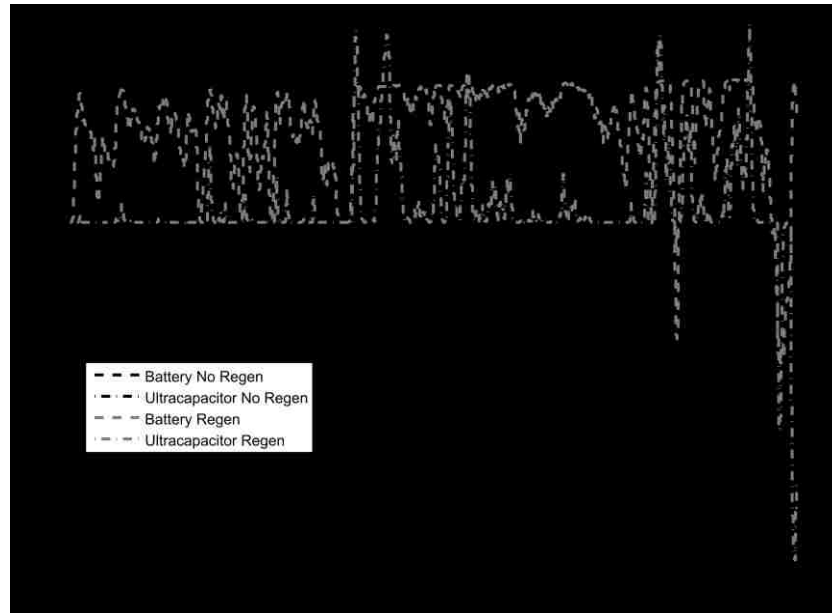


Figure 7.4: ERS-HWFET EV Currents

A large negative ultracapacitor current is seen at the end of the ERS-HWFET cycle in Figure 7.4. This is exactly as expected due to the braking event occurring at the end of the cycle. A significant portion of the HWFET drive cycle occurs at a power level slightly below the given battery power; this results in low current being transferred from the battery to the ultracapacitor during operation. The lack of braking events reduces the effectiveness of the regenerative braking system and the electric vehicle as a whole.

### 7.1.3 All Electric US06

The all electric ERS model is unable to trace the velocity profile of the US06 drive cycle due to the depletion of the ultracapacitor. Once the ultracapacitor is depleted, the battery becomes the sole power source, resulting in an underpowered electric motor. The resulting velocity profile of the all electric ERS model can be seen in Figure 7.5.

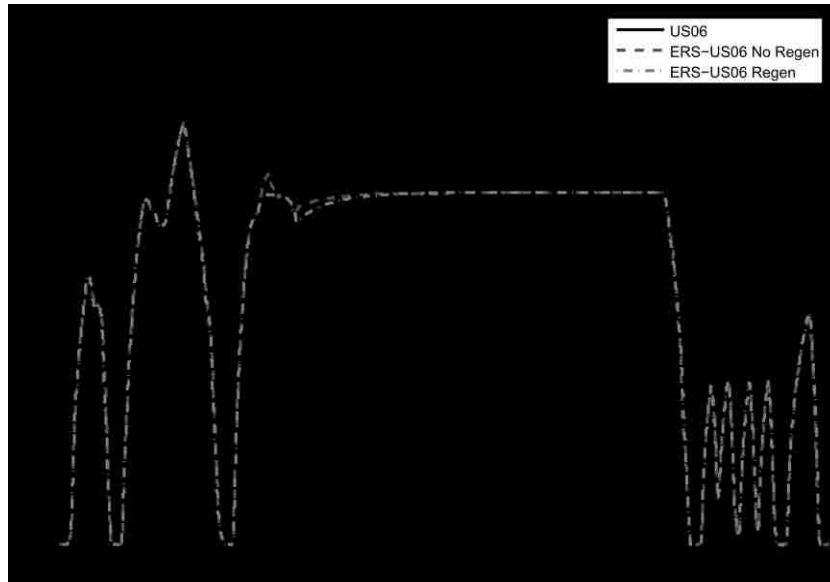


Figure 7.5: ERS-US06 EV Velocity Profile

The result shows the disadvantage of an electric vehicle configuration. Once the high power source is depleted, the system must operate with poor performance until the high power source can develop sufficient charge to restart operation. The battery and ultracapacitor state of charge can be seen in Figure 7.6.

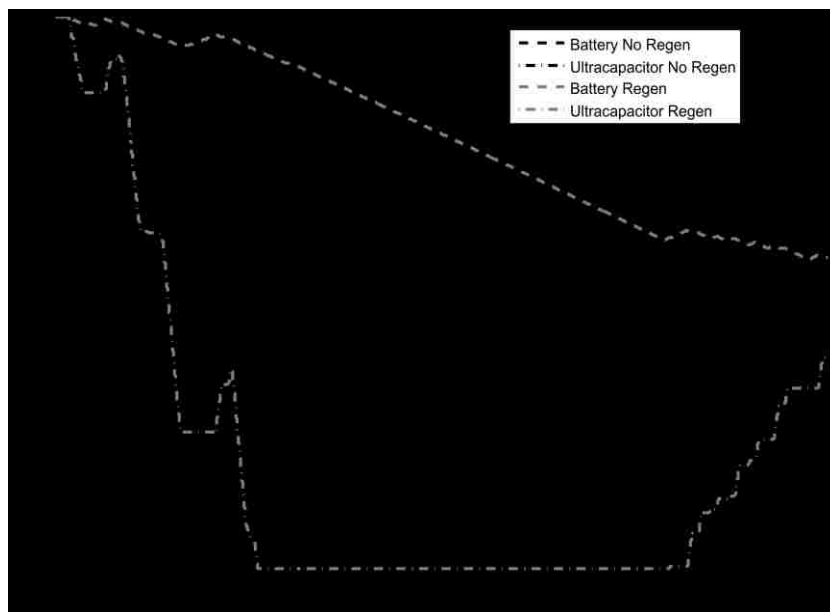


Figure 7.6: ERS-US06 EV State of Charge

Once again the importance of the regenerative braking system may be noted. The use of the regenerative braking system increases the final state of charge of the battery by 0.08. The high speed and aggressive nature of the US06 cycle allows for greater energy recovery. The battery and ultracapacitor currents can be seen in Figure 7.7.

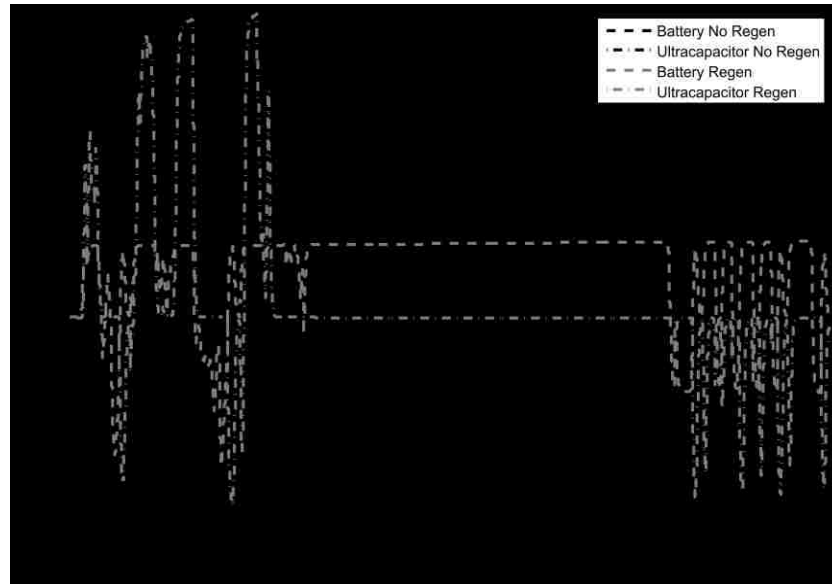


Figure 7.7: ERS-US06 EV Currents

Figure 7.7 shows the battery operating at maximum current for the duration in which the ultracapacitors have been completely discharged. The high speed braking event in combination with the reduction in traction power allows the ultracapacitors to regain charge towards the end of the cycle.

#### 7.1.4 All Electric SC03

The all electric ERS model is able to trace the SC03 drive cycle very accurately as seen in Table 7.1. The state of charge of the battery and ultracapacitor throughout the driving event can be seen in Figure 7.8.

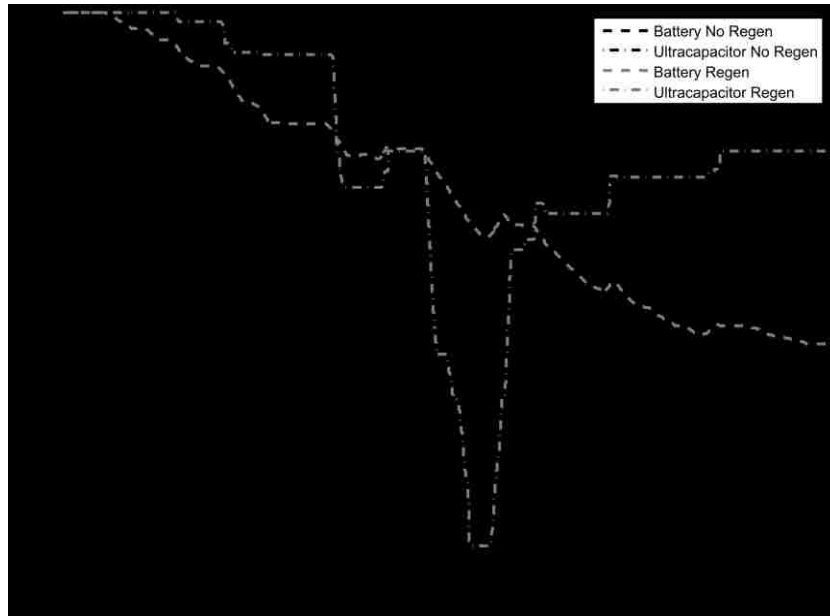


Figure 7.8: ERS-SC03 EV State of Charge

The regenerative braking system again shows considerable energy recovery. The battery state of charge is increased by 0.02 through the 600s drive cycle. The battery and ultracapacitor currents can be seen in Figure 7.9.

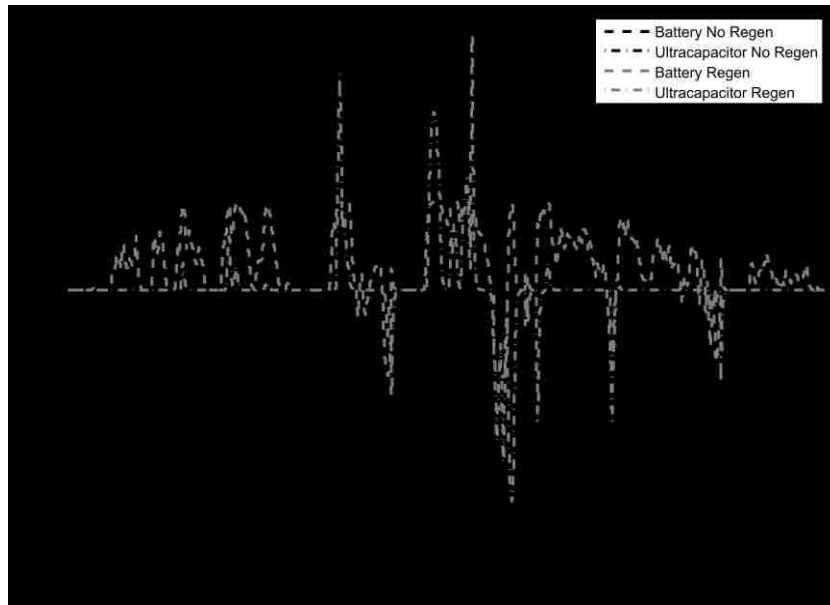
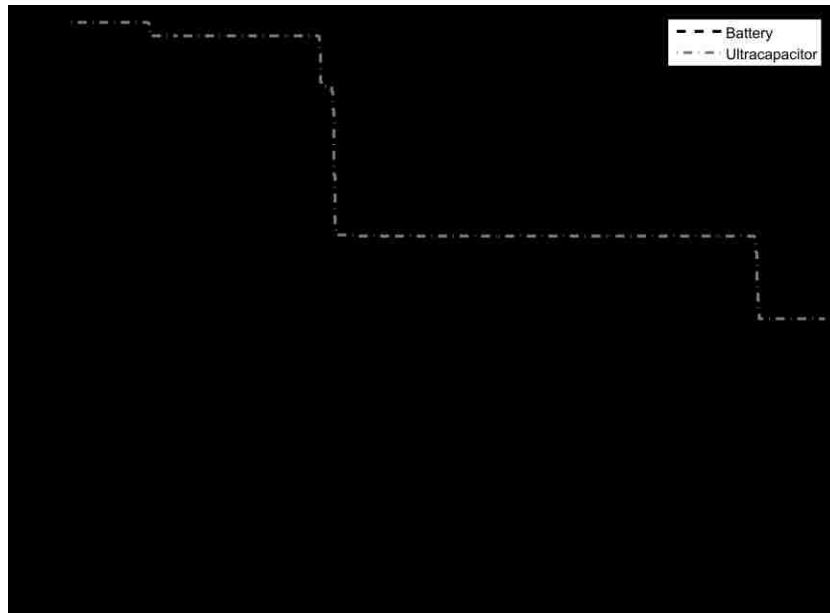


Figure 7.9: ERS-SC03 EV Currents

Figure 7.9 shows that the SC03 cycle is a relatively low power cycle, though does contain an aggressive acceleration and braking event occurring at approximately the midpoint of the cycle. The SC03 cycle shows a good indication of how battery and ultracapacitor current may be used for cycle indication and driver behaviour.

### 7.1.5 All Electric NYCC

The all electric ERS model is able to trace the NYCC drive cycle very accurately as seen in Table 7.1. The NYCC is the least efficient cycle in terms of fuel consumption found in Chapter 3. The large amount of low speed and idling operations makes the NYCC cycle ideal for electric operation. The state of charge of the battery and ultracapacitor during the drive cycle can be seen in Figure 7.10.



*Figure 7.10: ERS-NYCC EV State of Charge*

Figure 7.10 shows the state of charge of the battery depletes less than 5 percent in the completion of the NYCC drive cycle. This suggests that vehicles in operation under the NYCC could go days without recharge. It is also noted that the non-regenerative and regenerative simulations are identical due to the high state of charge of the battery and

ultracapacitor. The time history of the battery and ultracapacitor currents can be seen in Figure 7.11.

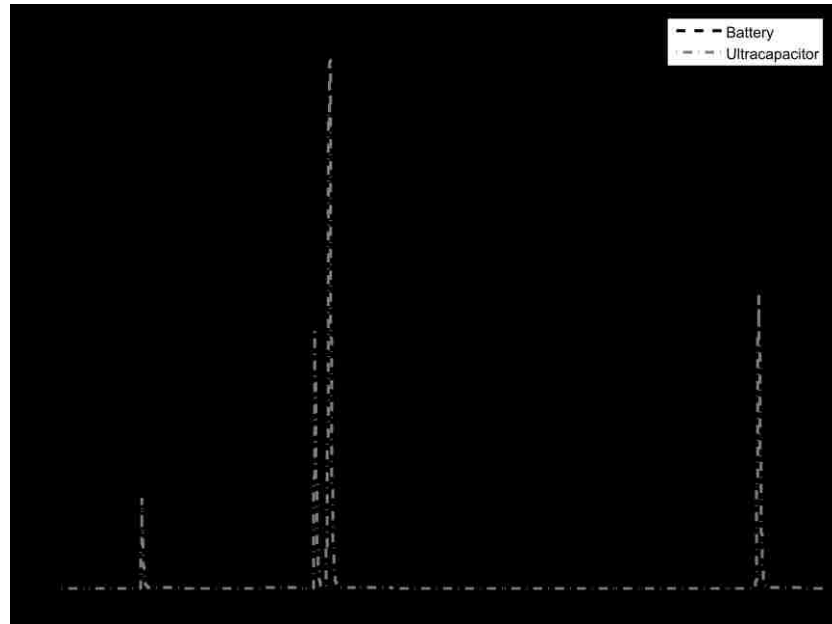


*Figure 7.11: ERS-NYCC EV Currents*

The ultracapacitor functions for a very brief amount of time suggesting that a multiple power source system may be too complex for vehicles with such operating conditions.

## **7.2 Blend Mode**

The preceding section showed that the electric vehicle had the capacity to complete all of the drive cycles except the US06. The high driver aggression resulted in full ultracapacitor depletion in a short period of time. The particular shortcomings of the all electric vehicle may be corrected by the use of the developed blend mode control. The following sections will evaluate the hybridized Pacifica for blend mode range and fuel consumption. Reduction in initial battery state of charge for all drive cycles will also be evaluated.

### 7.2.1 Blend Mode UDDS

The operation of blend mode for the UDDS cycle yields equivalent results to that of the all electric vehicle for initial battery state of charge equal to 1.0 and 0.7. The low driver throttle results in the engine requiring the ability to operate in a low inefficiency range which is not within the acceptable range of the integrated hybrid controller as outline by Equation 6.1. The resulting state of charge for the battery and ultracapacitor with varying initial conditions can be seen in Figure 7.12.

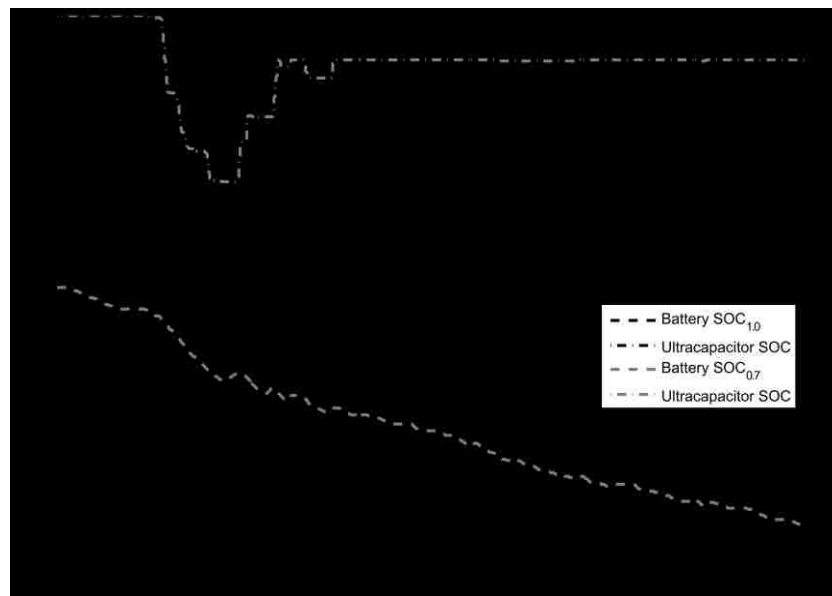


Figure 7.12: ERS-UDDS Blend Mode State of Charge

### 7.2.2 Blend Mode HWFET

The operation of the blend mode for the HWFET cycle shows differing results for initial battery state of charge of 1.0 and 0.7. The initial battery state of charge of 1.0 simulation demonstrates that the cycle is completed all electrically, though with initial battery state of charge of 0.7, the battery becomes completely depleted before the end of the drive cycle. The vehicle is then run on charge sustaining mode for the remainder of the event.

The battery and ultracapacitor state of charge for both the events can be seen in Figure 7.13.

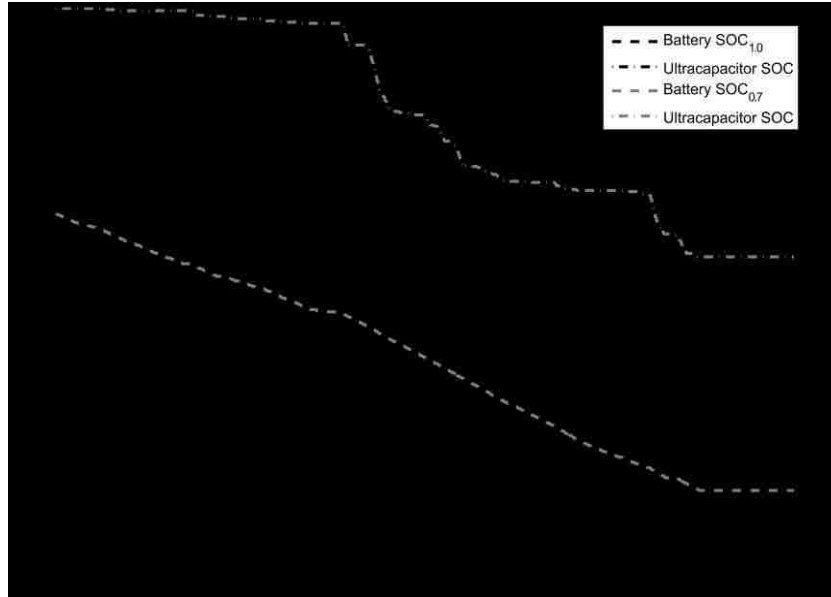


Figure 7.13: ERS-HWFET Blend Mode State of Charge

Figure 7.13 suggests that the ultracapacitor could be used to further power the vehicle all electrically and perhaps avoid the use of the internal combustion engine. The electric motor and internal combustion engine torques throughout the HWFET cycle are seen in Figure 7.14 and Figure 7.15.



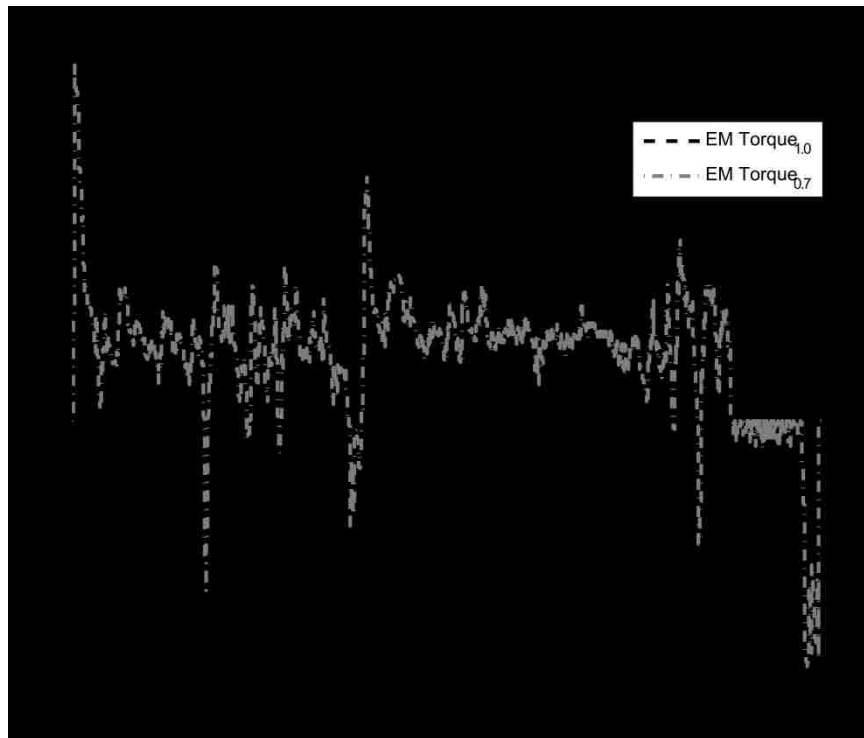


Figure 7.14: ERS-HWFET Blend Mode EM Torque

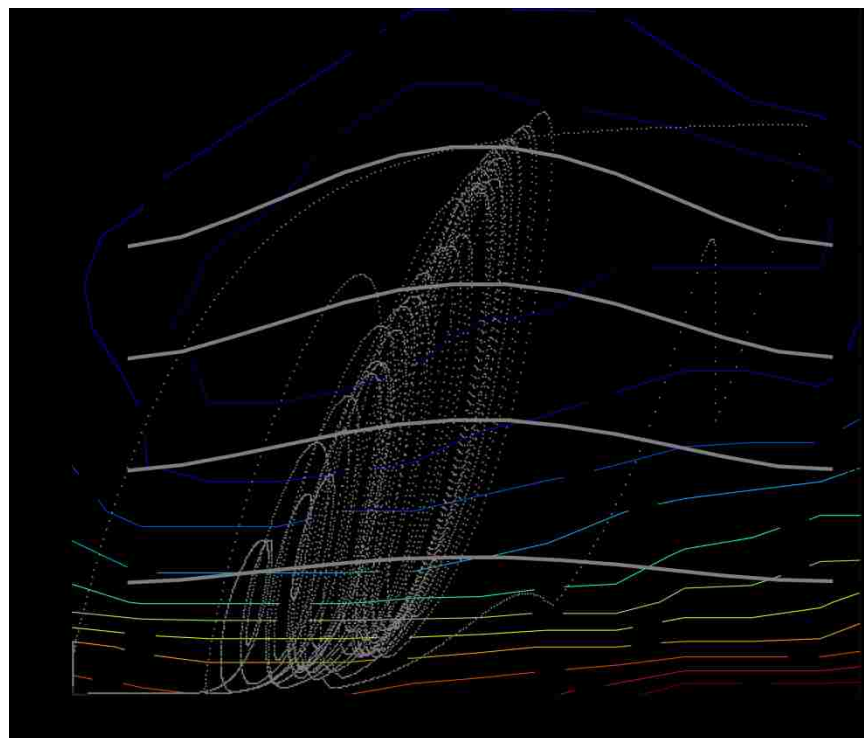


Figure 7.15: ERS-HWFET Blend Mode ICE Torque

### 7.2.3 Blend Mode US06

The blend mode ERS model shows one of the advantages of the integrated hybrid control. The all electric mode was unable to follow the desired velocity profile, though once the ultracapacitor reached the minimum state of charge the internal combustion engine was operated to provide the required torque. Once the velocity was reduced, the ultracapacitor regained charge through the battery and regenerative braking and the vehicle returned to electric vehicle mode. The state of charge of the battery and ultracapacitor throughout the event are seen in Figure 7.16.

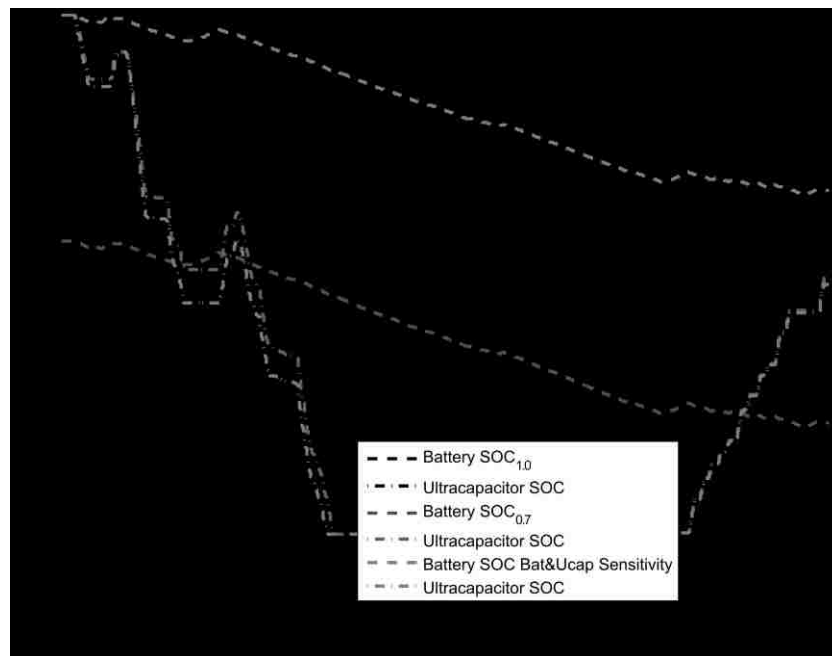


Figure 7.16: ERS-US06 Blend Mode State of Charge

Figure 7.16 shows a reduction in ultracapacitor depletion with the use of the integrated hybrid control when ultracapacitor and battery state of charge are both used to determine engine operation. The US06 cycle had a fuel consumption of 10 L/100km over the 600 second cycle, a reduction of over half the fuel displaced in the stock configuration. Improvements in fuel consumption are partially due to an increase in engine efficiency

and partially due to a reduction in battery state of charge. This is an inherent advantage of the plug-in hybrid electric vehicle; it may recharge at much lower cost than converting fuel energy to electric energy through a generator.

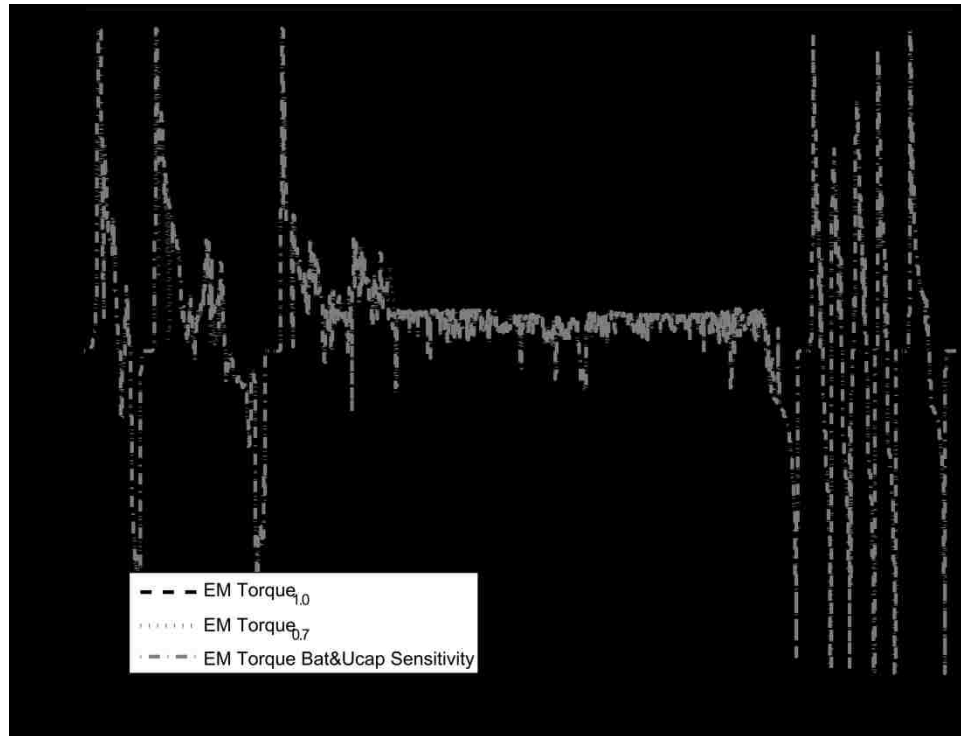


Figure 7.17: ERS-US06 Blend Mode EM Torque

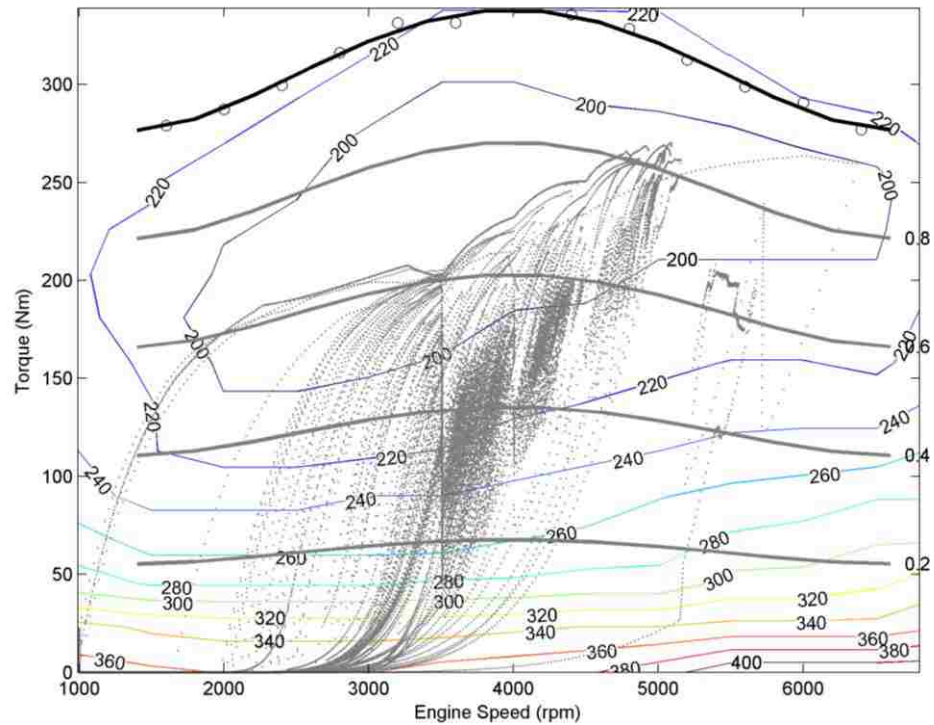


Figure 7.18: ERS-US06 Blend Mode ICE Torque

Figure 7.17 and Figure 7.18 show the electric motor and internal combustion engine torques throughout the US06 drive cycle. The results from the blend mode US06 simulation suggest that further investigation into the integrated hybrid control strategy with multiple peaking power sources is required.

### 7.2.4 Blend Mode SC03

The blend mode ERS model for the SC03 cycle with initial battery state of charge equal to 1.0 shows equivalent results to the all electric simulation results seen in Section 7.1.4. Once the initial battery state of charge is decreased to 0.7, the simulation runs in all electric mode with the exception of a short period in blend mode. The battery and ultracapacitor state of charge are seen in Figure 7.19. The short duration of the internal combustion operation suggests blend mode may be unnecessary for the SC03 drive cycle. The electric motor and internal combustion engine torques are seen in Figure 7.20 and Figure 7.21.

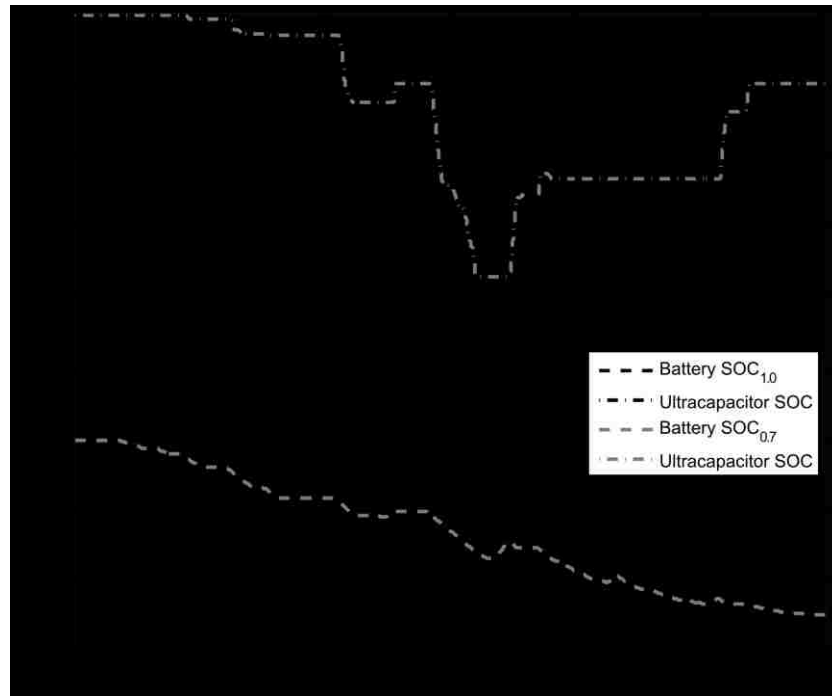


Figure 7.19: ERS-SC03 Blend Mode State of Charge

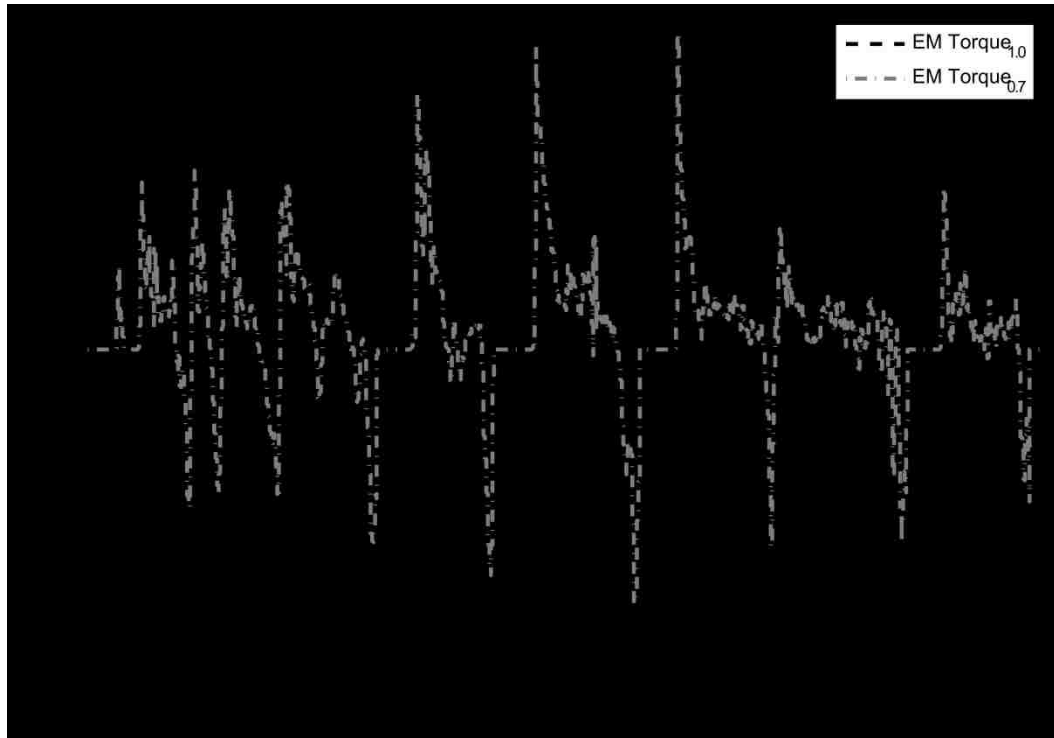


Figure 7.20: ERS-SC03 Blend Mode EM Torque

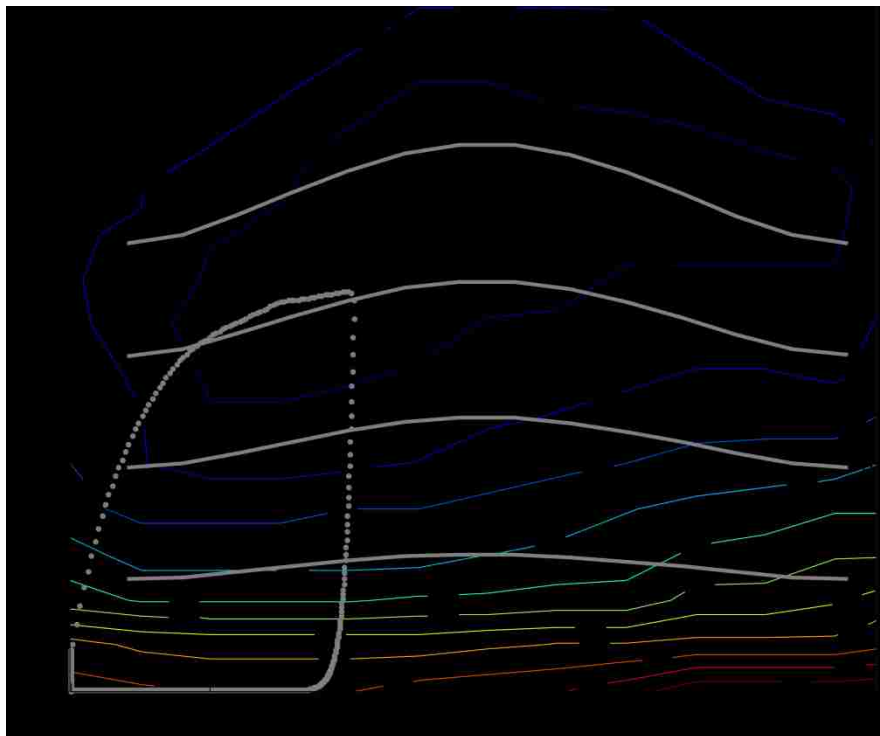


Figure 7.21: ERS-SC03 Blend Mode ICE Torque

### 7.2.5 Blend Mode NYCC

The operation of blend mode for the NYCC cycle yields equivalent results to that of the all electric vehicle for initial battery state of charge equal to 1 and 0.7. The low driver throttle results in the engine requiring the ability to operate in a low inefficiency range which is not within the acceptable range of the integrated hybrid controller as outlined by Equation 6.1. The resulting state of charge for the battery and ultracapacitor with varying initial conditions can be seen in Figure 7.22.

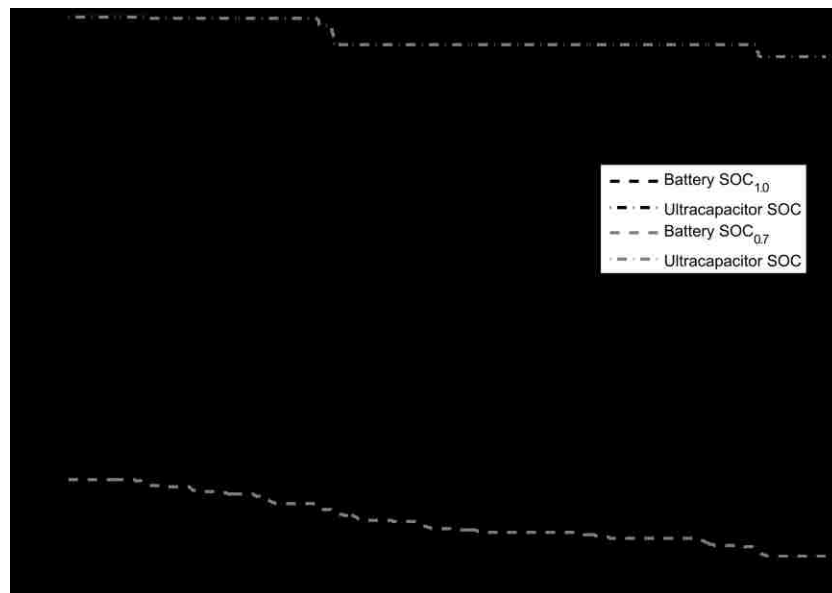


Figure 7.22: ERS-NYCC Blend Mode State of Charge

## **Chapter 8**

# **8 Conclusions and Recommendations**

The removal of global dependency on fossil fuels requires the development of new and innovative technologies such as hybrid electric vehicles. Empirical testing and development of PHEVs can prove to be extremely costly. Computational vehicle models and simulation allow for a reduction in cost of testing and development of PHEVs. The objective of the research discussed in this document was to develop a flexible vehicle model, minimize fuel consumption through integrated hybrid control, maximize regenerative capabilities while maintaining performance, and to utilize multiple power sources to improve vehicle performance over standard electric vehicles. The following section will assess the researcher's success at meeting the outlined objectives.

### **8.1 Thesis Summary**

Preliminary development of the vehicle model was done with the introduction of the ERS model. The resulting equations of motion, wheel speed stability, and tire behaviour for the ERS model were summarized. Validation of the ERS model in longitudinal acceleration, longitudinal braking, highway fuel consumption and city fuel consumption were completed. The highway fuel consumption and city fuel consumption did not match the advertised values but were certainly reasonable; as such, these newly calculated values were assumed to be representative of the vehicle's true performance.

Drive cycle analysis was introduced with the relevant cycles for the research. The ERS model was simulated through five drive cycles known as: the Urban Dynamometer



Driving Schedule, the Highway Fuel Economy Test Driving Schedule, the US06 or Supplemental FTP Driving Schedule, the Speed Correction 03 Driving Schedule and the New York City Cycle. Results showed strong correlation between the ERS model and the defined drive cycle velocity profile. Small variations in velocity were determined to be a result of the time lag in the mechanical drivetrain control system and the lack of a predictive driver model. The fuel consumption found from the ERS model was used as the benchmark for future hybrid electric vehicle simulation under such drive cycles.

Prior to hybridization, the electric vehicle driveline was developed. Due to the nature of plug-in hybrid electric vehicles, the all electric capabilities of the vehicle were evaluated. The electric motor was sized based upon a maximum all electric speed of 100 kph, resulting in a 32kW electric motor for maintained performance at high speed and improved energy recovery during regenerative braking. The battery and ultracapacitor were sized based upon the maximum allowable voltage and the power requirements of the electric motor. The electric motor was modeled using a steady state efficiency map to represent both the electric motor and the three phase inverter. The battery and ultracapacitor were modeled using simple equivalent circuits with internal resistance and open circuit voltage as functions of state of charge.

The electric driveline was implemented in the ERS model, and evaluated in longitudinal acceleration. The ERS EV model showed acceptable performance below 65 kph, suitable for the proposed PHEV configuration.

The integration of the mechanical and electrical drivelines required complex control algorithms. The focus of the research was to develop such controls as to fulfill the objectives outlined previously. The integrated hybrid control was developed to modulate the portions of throttle required by both propulsion systems in order to minimize fuel consumption while maintaining vehicle performance. The results of the simulation showed that the engine operation was maintained in the high efficiency range while the

supplemental torque required was developed by the electric motor. The efficiency range of the internal combustion engine was set based on a weighted percentage of the state of charge of the battery and ultracapacitor. Results showed that setting the engine efficiency range based solely on battery state of charge or solely on ultracapacitor state of charge had negative effects on fuel consumption.

To further minimize fuel consumption, regenerative braking was modeled and integrated into the hydraulic braking system. Results show the use of the electric motor alone to brake the vehicle allowed for the maximum recovered energy, though it deteriorated braking performance. The developed braking system was optimized to recover the maximum amount of energy without sacrificing braking performance. At a deceleration rate of 0.3g, the regenerative braking system was able to recover 85% of the available energy. At deceleration rates below 0.3g the system recovered a larger percentage of available energy, though at higher deceleration rates the percentage was reduced to ensure adequate braking during emergency events.

The high power demand of the electric driveline required both battery and ultracapacitor units. The issues of low power density of the battery and the low energy density of the ultracapacitor were addressed with the use of a hybrid power system. Due to the low energy capacity of the ultracapacitor, it was decided that the ultracapacitor be used solely for high power events and the battery be used for the low power events. The results show that the peaking power source control was able to minimize ultracapacitor currents and therefore minimize variations in the ultracapacitor state of charge. The peaking power source control also maintained the ultracapacitor state of charge based on vehicle speed.

Once the integration of the entire plug-in hybrid electric vehicle controls were made to the ERS model, the ERS model was simulated in the drive cycle events. The results showed that low driver aggression, less than 0.25g accelerations, limits the use of the internal combustion engine. The UDDS and NYCC cycle were able to be completed all

electrically even with a reduced initial state of charge in the battery. The HWFET cycle operated all electrically with an initial battery state of charge of 1.0, although it switched to charge sustaining mode when the initial state of charge was reduced to 0.7. The battery was completely depleted before the completion of the drive cycle for the second case. The high driver aggression of the US06 cycle was able to capture the operation of the integrated hybrid control. The original results of the US06 cycle showed the integrated hybrid control required more sensitivity to the ultracapacitor than the battery. The lack of ultracapacitor consideration to the engine efficiency range resulted in poor performance of the integrated hybrid control. The modified integrated hybrid control was able to complete the drive cycle with low variations in velocity. The all electric mode, blend mode and charge sustaining mode were all required to complete the drive cycle. The SC03 cycle operated the internal combustion engine for a five second period due to a low state of charge in the ultracapacitor, though it was not operated at any other time during the cycle.

The summarized results show that electric vehicles can perform equally to conventional vehicles on most drive cycles given minimal driver aggression. The inclusion of an internal combustion engine was proven necessary for high vehicle performance and range.

The developed Hybrid ERS vehicle model was flexible, able to minimize fuel consumption through the integrated hybrid control, maximize recovered energy through the regenerative braking system while maintaining performance, and utilize multiple peaking power sources to improve all electric performance.

## **8.2 Recommendations**

Although the results found showed potential, further development to the Hybrid ERS model would be desirable. The addition of dynamic battery, ultracapacitor, and electric motor models could be used to verify the results found from this study.

The Hybrid ERS model focused on the longitudinal behaviour of the vehicle. The inclusion of lateral effects could be developed for further analysis. Lateral effects may also suggest modifications to configurations and control schemes.

Further development in the integrated hybrid control could improve fuel efficiency. The all electric and blend mode ranges for the given drive cycles could be evaluated by modifying the initial conditions of the system or by modifying the drive cycle data.

The peaking power source control does not include power transfer from the ultracapacitor to the battery, which could prove to be beneficial at high speeds when the ultracapacitor is above the desired state of charge.

The advancement of Hybrid ERS model could function as a valuable tool in hybrid development avoiding large investment and potentially optimizing any hybrid system.

## References

- [1] J. K. Ahn, K. H. Jung, D. H. Kim, H. B. Jin, and S. H. Hwang, "Analysis of a Regenerative Braking System for Hybrid Electric Vehicles using Electro-Mechanical Brake," *International Journal of Automotive Technology*, pp. 229-234, 2009.
- [2] R. Apter and M. Prathaler, "Regeneration of Power in Hybrid Vehicles," p. 7.
- [3] Jonathan J. Awerbuch and C. R. Sullivan, "Control of Ultracapacitor-Battery Hybrid Power Source for Vehicular Applications," *IEEE Conference on Global Sustainable Energy Infrastructure*, p. 8, 2008.
- [4] K. E. Bailey and B. K. Powell, "A Hybrid Electric Vehicle Powertrain Dynamic Model," *Proceedings of the American Control Congress*, p. 6, 1995.
- [5] Mike Blundell and Damian Harty, *The Multibody Systems Approach to Vehicle Dynamics*. Burlington: Elsevier Butterworth-Heinemann, 2004.
- [6] V. Brslica, "Super-capacitor Integration into Hybrid Vehicle Power Source," *University of Defence in Brno*, p. 6.
- [7] Karen L. Bulter, Mehrdad Ehsani, and Preyas Kamath, "A Matlab-Based Modelling and Simulation Package for Electric and Hybrid Electric Vehicle Design," *IEEE*

- Transactions on Vehicular Technology*, pp. 1770-1778, 1999.
- [8] H. L. Chan and D. Sutanto, "A New Battery Model for use with Battery Energy Storage Systems and Electric Vehicles Power Systems," The Hong Kong Polytechnic University, 2000.
- [9] S. R. Cikanek, K. E. Bailey, and B. K. Powell, "Parallel Hybrid Electric Vehicle Dynamic Model and Powertrain Control," *Proceedings of The American Control Conference*, pp. 684-688, 1997.
- [10] Sebastien Delprat, Jimmy Lauber, Thierry Marie Guerra, and J. Rimaux, "Control of a Parallel Hybrid Powertrain: Optimal Control," *IEEE Transactions on Vehicular Technology*, pp. 872-881, 2004.
- [11] Juan W. Dixon, Micah Ortuzar, and Eduardo Wiechmann, "Regenerative Braking for an Electric Vehicle Using Ultracapacitors and a Buck-Boost Converter," *Catholic University of Chile*, p. 11.
- [12] Mehdrad Ehsani, Yimin Gao, and Ali Emadi, *Modern Electric, Hybrid Electric, and Fuel Cell Vehicles*. Boca Raton, FL: Taylor and Francis Group, LLC, 2010.
- [13] Hanrong Fan, Graham E. Dawson, and Tony R. Eastham, "Model of Electric Vehicle Induction Motor Drive System," Queen's University, Kingston,.
- [14] Ryan Fellini, Nestor Michelena, Panos Papalambros, and Michael Sasena, "Optimal Design of Automotive Hybrid Powertrain Systems," The University of Michigan, Ann Arbor,.
- [15] Lijun Gao, Shengyi Liu, and Roger A. Dougal, "Dynamic Lithium-Ion Battery

- Model for System Simulation," *IEEE Transactions on Components and Packaging Technologies*, pp. 495-505, 2002.
- [16] Giancarlo Genta, *Motor Vehicle Dynamics*. River Edge, NJ: World Scientific Publishing Co. Pte. Ltd., 1997.
- [17] Thomas D. Gillespie, *Fundamentals of Vehicle Dynamics*. Warrendale: Society of Automotive Engineers, 1992.
- [18] Masoud Aliakbar Golkar and Amin Hajizadeh, "Power Management Strategy for Parallel Hybrid Electric Vehicles," *International Conference on Sustainable Energy and Environment*, p. 6, 2006.
- [19] Yusuf Gurkaynak and Ali Emadi, "Adaptive Energy Management of Hybrid and Plug-in Hybrid Electric Vehicles Using Artificial Intelligence," 2007.
- [20] Bhag S. Guru and Huseyin R. Hiziroglu, *Electric Machinery and Transformers*. New York: Oxford University Press Inc., 2001.
- [21] Lino Guzzella and Antonio Sciarretta, *Vehicle Propulsion Systems*. Verlag Berlin Heidelberg: Springer, 2005.
- [22] Junjie He, David A. Crolla, Martin C. Levesley, and Warren J. Manning, "Integrated Active Steering and Variable Torque Distribution Control for Improving Vehicle Handling and Stability," *Vehicle Dynamics & Simulation*, 2004.
- [23] Saft Inc. (2007) Saft Batteries. [Online].  
<http://www.saftbatteries.com/Home/tabid/54/Language/en-US/Default.aspx>

- [24] Reza N. Jazar, *Vehicle Dynamics Theory and Application*. Riverdale: Springer, 2008.
- [25] Lars Johannesson, Mattias Asbogard, and Bo Egardt, "Assessing the Potential of Predictive Control for Hybrid Vehicle Powertrains using Stochastic Dynamic Programming," *IEEE Conference of Intelligent Transportation Systems*, pp. 366-371, 2005.
- [26] D. Karbowski, A. Rousseau, S. Pagerit, and P. Sharer, "Plug-in Vehicle Control Strategy: From Global Optimization to Real-Time Application," *Argonne National Laboratory*, p. 23.
- [27] U. Kiencke and L. Nielsen, *Automotive Control Systems*. Warrendale: Springer, 2000.
- [28] Jay Kwon, Aymeric Rousseau, and Phil Sharer, "Analyzing the Uncertainty in the Fuel Economy Prediction for the EPA MOVES Binning Methodology," *Argonne National Laboratory*, p. 17.
- [29] James Larminie and John Lowry, *Electric Vehicle Technology Explained*. West Sussex, England: John Wiley & Sons Ltd., 2003.
- [30] Tony Markel and Ahmad Pesaran, "PHEV Energy Storage and Drive Cycle Impacts," *National Renewable Energy Laboratory*, p. 26, 2007.
- [31] Tony Markel and Keith Wipke, "Modeling Grid-Connected Hybrid Electric Vehicles Using ADVISOR," *National Renewable Energy Laboratory*, p. 7.
- [32] Erik Lowndes McKenzie, *Development of an Intermediate DOF Vehicle Dynamics*



*Model for Optimal Design Studies.*: North Carolina State University, 1998.

- [33] William F. Milliken and Douglas L. Milliken, *Race Car Vehicle Dynamics*. Warrendale, PA: SAE International, 1995.
- [34] Ayman Moawad, Gurhari Singh, Simeon Hagspiel, Mohamed Fellah, and Aymeric Rousseau, "Impact of Real World Drive Cycles on PHEV Fuel Efficiency and Cost for Different Powertrain and Battery Characteristics," *EVS24*, p. 10, 2009.
- [35] Nathan C. Nantais, *Active Brake Proportioning and Its Effects on Safety and Performance*. Windsor: University of Windsor, 2006.
- [36] Evren Ozatay, Ben Zile, Joel Anstrom, and Sean Brennan, "Power Distribution Control Coordinating Ultracapacitors and Batteries for Electric Vehicles," *Proceedings of the American Control Conference*, pp. 4716-4721, 2004.
- [37] D. Peng, Y. Zhang, C. L. Yin, and J. W. Zhang, "Combined Control of a Regenerative Braking and Anti-Lock Braking System for Hybrid Electric Vehicles," *International Journal of Automotive Technology*, pp. 749-757, 2008.
- [38] Pierluigi Pisu and Giorgio Rizzoni, "A Comparative Study of Supervisory Control Strategies for Hybrid Electric Vehicles," *IEEE Transactions on Control Systems Technology*, pp. 506-518, 2007.
- [39] B. K. Powell, K. E. Bailey, and S. R. Cikanek, "Dynamic Modeling and Control of Hybrid Electric Vehicle Powertrain Systems," *IEEE Control Systems*, pp. 17-33, 1998.
- [40] Robert J. Rieveley and Bruce P. Minaker, *Variable Torque Distribution Yaw*

*Moment Control For Hybrid Powertrains.*: SAE Inc., 2007.

- [41] Aymeric Rousseau, "PSAT Training - Part 04," *Argonne National Laboratory*, p. 20.
- [42] Aymeric Rousseau and Neeraj Shidore, "Research on PHEV Battery Requirements and Evaluation of Early Prototypes ," *Argonne National Laboratory*, p. 29.
- [43] Phillip Sharer, Romain Leydier, and Aymeric Rousseau, "Impact of Drive Cycle Aggressiveness and Speed on HEVs Fuel Consumption," *Argonne National Laboratory*, p. 18.
- [44] Phil Sharer, Aymeric Rousseau, Dominik Karbowski, and Sylvain Pagerit, "Plug-in Electric Vehicle Control Strategy: Comparison between EV and Charge Depleting Options," *Argonne National Laboratory*, p. 15.
- [45] Phil Sharer, Aymeric Rousseau, Dominik Karbowski, and Sylvain Pagerit, "Plug-in Hybrid Electric Vehicle Control Strategy: Comparison between EV and Charge-Depleting Options," *Argonne National Laboratory*, p. 15.
- [46] Phil Sharer, Aymeric Rousseau, Sylvain Pagerit, and Paul Nelson, "Midsize and SUV Vehicle Simulation Results for Plug-in HEV Component Requirements," *Argonne National Laboratory*, p. 16.
- [47] Ruud Van Gaal and B. V. Dolphinty. (2009, November) Pacejka's Magic Formula. [Online]. <http://www.racer.nl/reference/pacejka.htm>
- [48] F. Wang and B. Zhuo, "Regenerative braking strategy for hybrid electric vehicles based on regenerative torque optimization control," *Proc. IMechE* , pp. 499-513, 2008.

- [49] Sebastien Wasterlain, Alcicek Guven, Hamid Gualous, Jean Francois Fauvarque, and Roland Gallay, "Hybrid power source with batteries and supercapacitor for vehicle applications," *L2ES Laboratory UFC-UTBM*, p. 5.
- [50] Barry Winfield. (2003, June) 2004 Chrysler Pacifica AWD - Road Test. [Online]. [http://www.caranddriver.com/reviews/car/03q2/2004\\_chrysler\\_pacifica\\_awd-road\\_test](http://www.caranddriver.com/reviews/car/03q2/2004_chrysler_pacifica_awd-road_test)

# Appendix A: Vehicle Specifications

The vehicle model developed allows for flexibility in design and configuration. The major nominal vehicle parameters are summarized in Table A.1. All vehicle specifications, battery parameters, and ultracapacitor parameters are taken from [50] [23].

Item	Value
Vehicle mass	2299 kg
Yaw moment of inertia	3365 kg·m <sup>2</sup>
Roll moment of inertia	750 kg·m <sup>2</sup>
Wheel roll moment of inertia	2 kg·m <sup>2</sup>
Distance from center of gravity to front axle	1.3293 m
Distance from center of gravity to rear axle	1.6247 m
Height of center of gravity	0.644 m
Distance from center to center of gravity	0.35 m
Effective rolling radius	0.432 m
Frontal Area	2.84 m <sup>2</sup>
Aerodynamic drag coefficient	0.355
Density of air	1.23 kg/m <sup>3</sup>

---

Density of isooctane	0.688 kg/L
Engine moment of inertia	0.7 kg·m <sup>2</sup>
Electric motor torque	190 N·m
Electric motor maximum power	67 kW
Electric motor continuous power	32 kW
Electric motor gear ratio	17.5
Ultracapacitor capacity	6 Ah
Ultracapacitor maximum power	65.7 kW
Ultracapacitor energy	657 Wh
Battery capacity	35 Ah
Battery maximum power	27.3 kW
Battery energy	9.5 kWh
Automatic transmission ratios	2.84, 1.57, 1, 0.69
Drivetrain efficiency	0.92

---

Table A.1: Vehicle Parameters

The Magic Formula Tire model contains coefficients  $b_0$  through  $b_{12}$  for the pure slip calculations. The coefficients are summarized in Table A.2.

<b>Coefficient</b>	<b>Value</b>
$b_0$	2.68
$b_1$	-47.6118
$b_2$	1350
$b_3$	-0.0736
$b_4$	124.82
$b_5$	-0.076614
$b_6$	-0.00386
$b_7$	0.085055
$b_8$	0.75719
$b_9$	0
$b_{10}$	0
$b_{11}$	0.005
$b_{12}$	0

*Table A.2: Magic Formula Tire Model Pure Slip Coefficients*

## Appendix B: Drive Cycles

The drive cycles of interest for this study are outlined in Chapter 4. To further examine the characteristics of the UDDS, HWFET, US06, SC03 and NYCC drive cycles, their displacements, velocities, and accelerations are plotted as functions of time.

### Hybrid Control Evaluation Cycle

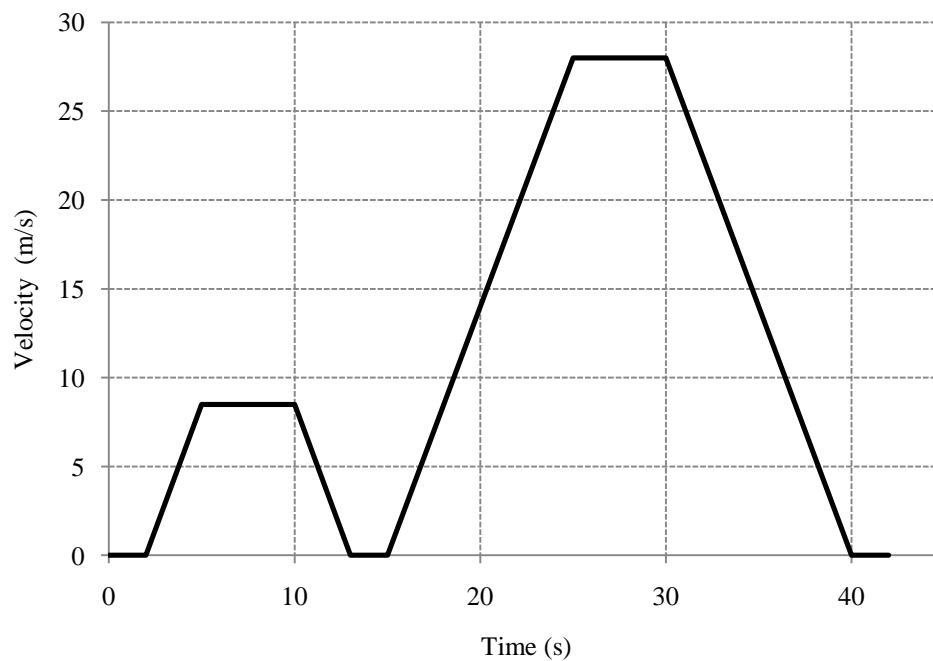


Figure B.1: Hybrid Control Cycle Velocity

### Urban Dynamometer Driving Schedule

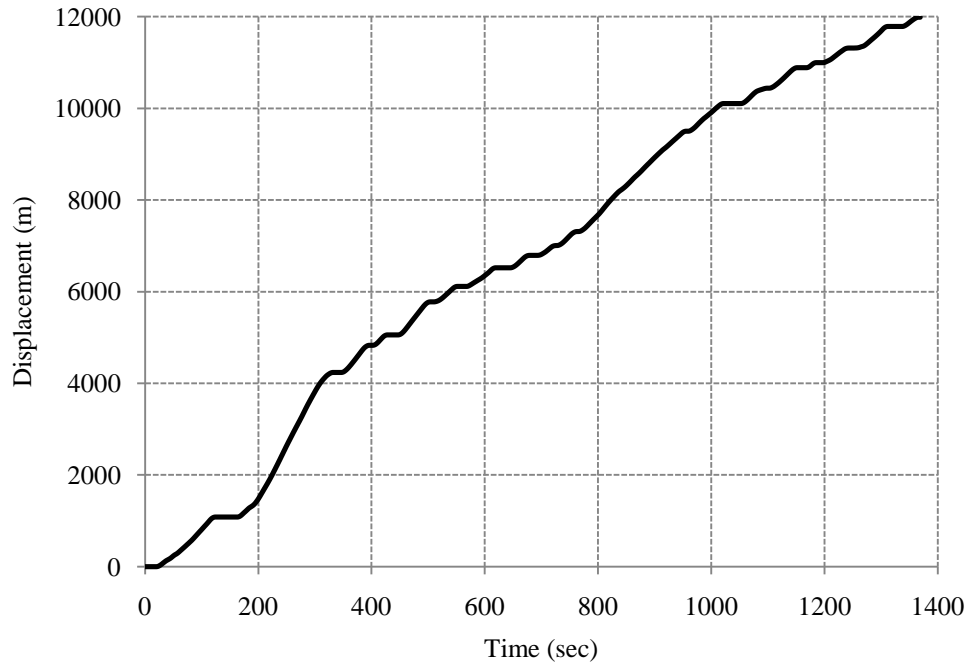


Figure B.2: UDDS Displacement

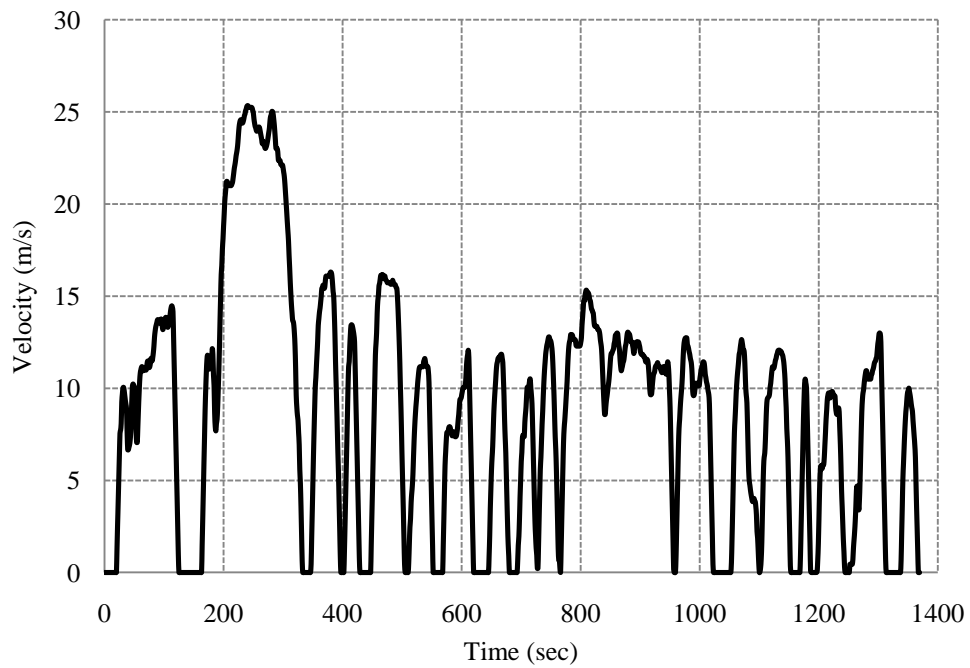


Figure B.3: UDDS Velocity



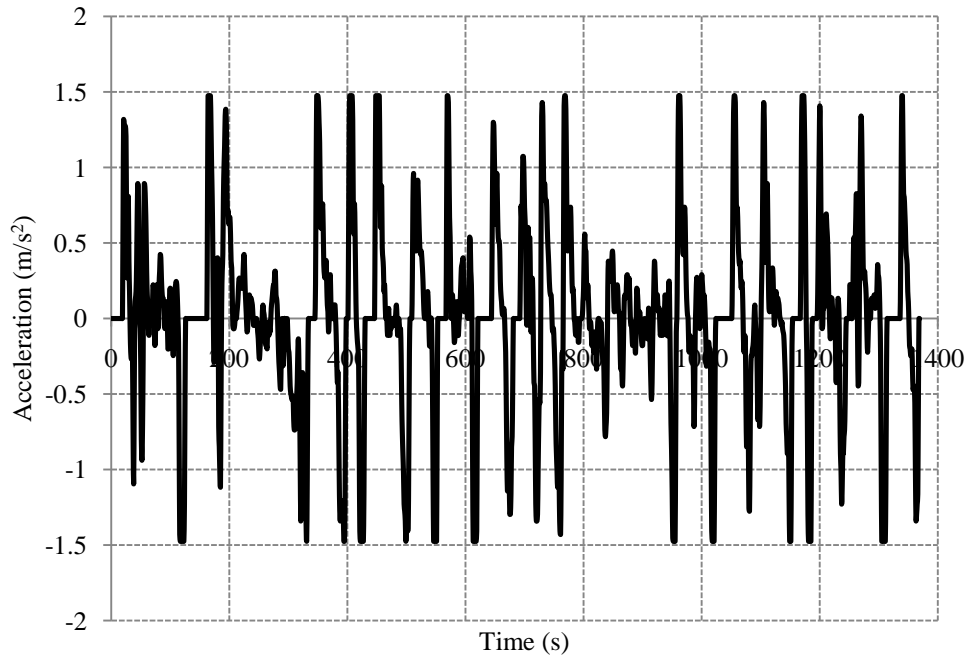


Figure B.4: UDDS Acceleration

### EPA Highway Fuel Economy Test Driving Schedule

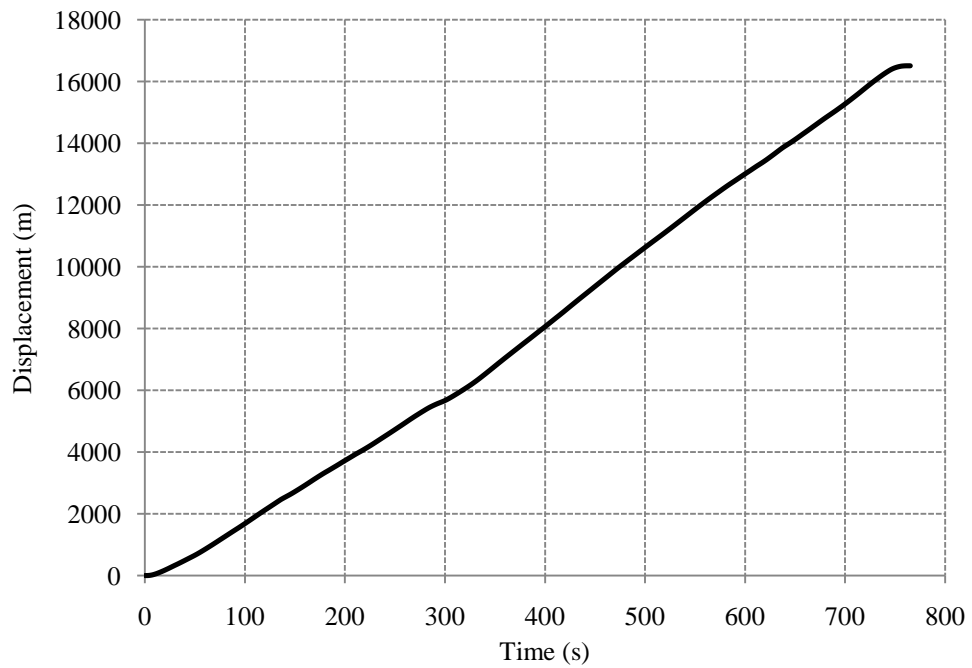


Figure B.5: HWFET Displacement

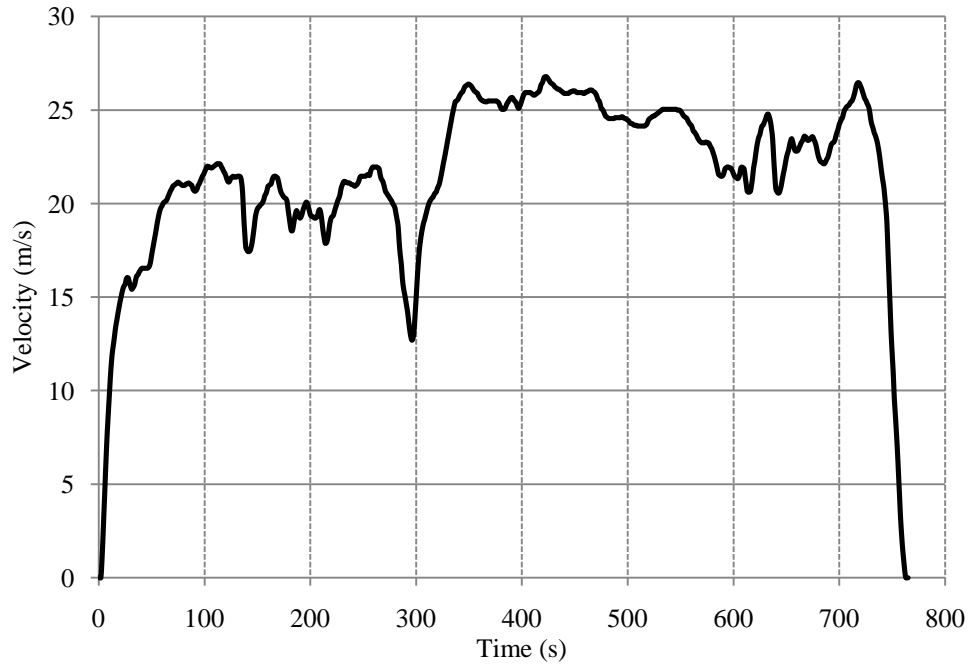


Figure B.6: HWFET Velocity

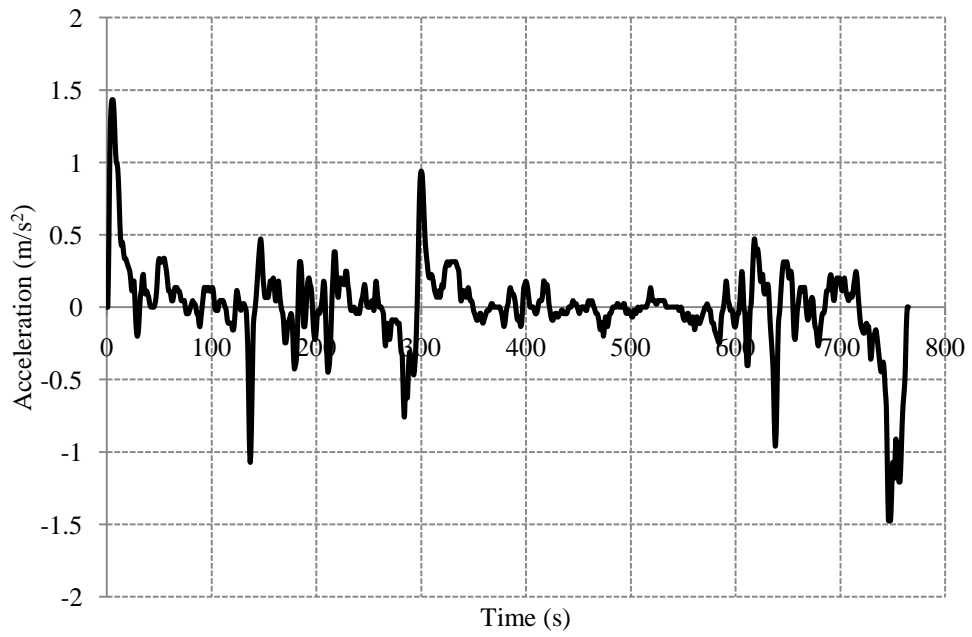


Figure B.7: HWFET Acceleration

### US06 or Supplemental FTP Driving Schedule

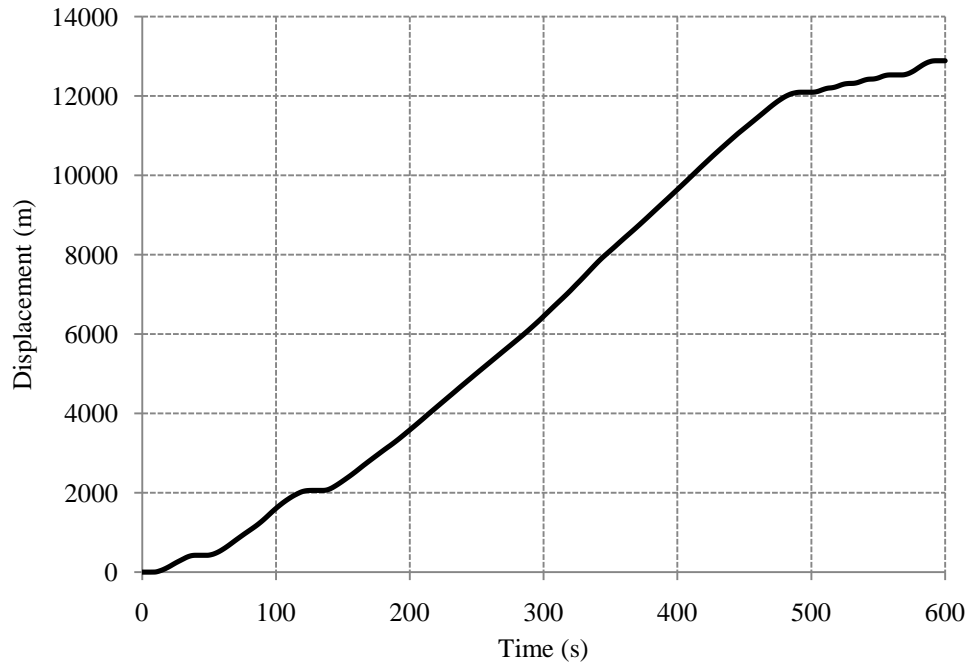


Figure B.8: US06 Displacement

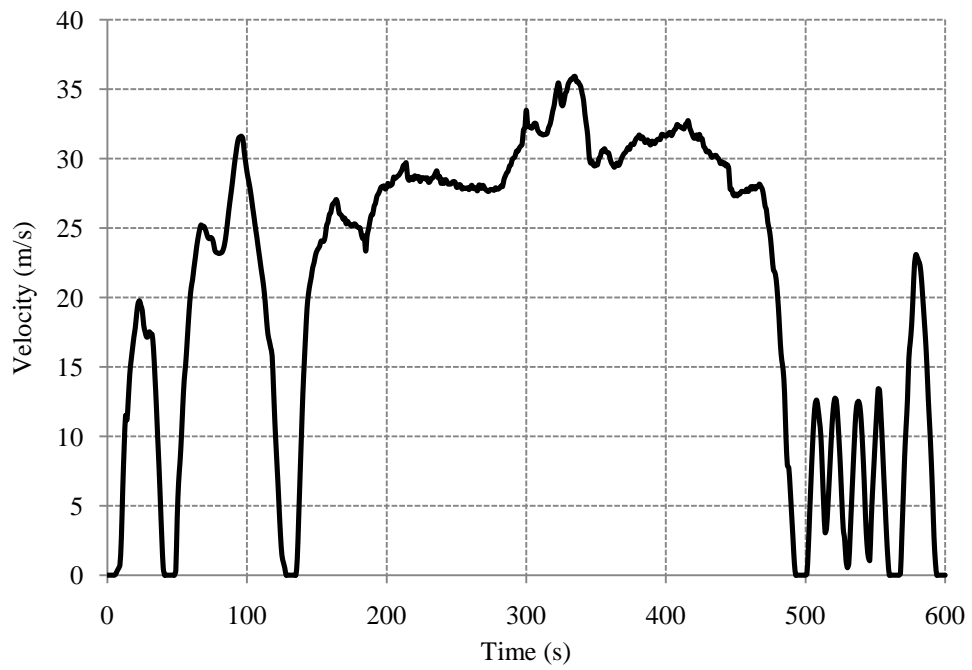


Figure B.9: US06 Velocity

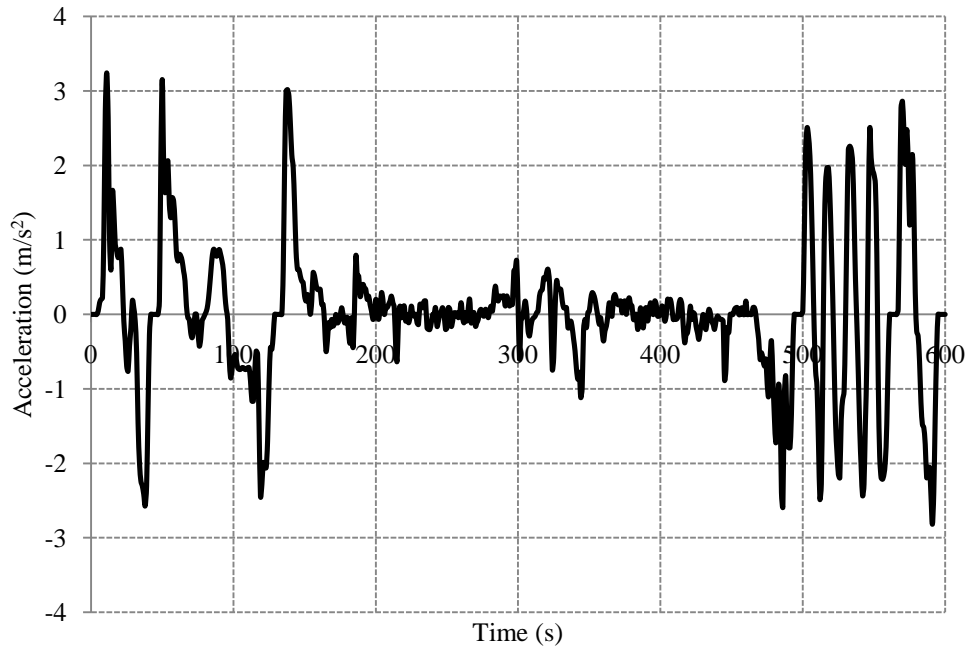


Figure B.10: US06 Acceleration

### Speed Correction 03 Driving Schedule

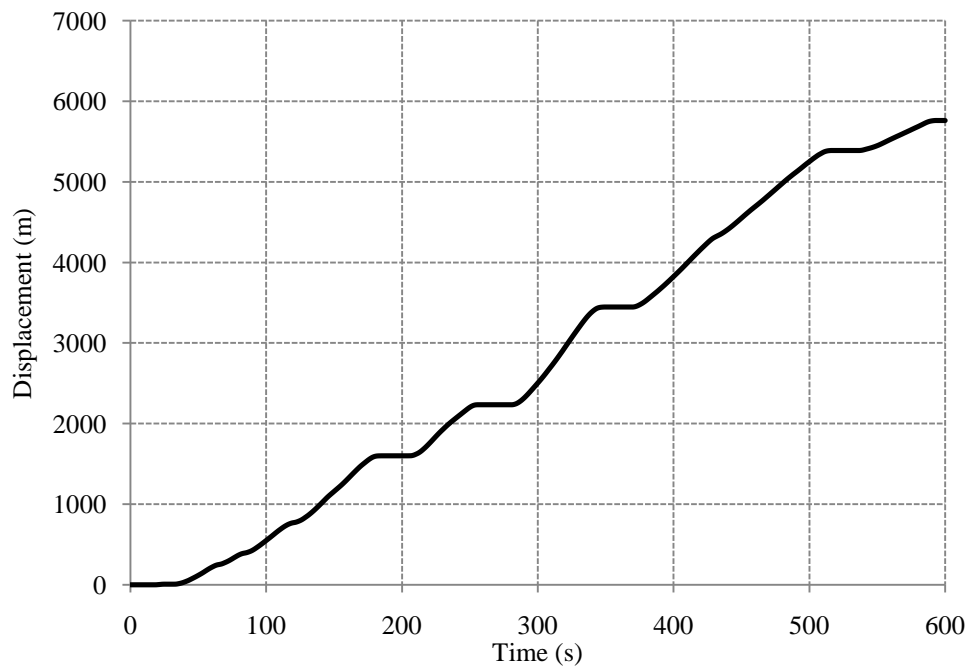


Figure B.11: SC03 Displacement

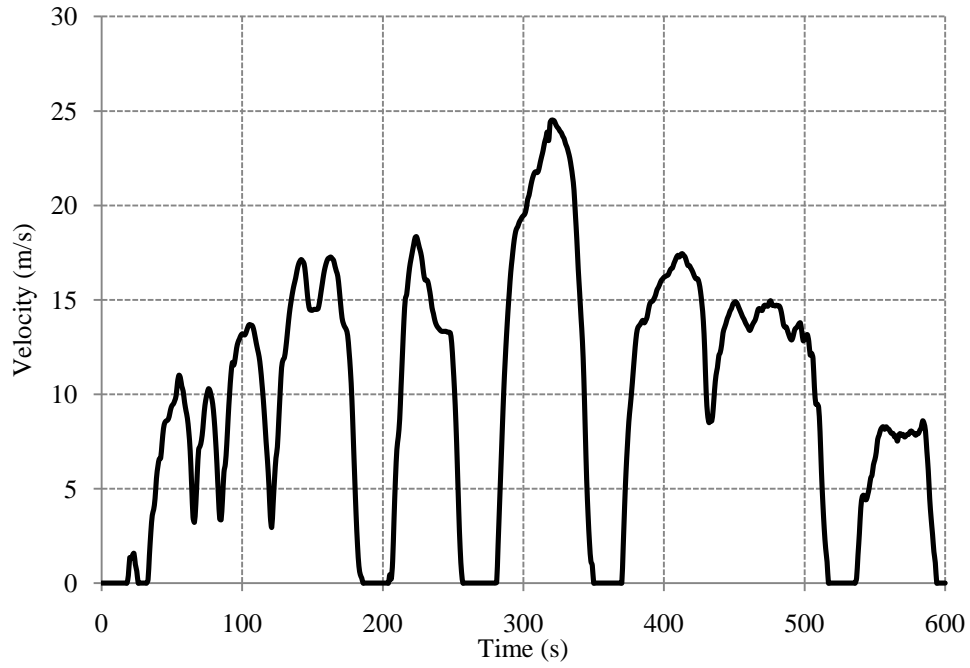


Figure B.12: SC03 Velocity

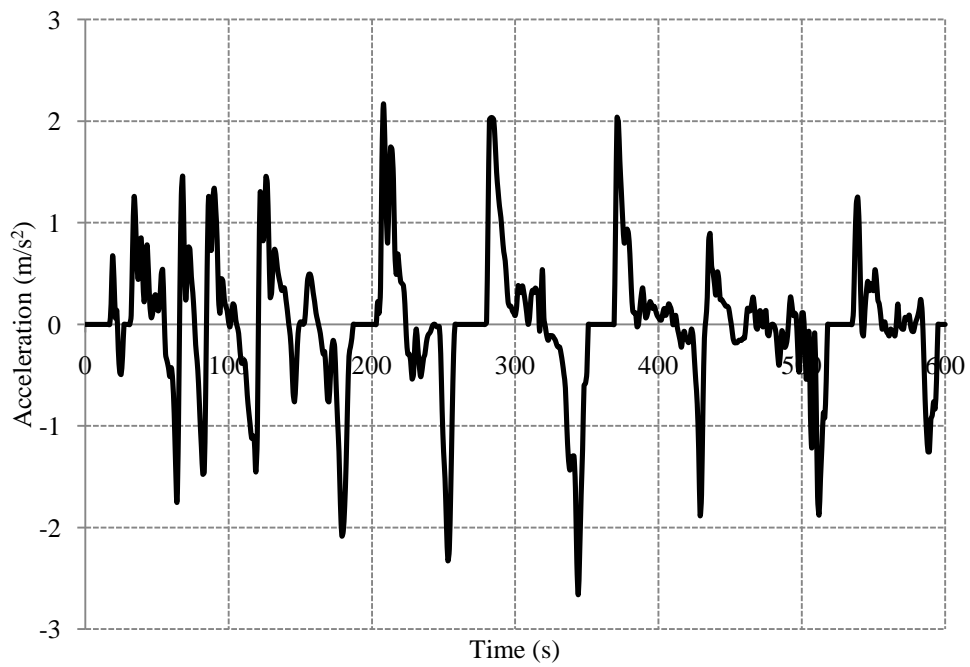


Figure B.13: SC03 Acceleration

### New York City Cycle

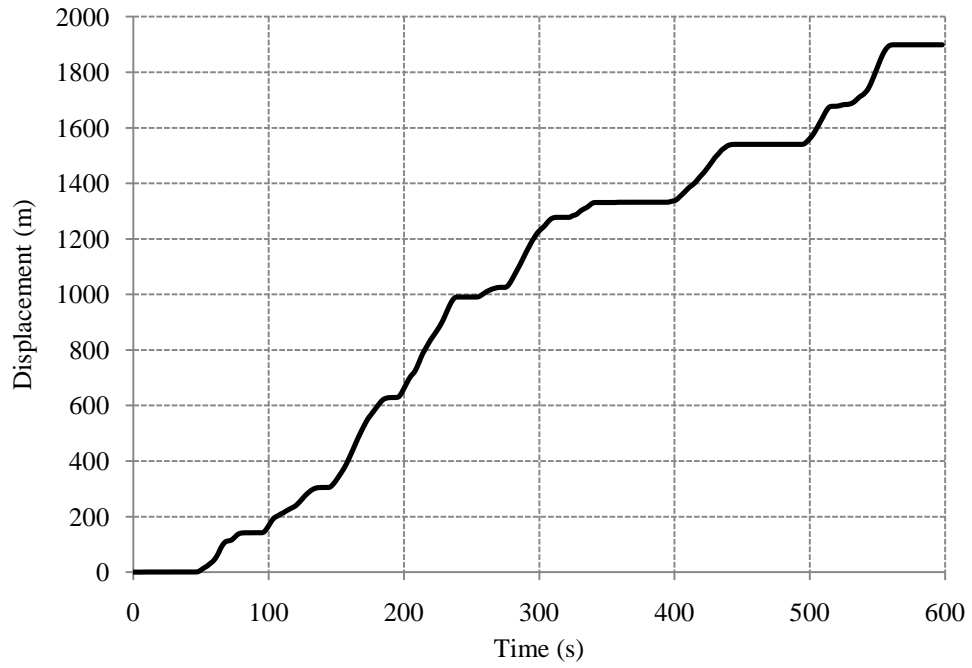


Figure B.14: NYCC Displacement

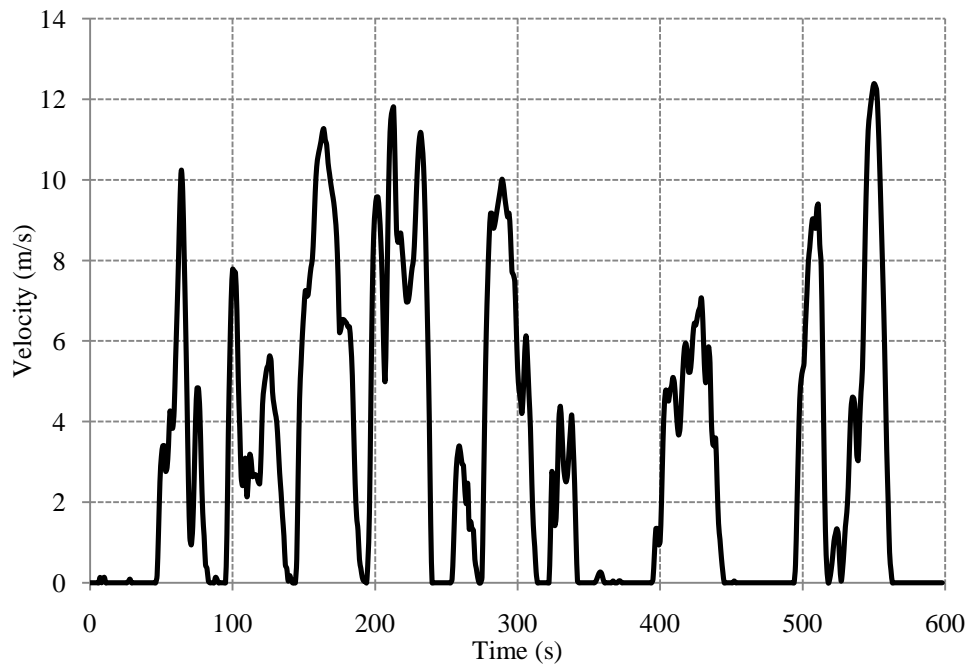


Figure B.15: NYCC Velocity

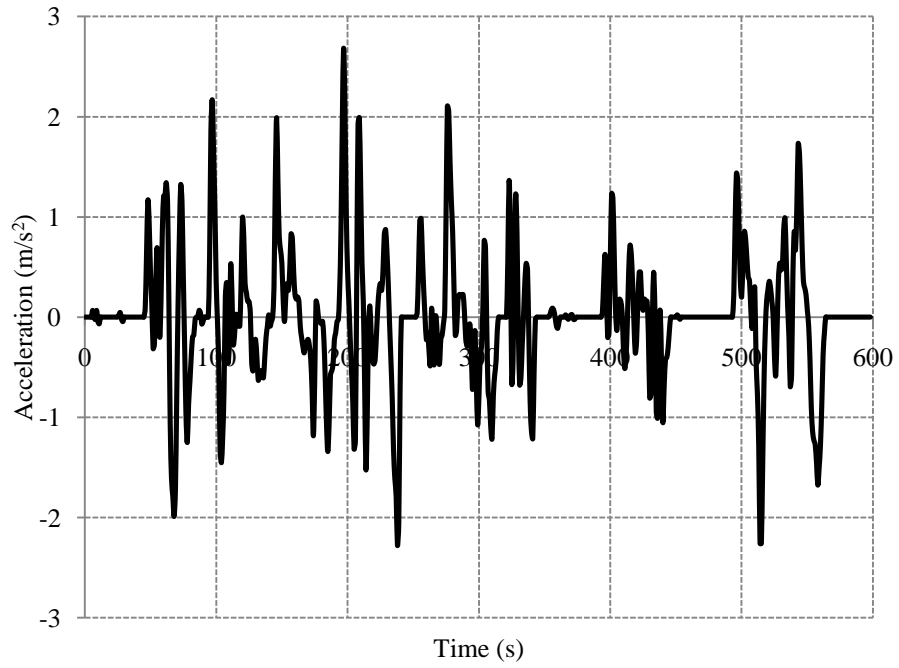


Figure B.16: NYCC Acceleration

# **Vita Auctoris**

Name: Kevin J. Martin

Born: Oshawa, Ontario, Canada, 1986

Education: St. Stephen's Secondary School, Bowmanville, Ontario, Canada

Bachelor of Applied Science – Honours Mechanical Engineering with Automotive Option, University of Windsor, Windsor, Ontario, Canada